https://doi.org/10.1070/RCR4985

BODIPY derivatives as fluorescent reporters of molecular activities in living cells

Vladimir I. Martynov, Alexey A. Pakhomov

Shemyakin – Ovchinnikov Institute of Bioorganic Chemistry, Russian Academy of Sciences, ul. Miklukho-Maklaya 16/10, 117997 Moscow, Russian Federation

Fluorescent compounds have become indispensable tools for imaging molecular activities in the living cell. 4,4-Difluoro-4-bora-3a,4a-diaza-*s*-indacene (BODIPY) is currently one of the most popular fluorescent reporters due to its unique photophysical properties. This review provides a general survey and presents a summary of recent advances in the development of new BODIPY-based cellular biomarkers and biosensors. The review starts with the consideration of the properties of BODIPY derivatives required for their application as cellular reporters. Then review provides examples of the design of sensors for different biologically important molecules, ions, membrane potential, temperature and viscosity defining the live cell status. Special attention is payed to BODPY-based phototransformable reporters.
The bibliography includes 339 references.

Contents

1. Introduction 1213
2. Properties of BODIPY derivatives required for their use as cellular reporters 1214
 2.1. Properties of the BODIPY core structure 1214
 2.2. Dependence of spectral properties of BODIPY derivatives on the structure 1214
 2.3. Properties of water-soluble BODIPY derivatives 1219
 2.4. Photostability 1221
 2.5. Brightness 1221
 2.6. Cytotoxicity and biocompatibility 1222
3. Targeted delivery of BODIPY derivatives to various intracellular compartments 1223
 3.1. Plasma membrane 1223
 3.2. Cytoplasm 1224
 3.3. Golgi apparatus and endoplasmic reticulum 1225
 3.4. Mitochondria 1226
 3.5. Lysosomes and endosomes 1226
4. Targeted labelling of individual cellular proteins with BODIPY derivatives 1227
5. BODIPY derivatives as the basis for the design of cell sensors 1230
 5.1. Cation sensors 1233
  5.1.1. pH indicators 1233
  5.1.2. Calcium ions 1235
  5.1.3. Potassium ions 1236
  5.1.4. Manganese cations 1237
  5.1.5. Intracellular sensors for zinc cations 1238
 5.2. Anion sensors 1238
  5.2.1. Chloride ions 1239
  5.2.2. Carbonate ions 1239
  5.2.3. Cyanide ions 1240
 5.3. Thiols 1240
 5.4. Sensors of reactive oxygen and nitrogen species 1242
  5.4.1. Hydrogen peroxide 1242
  5.4.2. Hydroxyl radical 1243
  5.4.3. Superoxide anion radical 1245
  5.4.4. Peroxyl radical 1245
  5.4.5. Hypochlorous acid 1246
  5.4.6. Nitrogen(II) oxide 1247
  5.4.7. Nitroxyl 1248
  5.4.8. Peroxynitrite 1249
 5.5. Membrane potential sensor 1250
 5.6. Viscosity and temperature sensors 1250
6. BODIPY phototransformable reporters 1252
7. Conclusion 1255
8. List of acronyms 1256

1. Introduction

Biological fluorescence markers have long been used as a tool for biomolecule detection and for the analysis of cell structure. However up to the 1980s, fluorescent labelling was used predominantly for fixed biological specimens due to the lack of fluorescent markers at that time suitable for live cell applications. Nowadays, fluorescence microscopy and fluorescent compounds of different types have become one of the most important tools for visualizing the mole-

V.I.Martynov. Doctor of Chemical Sciences, Chief Researcher, Head of the Laboratory of Molecular Theranostics, IBCH RAS.
E-mail: vimart@list.ru
Current research interests: protein posttranslational modifications, photosensitive proteins, application of fluorescent compounds as biosensors in cell biology and as theranostic agents in medicine.

A.A.Pakhomov. PhD, Senior Researcher at the same Laboratory, IBCH RAS. E-mail: alpah@mail.ru
Current research interests: fluorescent compounds for biotechnology including low-molecular-weight dyes and GFP-like proteins, mechanisms of fluorescent protein chromophore synthesis and its modifications, intracellular fluorescent probes and their targeted delivery.

Received 23 July 2020

© 2021 Uspekhi Khimii, ZIOC RAS, Russian Academy of Sciences and IOP Publishing Limited

cular organization and for detecting molecular activity in live cells. Fluorescent molecules function as cellular reporters displaying molecular processes in real time as changes in various fluorescence parameters.

For the most part, the increased interest in fluorescent reporters in recent years is associated with the discovery of different coloured variants of fluorescent proteins (FPs).[1] This technology allows the construction of genetically encoded fused structures of a target cellular protein with FP. However, the FP technology has limitations. In particular, there are several drawbacks including a significant size of the fluorophore itself,[2] a low maturation rate of many FPs (protein does not acquire fluorescence immediately),[3,4] rather complicated operations in preparing FPs with necessary photophysical properties.[5] Therefore, the synthesis of new fluorescent sensors based on small organic molecules represents a distinct trend in this field.[6,7]

The most popular synthetic fluorophores widely used in biochemistry and cell biology are coumarins, fluoresceins, rhodamines, phenoxazines, cyanines and derivatives of dipyrrometheneboron difluoride **1** (4,4-difluoro-4-boron-3a,4a-diaza-*s*-indacene, BODIPY).[8–10] Among these compounds, BODIPY derivatives are of particular interest, which is reflected in a number of recent review articles.[11–24] They possess high photostability[25] and fluorescence quantum yield, have a neutral charge, and show narrow absorption and emission bands.[12] The incorporation of specific substituents at different positions of the BODIPY structure makes it quite easy to obtain derivatives with desired chemical and photophysical properties.[11] Various BODIPY derivatives span virtually the entire visible and NIR wavelength range. Most fluorophores derived from BODIPY belong to stable fluorescent labels. Moreover, fluorescent BODIPY derivatives were also obtained with optical properties that change upon illumination with light of a specific wavelength (phototransformation)[26] or in the presence of certain analytes.[27,28]

The original BODIPY molecule and some its derivatives exhibit significant lipophilicity and, therefore, they are suitable for studying the processes within the plasma membrane and membranes of subcellular structures.[13,29] Modified BODIPY derivatives containing hydrophilic substituents are required to visualize the activities that take place in the cytosol. In this review, we will try to discuss all of the above-mentioned issues in light of the most recent data, as well as to provide an overview and summary of the latest advances in the development of BODIPY-based biomarkers and biosensors.

The range of topics related to BODIPY is extremely wide, and therefore it is impossible to cover all areas in one review. Some modern trends, in particular, the use of FLIM spectroscopy, the application of quantum dots in conjunction with BODIPY as FRET partners and surface plasmon-enhanced FRET are well covered in recent years, including review papers[30–36] and therefore are beyond the scope of this review. Comprehensive information on the synthesis of various BODIPY derivatives can be found in reviews by Kevin Burgess[11] and Wim Dehaen.[12] We also consider that the sensorics of transition and heavy metals deserves a more detailed analysis in the form of a separate publication. Since our main interest is in biomarkers and biosensors of the most important physiological compounds, the review focuses on this subject.

2. Properties of BODIPY derivatives required for their use as cellular reporters

The possibility of using a fluorophore as a reporter in a living cell is determined by its chemical (reactivity, solubility, lipophilicity, chemical stability, cytotoxicity), photophysical (absorption and emission maxima, extinction coefficient, fluorescence quantum yield, lifetime of the excited state,) properties, photostability and phototoxicity. Most BODIPY derivatives demonstrate negligible cytotoxicity,[37] narrow absorption bands (the absorption half-width is usually 20–30 nm),[38] high molar extinction coefficients (up to 10^5 L mol^{-1} cm^{-1}) and quantum yields (up to 1.0), with sufficiently long lifetimes of the excited singlet state (up to 10 ns)[38] and high chemical and photochemical stability in solutions. However, the original BODIPY structure does not possess all the necessary characteristics of an ideal cellular reporter. Yet, by derivatization, it is possible to optimize properties of BODIPY for its further application in *in vitro* and *in vivo* experiments.

2.1. Properties of the BODIPY core structure

Fluorescent derivatives of BODIPY were first synthesized by Alfred Treibs and Franz-Heinrich Kreuzer in 1968.[39] Since that time, many different analogues of this compound have been obtained; however, the unsubstituted green fluorescent BODIPY core structure **1** was synthetized only in 2009.[40,41] BODIPY **1** is characterized by a high fluorescence quantum yield in organic solvents (Φ_{fl} = 0.69–0.97). The position of the absorption maximum of **1** is almost independent of the solvent polarity ($\lambda_{abs} \approx 500$ nm); however, the emission maximum position is somewhat dependent on the solvent used (λ_{em} = 515–535 nm). It was also shown that the fluorescence quantum yield of **1** increases with increasing polarity of the solvent. Besides, compound **1** shows moderate water solubility and, in water, has an absorption maximum at 516 nm and a fluorescence quantum yield of 0.90.[40] The determined very close values of the B1-N1 and B1-N2 bond lengths (according to the crystallographic data, 1.551 Å and 1.547 Å, respectively) are indicative of the delocalization in the BODIPY structure.[41] The crystal structure also demonstrates that compound **1** is planar, with the exception of the boron atom, which slightly deviates from the plane of the molecule. According to DFT calculations, the structure should have a completely planar configuration, and a slight deviation from planarity is most likely due to intermolecular interactions in the crystal packing.[40]

2.2. Dependence of spectral properties of BODIPY derivatives on the structure

Compounds that absorb and emit light in the longer wavelength region, especially in the near-IR range (650–900 nm), are preferable for applications in living systems as compared to shorter wavelength fluorophores. Fluorophores with excitation and emission in the long wavelength region make it possible to avoid cell photodegradation, which is typical of UV light excitation. The use of longer wavelength fluorophores reduces autofluorescence and eventually increases the sensitivity of fluorescence microscopy. Other aspects that are very important for *in vivo* experiments is the reduced light scattering and the greater tissue penetration depth for the long wavelength light. On the other hand, concurrent application of several fluorophores with different emission maxima allows the

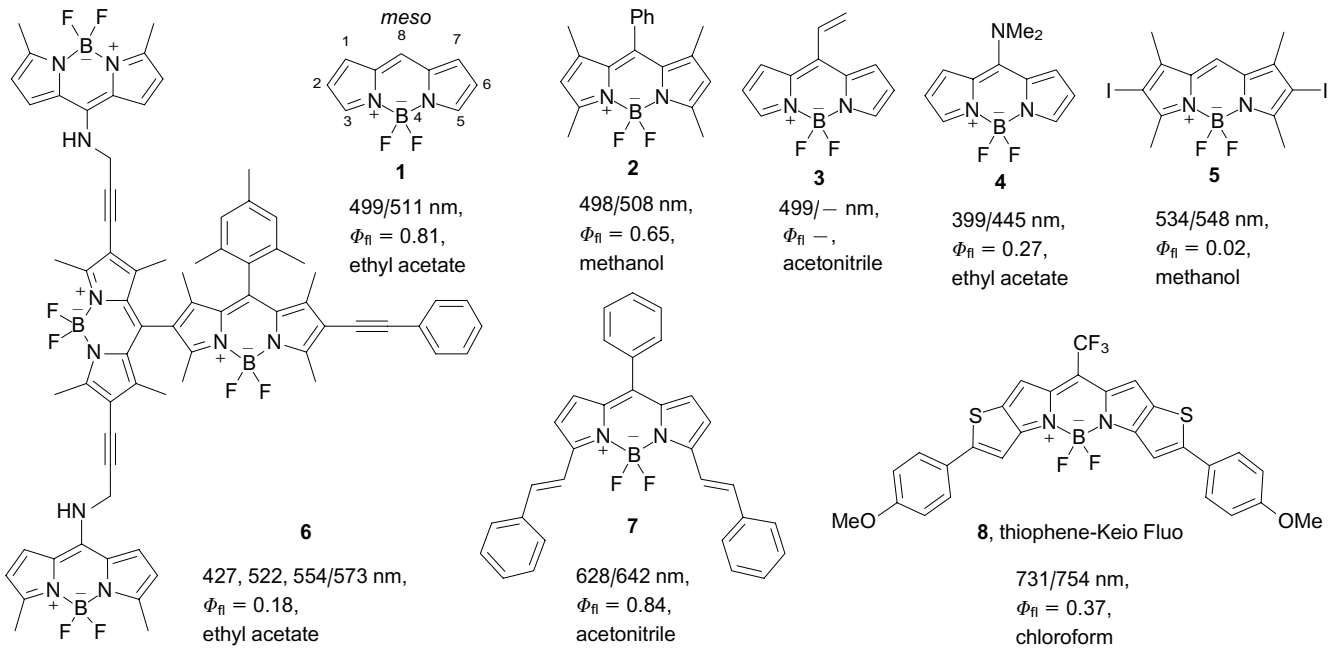


Figure 1. The influence of different substituents on spectral properties of BODIPY. Here and below, in addition to the compound number and its name, absorption and emission maxima separated by a slash, the quantum yield and the solvent, in which the data were obtained, are given under the structures.

monitoring of different cellular processes simultaneously by multichannel imaging.[42, 43]

Spectral properties of BODIPY derivatives can be rather easily tuned to the desired spectral range using various electron-donating, electron-withdrawing groups or substituents extending the π-electron system.[11] Up to now, BODIPY derivatives with fluorescence emission covering almost the entire visible spectrum and the near-infrared region have been obtained.[42, 44, 45] As noted above, BODIPY **1** has an emission maximum in the green spectral range. The incorporation of alkyl substituents in pyrrole rings of BODIPY[46] has virtually no effect on the spectral properties, as compared with structure **1**. The introduction of *meso*-substituents [C(8) atom] may lead to various effects.[47] For example, aromatic substituents in this position are oriented perpendicular to the BODIPY plane due to steric constraints and have only a slight effect on the spectral properties[11] (Fig. 1, compound **2**). Meanwhile, the introduction of vinyl substituents in this position (compound **3**) leads to a decrease in the fluorescence quantum yield almost to zero due to a significant deformation of the chromophore upon excitation and subsequent transition to the ground state *via* vibrational relaxation.[48, 49] Electron-donating substituents at the *meso* position of BODIPY cause a hypsochromic shift of fluorescence to the blue spectral region. For example, the 8-dimethylamino derivative of BODIPY (compound **4**) exhibits the absorption maximum at 399 nm and the emission maximum at 445 nm with a reduced quantum yield (Φ_{fl} = 0.27).[50] The fluorescence quantum yield also drastically reduces when heavy atom substituents, for example, halogen atoms (compound **5**),[51] fullerenes or other BODIPY fluorophores are introduced into the BODIPY core, if these substituents are not involved in the overall π-electron system (compound **6**).[52] Meanwhile, the presence of heavy atoms is associated with the photosensitizing properties of BODIPY, which makes it possible to use BODIPY derivatives in photodynamic therapy.[53 – 55] As expected, the introduction of aromatic substituents at the 3- and 5-positions (compounds **7**, **8**) leads to a bathochromic shift to the far-red and NIR spectral region.[23, 56, 57]

For the labelling of biomolecules, a series of commercially available BODIPY derivatives with aromatic electron-donating substituents at the 3- and 5-positions and with emission from the green to red spectral range were prepared (Fig. 2, compounds **9** – **17**).

The addition of styryl and other arylethylenyl substituents with electron-donating properties to BODIPY pyrrole rings shifts the fluorescence excitation/emission maxima up to 700 nm (Fig. 3, compounds **19** – **22**).[58, 59] It should be noted that the introduction of the first and the second styryl residues at the 3- and 5-positions (compounds **19**, **20**) leads to bathochromic shifts of ~70 and ~140 nm, respectively, as compared to original compound **18**. However, the introduction of the third and the fourth styryl substituents at the 1- and 7-positions has a negligible effect on spectral properties, while the reaction yield of these compounds drops sharply. For example, compound **22** has a yield of only 2%, whereas under similar conditions distyryl derivative **20** has a yield of 58%.[59] Thus, it should be taken into account that substituents at the 1- and 7-positions have an insignificant effect on the bathochromic shift, which is also evidenced by a small difference in the maxima of fluorescence excitation/emission of compounds **10** and **11** (Fig. 2). This phenomenon is probably due to steric constraints, which, similar to substituents in the *meso* position, do not allow the substituents at the 1- and 7-positions to participate in the conjugation with the BODIPY core structure.

The fluorophore π-electron system can be extended not only by the attachment of aromatic substituents, but also at the expense of multiplication of BODIPY residues (Fig. 4, compounds **23** – **25**).[60, 61] The fusion of BODIPY pyrrole rings with aromatic substituents (see compound **8** in Fig. 1 and compounds **26** – **31** in Fig. 4)[12, 61 – 66] also leads to a shift of fluorescence excitation/emission maxima to the NIR

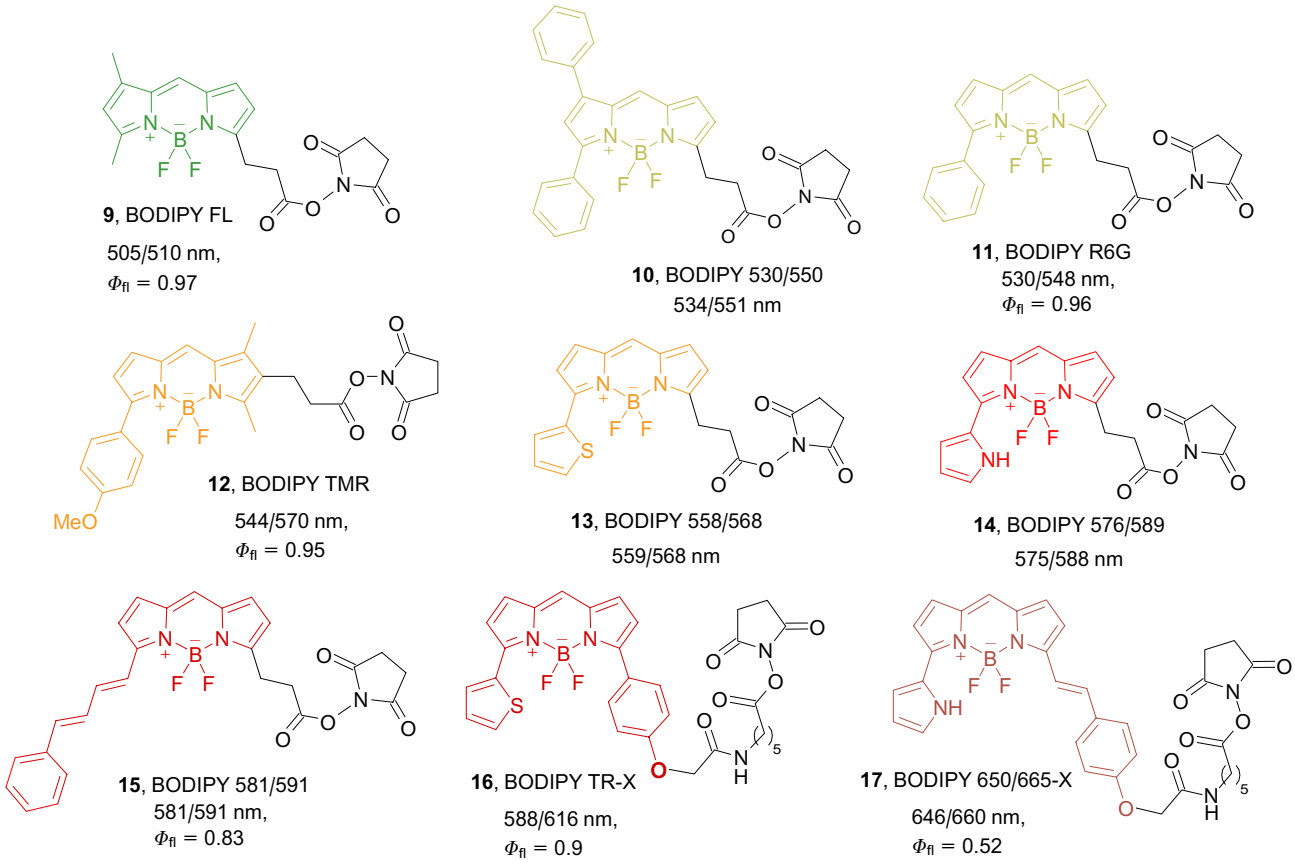


Figure 2. Commercially available BODIPY-based fluorescent dyes with emission ranging from green to red for labelling of biomolecules at their amino groups.

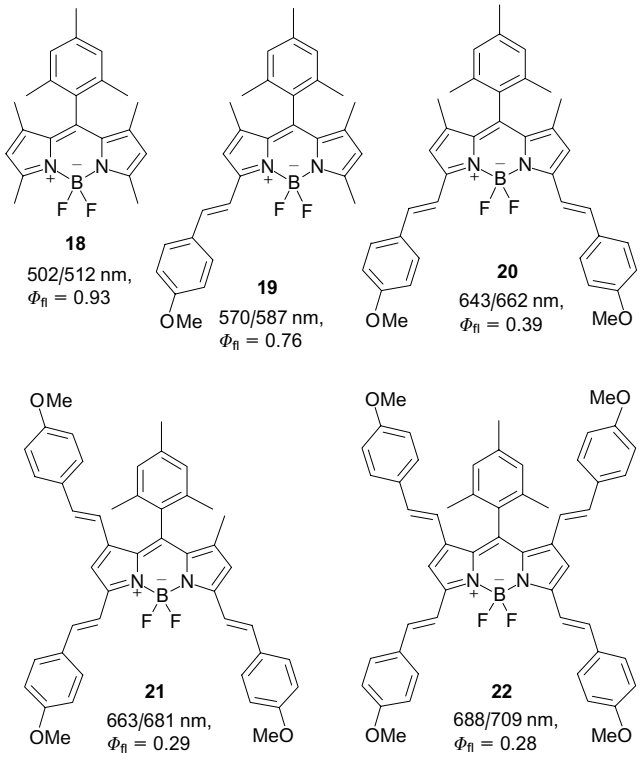


Figure 3. Influence of the number of styryl substituents on the spectral properties of BODIPY (dichloromethane solvent).

region (700 – 800 nm) and for bis-BODIPY derivatives, in some cases, beyond 900 nm. Unfortunately, excessive extension of the π-system can lead to a decrease in the stability of the compounds. For example, bis-BODIPYs, such as **28** – **30**, are highly susceptible to reactions with singlet oxygen generated by their own upon exposure to light.[12]

The replacement of carbon at the 8-position of BODIPY with nitrogen results in the aza-BODIPY derivatives (Fig. 5, compounds **32** – **34**),[35, 67, 68] which exhibit a significant bathochromic shift to the NIR region of the spectrum. Compared to the common BODIPY derivatives, aza derivatives with the same substituents exhibit ~150 nm larger bathochromic shifts. B,O-Chelated aza-BODIPY derivatives (*e.g.*, compound **33**) have a relatively high quantum yield due to the formation of intramolecular B,O-containing rings, which restricts the aromatic ring mobility.[67]

Wilden and co-workers[69] synthesized a library of BODIPY derivatives carrying substituents in different positions and systematically investigated the dependence of their photophysical properties on the nature and position of the substituent. In this publication, the data obtained were combined in a table that allows the prediction of the properties of new BODIPY derivatives. Using these data, the authors synthesized BODIPY derivative **35** with photophysical properties similar to the predicted ones.[69]

An additional shift of the spectra to longer wavelengths can be attained by introducing electron-withdrawing groups at the *meso* position. For example, the introduction of the CF_3 group in the *meso* position (Fig. 6, compounds **36** and **37**) leads to a shift of the fluorescence excitation/emission

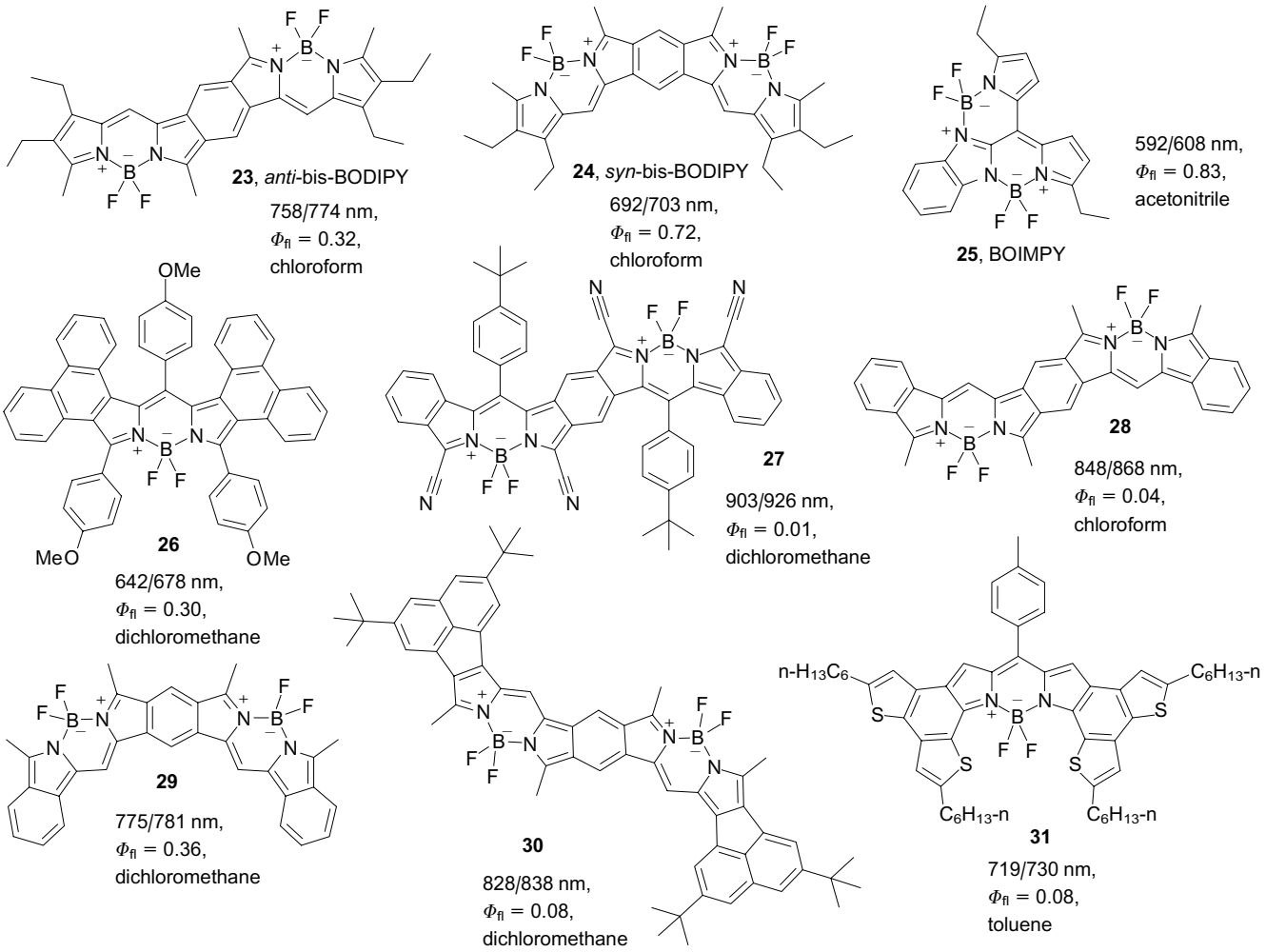


Figure 4. Multiplexed BODIPYs and derivatives with aromatic substituents fused to pyrrole rings.[51, 52 – 57]

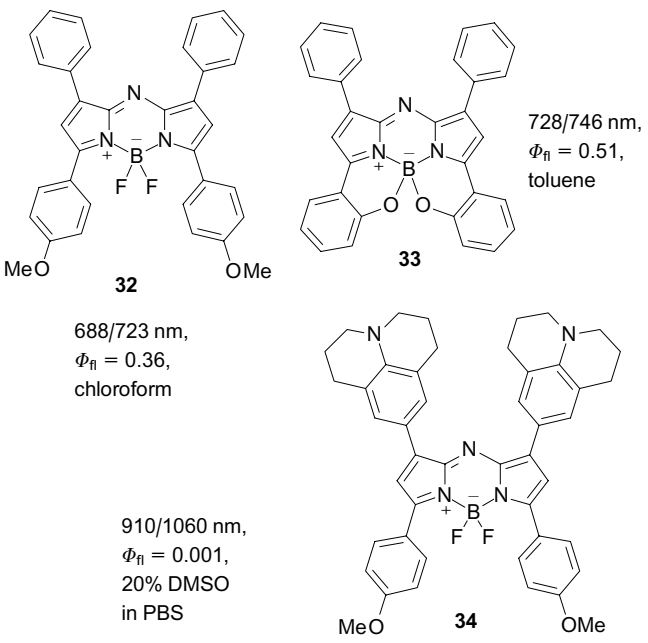
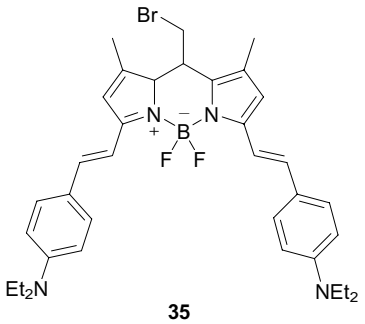


Figure 5. Aza-BODIPY derivatives with emission in the near-IR range.[35, 58, 59] PBS is phosphate buffer saline.

Structure 35



maxima by ~30 nm to the red region compared to related compounds **11** and **13** unsubstituted in the *meso* position.[70] An additional bathochromic shift (up to ~40 nm and 70 nm, respectively) is observed when electron-donating substituents, such as amino or dimethylamino groups, are introduced at the opposite side of the molecule **38** (Fig. 6, compounds **39** and **40**, respectively).[71, 72] According to quantum mechanical calculations, these effects are explained by a decrease in the LUMO (lowest unoccupied molecular orbital) levels and the corresponding decrease in the LUMO – HOMO (HOMO is the highest occupied molecular orbital) difference upon the introduction of electron-withdrawing substituents in the *meso* position[73]

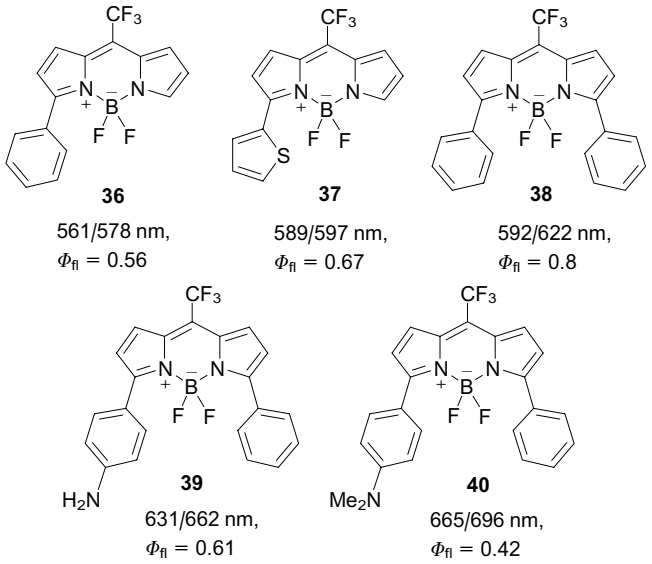


Figure 6. BODIPY derivatives with an electron-withdrawing CF_3 group in the *meso* position. Photophysical data were obtained in hexane.

and, in the case of electron-donating groups, at the opposite side of the fluorophore, due to the intramolecular charge transfer (ICT) and more significant decrease in the LUMO level compared with a decrease in HOMO.[71,72]

A characteristic property of most BODIPY derivatives is a small Stokes shift (usually 5 – 15 nm),[38,74] which can lead to fluorescence self-quenching. Moreover, small Stokes shifts can lead to partial overlap of the excitation and emission peaks. As a result, fluorescence emission is rather difficult to distinguish from scattered excitation light, which may cause some measurement errors.[75] This problem was addressed by the creation of systems (cassettes)[76,77] consisting of two fluorophores separated by a spacer group (see Fig. 1, compound **6**, and Fig. 7, compounds **41** – **45**). When one fluorophore (donor) is excited, the fluorescence energy (FRET) is resonantly transferred to the second fluorophore (acceptor), and the fluorescence emission of the second fluorophore is characterized by a significantly larger pseudo-Stokes shift as compared with those when fluorophores are used separately.[78,79] The spacer is necessary for the spatial separation of two π-electron systems; otherwise, the conjugated π-systems will behave as a single fluorophore. Noteworthy, the benzene ring in the *meso* position can also serve to separate π-systems, because it is oriented perpendicular to the BODIPY chromophore plane and does not participate in conjugation. One of the necessary conditions for efficient FRET is the overlapping of the donor emission and acceptor absorption peaks, which limits the choice of fluorophores. In contrast, upon through-bond energy transfer (TBET), the fluorophore donor and the

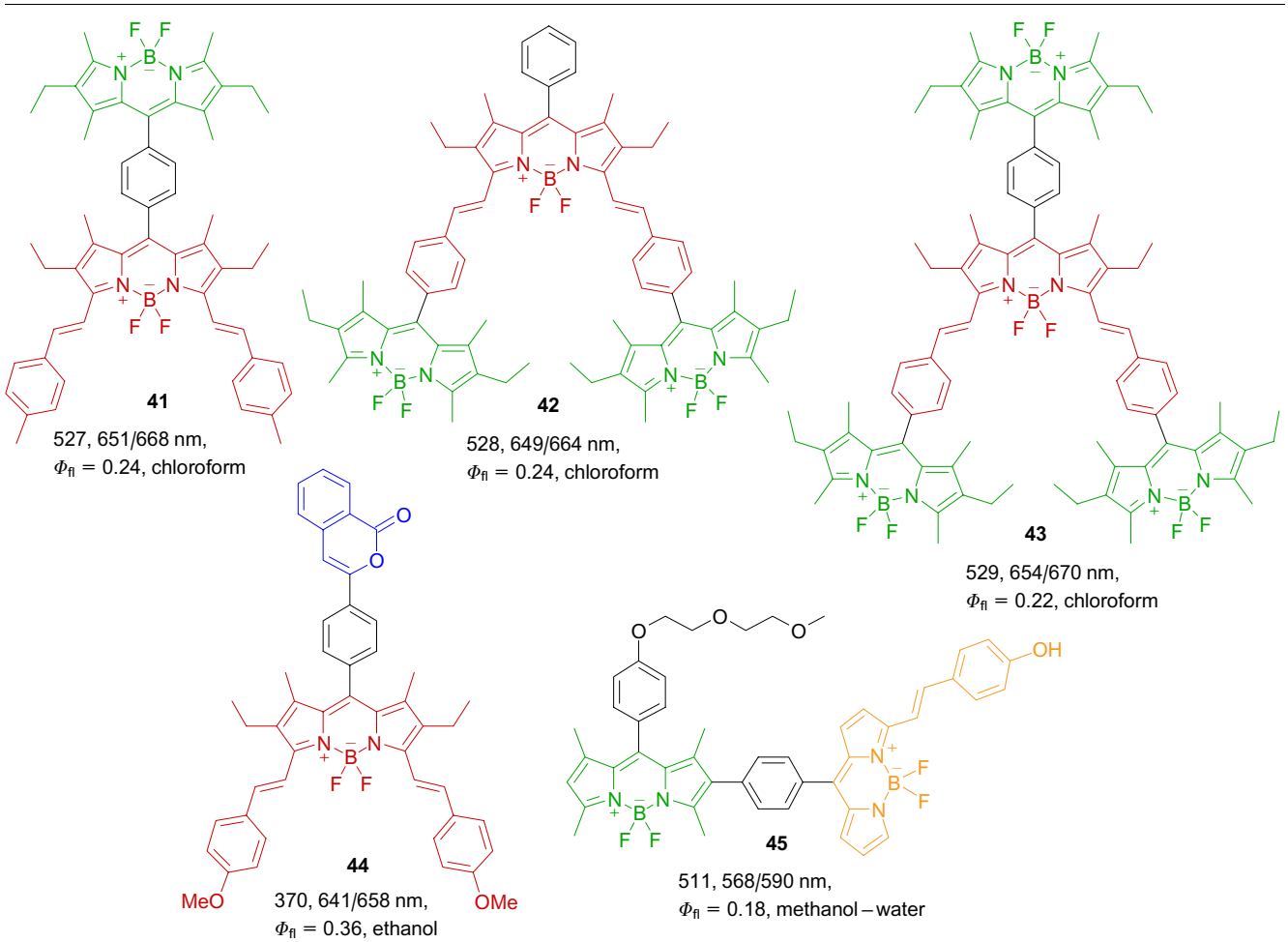
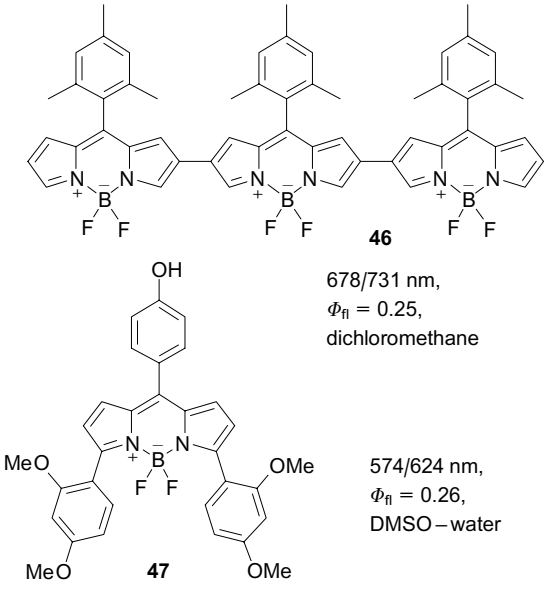


Figure 7. BODIPY multi-chromophore cassettes with an increased Stokes shift.

fluorophore acceptor are connected *via* a conjugating spacer;[75, 80, 81] in this case, the energy transfer process does not require overlap of the emission and absorption peaks, which implies greater possibilities for the fluorophore choice. In other approaches to increase the Stokes shift, BODIPY oligomers[82] (compound **46**) and BODIPY complexes with metals[83] were used. Wang and co-workers[84, 85] investigated the effects of various substituents and showed that the introduction of methoxyphenyl groups into BODIPY structure **47** significantly increases the Stokes shift. In this case, the dimethoxyphenyl derivative exhibited a 10 nm larger Stokes shift compared with the 38 nm shift of the monosubstituted BODIPY. In this work, the dimethoxyphenyl derivatives were successfully used as NO (Ref. 84) and H_2S (Ref. 85) sensors in living cells and tissues.

In conclusion, it should be noted that the introduction of substituents with different properties at different positions of BODIPY makes it possible to quite easily obtain derivatives with the required spectral properties. For example, the extension of the fluorophore π-system at the expense of aromatic substituents makes it possible to significantly shift the emission maxima to the red and near-IR regions, which is one of the essential prerequisite for application of these compounds in *in vivo* experiments. However, an excessive extension of the π-electron system often leads to a decrease in stability of the compounds due to photoreactions with oxygen. The optical properties are significantly affected by electron-donating and electron-withdrawing substituents in the BODIPY structure. Thus, the presence of an electron-donating group in the *meso* position leads to a hypsochromic shift, whereas the electron-withdrawing groups promote a bathochromic shift. A further red shift of the fluorescence excitation/emission spectra can be achieved by introducing electron-donating groups that provide ICT within the fluorophore π-system. It is also worth noting that a significant bathochromic shift occurs when the C(8) atom is replaced with nitrogen. Such aza-BODIPY fluorophores are characterized by ~150 nm larger bathochromic shifts compared to compounds containing a carbon atom in the 8-position.

Structures 46, 47



2.3. Properties of water-soluble BODIPY derivatives

Most BODIPY derivatives possess significant lipophilicity and, as the result, these compounds mainly accumulate in the plasma membrane and membranes of subcellular structures, such as endoplasmic reticulum, lysosomes, mitochondria and Golgi apparatus.[86] Hence, compounds of this type are advantageous for the study of processes occurring in cell membranes. In general, however, the lipophilicity of BODIPY is considered to be a disadvantage for experiments with living cells, although there are a number of studies where this property was successfully applied for instant cell staining.[87, 88] In aquatic environments, these derivatives form aggregates, which cause fluorescence quenching (aggregation-caused quenching, ACQ).[89] To visualize biomolecules localized in the cell cytosol, it is necessary to obtain modified water-soluble derivatives of BODIPY containing hydrophilic substituents.[90]

1,3,5,7-Substituted derivatives of BODIPY sulfonated at the 2- and 6-positions (Fig. 8, compound **48**) were synthesized to enhance aqueous solubility.[91] Notably, the introduction of sulfonate groups does not significantly change the absorption and fluorescence emission spectra compared to those of the unsulfonated fluorophore. Sulfonated BODIPY derivatives suitable for conjugation with biomolecules were synthesized by means of various approaches.[92, 93] However, the introduction of substituents bearing negatively charged ionizable groups can significantly reduce the cell membrane permeability of the fluorophore.[94, 95] To overcome this drawback, zwitterionic sulfobetaine substituents were introduced into the BODIPY structure both at the 2- and 6-positions and the boron atom (compounds **49**, **50**).[96] It was shown that the presence of sulfobetaine moieties at the boron atom does not affect the spectral properties of the fluorophore.[96] while a slight bathochromic shift is observed for the 2- and 6-dialkine-substituted dyes.[97] Furthermore, BODIPY derivatives that include a sulfonated peptide consisting of two (compound **51**) or three α-sulfo-β-alanine residues were synthesized in order to improve water solubility.[97] It was also shown that BODIPY conjugates with histidine and tyrosine residues are highly soluble in polar solvents.[98]

As an alternative, BODIPY derivatives with non-ionic polyethylene glycol (PEG) chains of various lengths were synthesized (compounds **52** and **53**).[99] The presence of PEG substituents not only led to increased water solubility, but also efficiently prevented the BODIPY aggregation and reduced the aggregation-caused fluorescence quenching (ACQ). As a result, neutral PEG derivatives of BODIPY with high quantum yields in aqueous media were obtained.[99] Kim and co-workers[100] synthesized a series of water-soluble PEG-substituted BODIPY derivatives, such as compound **54**. The bulky PEG groups were introduced at the *meso* position, resulting in an increase in water solubility and fairly high fluorescence quantum yields (up to 0.512) in water. The potential applicability of the synthesized dyes in fluorescence bioimaging was demonstrated in the MCF-7 human breast cancer cell line. The synthesized fluorophores were shown to penetrate the cell membrane and accumulate in the cytoplasm.[100]

The water solubility can be increased by the introduction of polysaccharides[101] or alkoxy groups into the BODIPY core instead of fluorine atoms (compounds **55** – **57**).[102, 103] Fluorescent BODIPY derivatives carrying from one to three glucose residues (Fig. 9, compound **58**) were synthesized by the Cu(I)-catalyzed azide-alkyne cyclo-

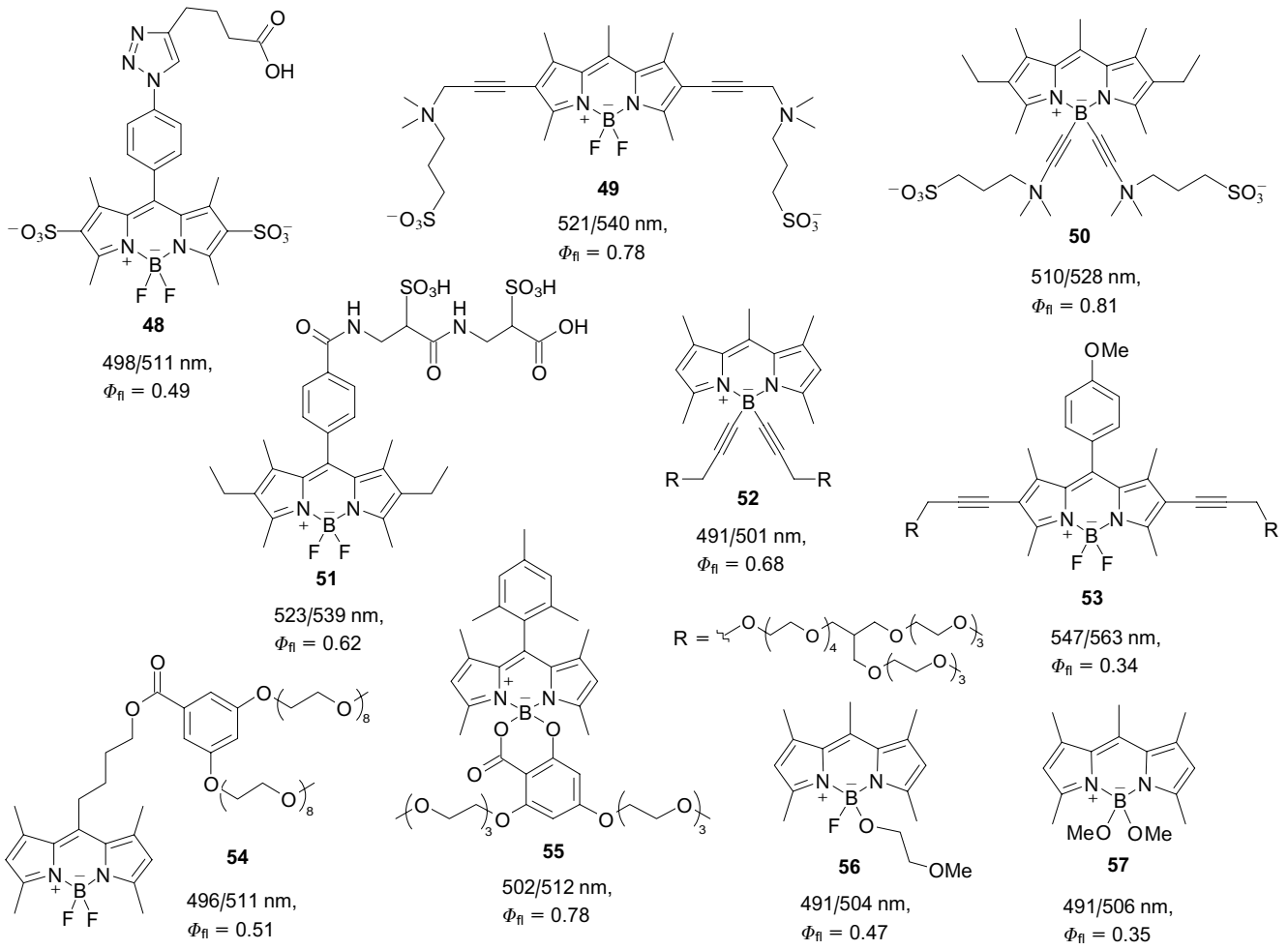


Figure 8. Water-soluble BODIPY derivatives. Absorption/emission maxima and quantum yields are given for aqueous solutions.

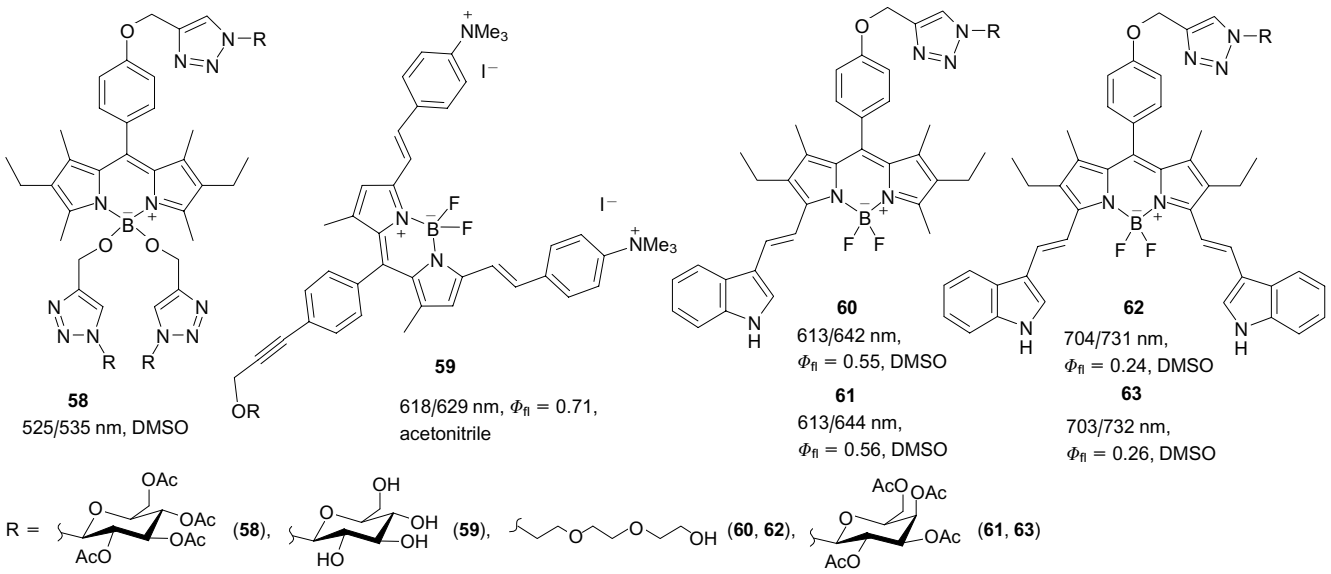


Figure 9. BODIPY derivatives with carbohydrate and PEG substituents.

addition.[101] Experiments with the human carcinoma HEp2 cell line showed that, apart from improved water solubility, all three derivatives have high intracellular permeability and low cytotoxicity, both in the dark and upon exposure to light, with half maximal inhibitory concentration (IC_{50}) exceeding 100 μM. The increased membrane permeability

is proposed to be caused by interactions with glycoprotein receptors on the cell surface. The degree of accumulation of these derivatives inside the cell was shown to depend on the amount of glucose residues, with the highest degree of accumulation for the trisubstituted BODIPY derivative (after 24 h of incubation). In another work, it was shown that internalization of BODIPY derivatives containing carbohydrate residues (compound **59**) by cells presumably occurs *via* clathrin-dependent endocytosis.[104] To improve water solubility, Kim and co-workers[105] introduced lactose substituents into iodine derivatives of BODIPY. The resulting compounds had significant intracellular permeability and, due to the presence of iodine atoms, can be used as photosensitizers in photodynamic therapy of cancer.

As noted above, the shift of the fluorescence spectra of BODIPY derivatives to the far-red and NIR regions can be achieved by extending the π-electron system of the fluorophore *via* the addition of aromatic substituents at the 3- and 5-positions. However, the extension of the aromatic system is usually associated with an increase in the hydrophobicity of these compounds. Vicente and co-workers[106] synthesized 3-mono, 5-mono- and diindolylethylenyl derivatives of BODIPY. Besides, related compounds with galactose and PEG substituents were synthesized by azide-alkyne cycloaddition in order to improve water solubility and increase membrane permeability. Compounds **60** – **63** have fluorescence emission maxima in the region of 642 – 732 nm and quantum yields Φ_{fl} = 0.24 – 0.56. *In vitro* experiments with the HEp2 cell line showed that all these derivatives do not exhibit cytotoxicity up to 100 μM concentrations. Compared to the original unsubstituted derivatives, compounds with galactose and PEG substituents are much more efficiently internalized by cells and accumulate in the endoplasmic reticulum (ER) (Fig. 10). It is worth noting that 3-monoindolylstyryl derivative **60** is 5 times more efficiently internalized by cells and has higher quantum yields compared to 3,5-diindolylstyryl derivative of BODIPY **62**.

The synthesis of water-soluble zwitterionic BODIPY compounds containing trimethylammonium and oxo or imino substituents at the 3 and 5-positions was reported by Sekhar *et al.*[107] (Fig. 11). These compounds have a significant Stokes shift (70 nm), high fluorescence quantum yields (0.68 and 0.95, respectively) and low cytotoxicity. It was also shown that derivatives **64** and **65** penetrate the cell membrane, accumulating in yeast (SCY62 and H1246) cells.[107] Some other BODIPY derivatives with electron-donating groups in the *meso* position and emitting light in the blue range also possess large Stokes shift (see compound **4** in Fig. 1). In another approach, the encapsulation of BODIPY derivatives into nanoparticles was used to overcome poor water solubility (see also Section 6).[108 – 111]

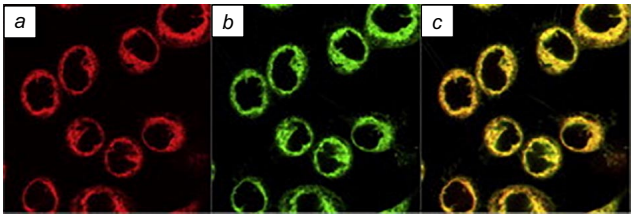


Figure 10. Subcellular distribution of fluorescence after HEp2 incubation with compound **63** (*a*), ER Tracker (green fluorescence) (*b*), ER Tracker and compound **63** (merged) (*c*).[106] Published with the permission from Elsevier.

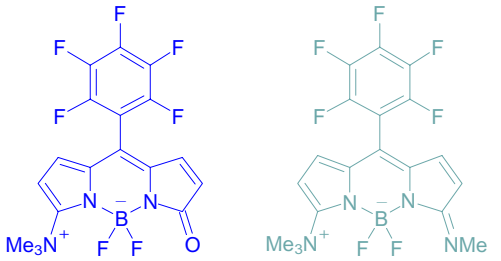


Figure 11. Water-soluble zwitterionic BODIPY derivatives with a large Stokes shift.[107]

2.4. Photostability

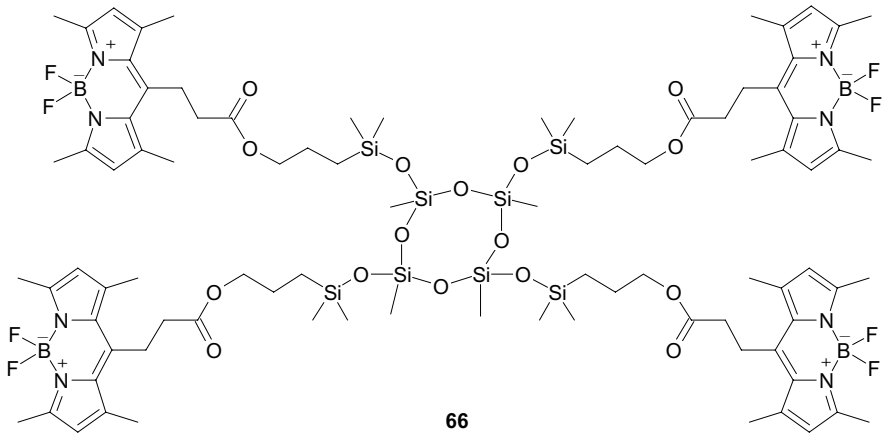
Nowadays, various techniques of super resolution fluorescence microscopy have found application in the study of biological processes. For example, fluorescence correlation spectroscopy (FCS) provides information on the movement speed of various intracellular molecules, their molecular weights and chemical reaction rates.[112] One of the key parameters in these methods is the photostability of the fluorophore. Fluorescence methods are based on multiple repeated photocycles of excitation and transition to the ground state. However, in its high-energy excited state, the fluorophore can degrade (particularly due to reactions with other compounds) and lose its fluorescent properties (photobleaching). Therefore, the maximum number of these cycles and, ultimately, the duration of imaging of intracellular processes depends on the photostability of the fluorophore. Photostability depends on many factors, such as the structure of the fluorophore, the composition of the medium, the light flux power, *etc.*[113]

Jang and co-workers[114] accomplished a comparative study of the photostability of various derivatives of fluorescein and BODIPY. They showed that, upon FCS, BODIPY derivatives generally have greater photostability as compared to fluorescein. The photobleaching was hypothesized to occur during the transition of the fluorophore to the S1 excited singlet state and it was attributed to one-electron oxidation with the participation of an oxygen molecule.[114]

Nagano and co-workers[25] reported that the photostability of BODIPY derivatives depends on the electron-withdrawing properties of the substituents. Seven 2,6-substituted BODIPY derivatives with different electron-withdrawing properties were synthesized. It was shown that the more electron-deficient BODIPY compounds produce smaller amounts of singlet oxygen, undergo reactions with $^1O_2$ to a lesser extent and, as a consequence, are less susceptible to photobleaching.

2.5. Brightness

Brightness is one of the most important parameters that defines the efficiency of fluorophores as molecular reporters. It is directly proportional to the product of the molar extinction coefficient and the fluorescence quantum yield ($\varepsilon \times \Phi_{fl}$). Brightness is of great importance in microscopy since the intensity of the light emitted by the dye should significantly exceed the background level of intrinsic cell fluorescence.



66

Structure 66

505/517 nm,
Φ_{fl} = 0.64, toluene;
498/506 nm,
Φ_{fl} = 0.08, acetonitrile

BODIPY derivatives are usually characterized by high molar extinction coefficients (up to 2.9×10^5 L mol^{-1} cm^{-1}), high quantum yields (up to 1) and, correspondingly, high values of brightness. The brightness of the fluorophore, including BODIPY derivatives, is greatly influenced by substituents that can participate in photoinduced electron transfer (PET) and intramolecular charge transfer (ICT) processes, which reduce the fluorescence quantum yield. Furthermore, brightness of some BODIPY derivatives also largely depends on the polarity of the solvent, ensuring the solvatochromic properties of the fluorophore.[12, 62, 115] In polar solvents, BODIPY derivatives tend to aggregate, with fluorescence quenching caused by aggregation (aggregation-caused quenching, ACQ).

A possible way to obtain reporters with increased brightness is the synthesis of molecules containing several fluorophores. To this end, compound **66** was obtained, in which four tetramethyl-substituted BODIPY residues were attached to the cyclotetrasiloxane matrix.[116] In low-polarity solvents, tetra-BODIPY derivative **66** exhibited brightness almost three times higher compared to mono-BODIPY. In contrast, in polar solvents, the brightness of the tetra-BODIPY derivative decreased, which is likely due to ACQ as a result of intramolecular interactions of nonpolar BODIPY fluorophores.

2.6. Cytotoxicity and biocompatibility

The possibility of using BODIPY derivatives in *in vitro* and *in vivo* experiments is largely determined by the cytotoxicity of these compounds. Cytotoxicity can manifest itself in the form of cell necrosis due to disruption of the plasma membrane and subsequent lysis. Also, a whole group of compounds (cytostatics) can activate apopotosis, the process of programmed cell death. In addition, some compounds reduce the growth and division rates of cells, affecting their viability. It should also be borne in mind that some fluorophores, when exposed to exciting light, generate reactive oxygen species,[117] which are toxic to the cell (phototoxicity).

A number of methods are used to assess the cell viability and determine the toxicity of various compounds, including the MTT colorimetric assay, which evaluates the metabolic activity of a cell,[118] flow cytometry and the bioluminescence method for determining intracellular ATP. Also, there are a number of commercially available test systems for the evaluation of cell viability. The cytotoxicity can be quantified by determining the molar concentration of a substance at which the number of viable cells is reduced by 50% (IC_{50}, the half-maximal inhibitory concentration).

In 2014, a new class of fluorophores based on monoalkoxy-substituted boron derivatives of BODIPY was synthesized and the possibility of using these compounds in bioimaging in comparison with the parent methyl-substituted BODIPY derivatives was evaluated.[102] For the human breast cancer cell line MCF-7, it was shown that the 48-h incubation of cells in the presence of 10 μM monoalkoxy-substituted and 1,3,5,7,8-methyl-substituted BODIPY derivatives did not lead to a change in the number of viable cells.

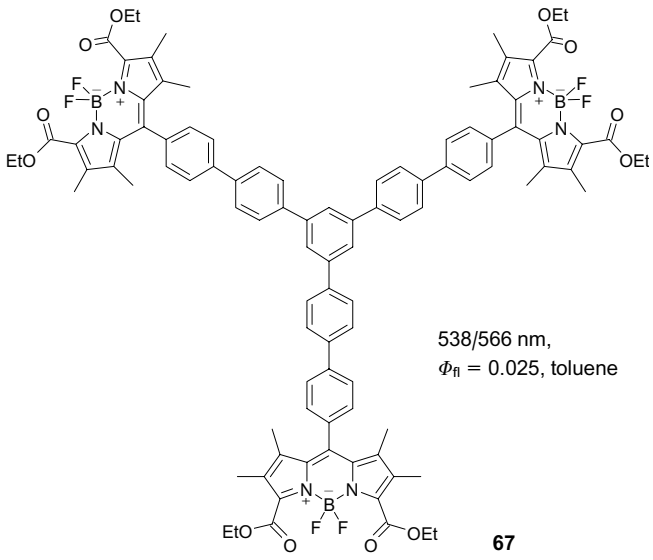
Liang, Mack, Chen and co-workers[119] investigated the dependence of cytotoxicity of various derivatives on the nature, the number of substituents and their position in the BODIPY structure. A number of 3,5-distyryl and *meso*-morpholine-(isoquinoline) derivatives of BODIPY were synthesized. Using the HepG-2 cell line of human hepatocellular carcinoma, it was shown that *meso*-morpholine-substituted BODIPYs have lower IC_{50} values compared to various styrene- and *meso*-isoquinoline-substituted BODIPYs. In general, the IC_{50} value of all compounds exceeded the 100 μM level.

In order to determine the intracellular pH, the *meso*-calix [4] arene derivative of BODIPY[120] was synthesized (see Section 5.1.1). The resulting indicator was used to monitor pH changes within a living cell at the initial stages of apoptosis. The cytotoxicity of this compound was evaluated in the HeLa cervical cancer cell line using the MTT assay. The IC_{50} value of 162 μM was determined for this derivative.

Vicente and co-workers[86] investigated the properties of mono- and dibenzo-fused BODIPY derivatives. Using the human carcinoma cell line HEp2, IC_{50} values were determined for all derivatives, both in the dark and under constant illumination with a halogen lamp. All BODIPY derivatives had extremely low cytotoxicity with half-maximal inhibitory concentrations IC_{50} of more than 200 μM in the dark and over 100 μM upon illumination with light (1.5 J cm^{-2}).

Furthermore, using a symmetric star-shaped molecule **67** with a polyphenylene core and three BODIPY substituents, the toxicity and biocompatibility were studied at the whole organism level.[121] Embryos and mature zebrafish were used as the model. More specifically, mature fish were exposed to this compound at various concentrations for 24, 48, 72 and 96 h. At concentrations of compound **67**

Structure 67



67

above 100 mg L^{-1}, no lethal outcomes were observed in a group of eight fish.

3. Targeted delivery of BODIPY derivatives to various intracellular compartments

Several BODIPY variants with targeted delivery to lysosomes and the endoplasmic reticulum are commercially available under the trade names LysoTracker and ER-Tracker (Fig. 12, compounds **68** – **71**).[122] Nevertheless, the active development of new BODIPY derivatives with targeted delivery to various intracellular compartments is now underway. As already noted, most BODIPY derivatives have a neutral charge and significant lipophilicity. As a result, these compounds penetrate the cell membrane, accumulating in the membranes of subcellular structures. Various vector groups are introduced into the BODIPY molecule to achieve targeted delivery to a specific cell compartment.

Weinstein and co-workers[123] synthesized a number of BODIPY derivatives with targeted delivery to lysosomes, mitochondria and the endoplasmic reticulum (Fig. 13, compounds **72** – **74**). These derivatives contained biologically active substituents in the *meso* position, which were activated and released into cell compartments *via* the photolysis under visible light (see also Sections 3.3 and 3.4).

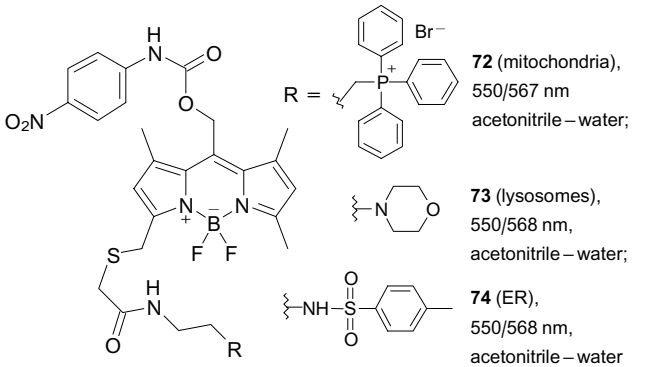


Figure 13. Examples of vector groups for targeted delivery of BODIPY derivatives to the endoplasmic reticulum, lysosomes and mitochondria. Here and in Fig. 14, the target cellular localization of the dye is indicated in parentheses.[123]

3.1. Plasma membrane

The plasma membrane plays a crucial role as a barrier separating the cytoplasm from the extracellular medium. Besides, the plasma membrane is involved in various active processes in a living cell, such as passive and active directed transmembrane transport of substances (endocytosis and exocytosis, respectively). It participates in intercellular interactions and performs a signaling function, interacting with various substances and stimuli that have a great impact on the cell growth and proliferation. Plasma membrane imaging with fluorescence microscopy provides information on the cell status, the cell division stage and the cell death *via* apoptosis or necrosis.[124] Since many synthetic fluorophores have significant lipophilicity, they are most often

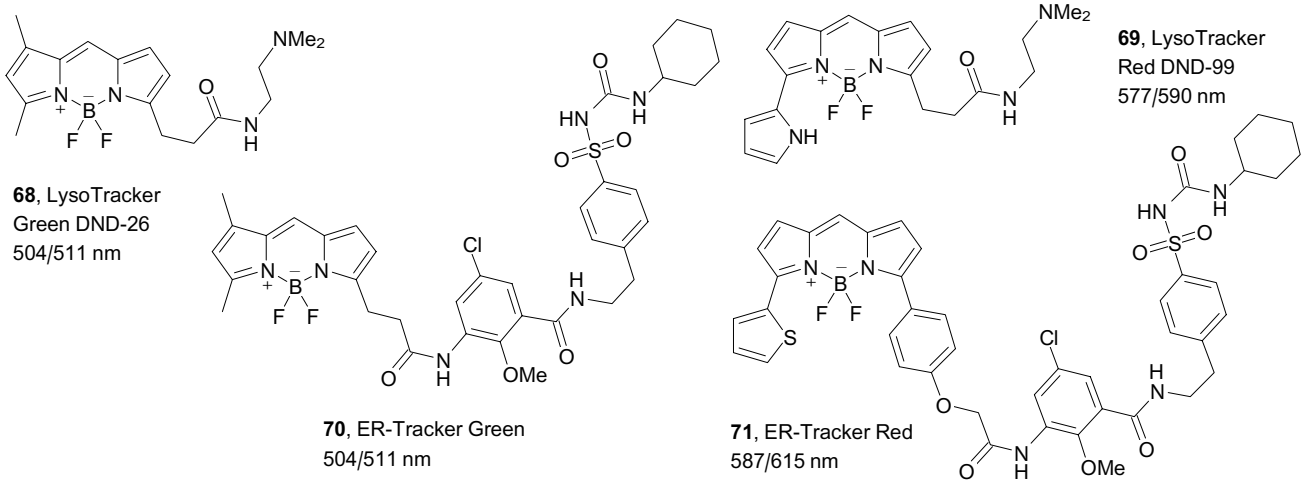


Figure 12. Commercially available BODIPY variants with targeted delivery to lysosomes and the endoplasmic reticulum.[122]

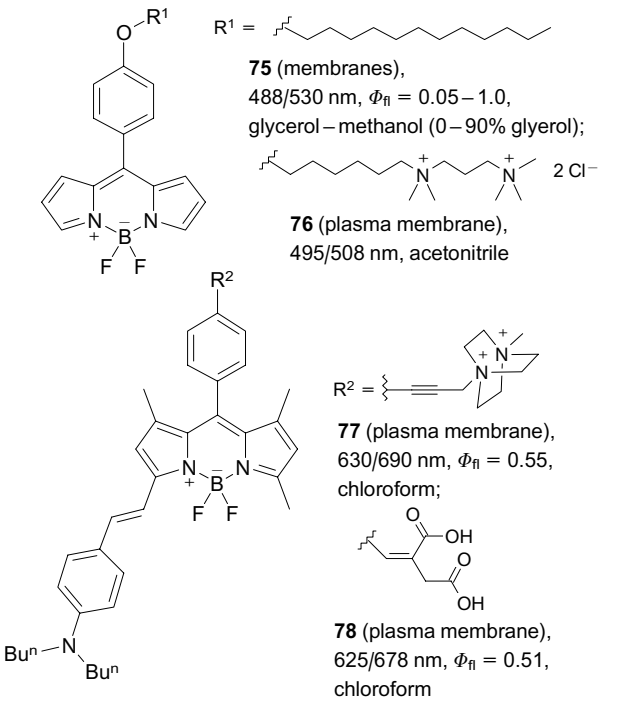


Figure 14. BODIPY derivatives for fluorescent labelling of the plasma membrane.

used for labelling cell membranes. However, labelling the plasma membrane of a living cell is procedure challenge due to the precipitation of BODIPY dye in aqueous solutions and penetration of these fluorophores into the cell followed by the dye accumulation in the membranes of intracellular organelles (*e.g.*, structure **75** in Fig. 14).[86, 125] (It is worth noting that compound **75** is used for labelling membrane structures of the cell.)

To overcome this problem, Kuimova and co-workers[126] synthesized BODIPY derivative **76** (Fig. 14), in which two ammonium groups are incorporated into the hydrocarbon chain. A double positive charge of nitrogen atoms prevents the reporter from penetrating the plasma membrane. Less than a 30-min incubation of human ovarian adenocarcinoma SK-OV-3 cells with compound **76** resulted in selective fluorescent staining of the plasma membrane. Noteworthy, the fluorescence quantum yield of this compound depends on the viscosity of the medium.

Selfridge and co-workers[94] synthesized two water-soluble BODIPY derivatives **77** and **78**, which acquire near-infrared fluorescence after binding to the membrane. The introduction of dicationic or dianionic substituents into the reporter molecule prevents dye translocation through the membrane and ensures selective incorporation into the plasma membrane. Labelling with a dicationic form was particularly efficient taking into account the significant photostability of the dye, which allowed a long-term light exposure without noticeable bleaching. The synthesized compounds exhibited solvatochromic properties and were nonemissive in water and other polar solvents but displayed high-fluorescence intensity upon insertion into the membrane.

To fine tune the amphiphilic properties, Klymchenko, Collot and co-workers[88] obtained three types of BODIPY derivatives functionalized by both zwitterionic and aliphatic groups (Fig. 15, compounds **79** – **81**). Monosubstituted compound **79** possessed strong fluorescence and high solubility in water, while exhibiting low affinity for membrane structures. BODIPY derivative **81** with three such substituents formed aggregates in an aqueous medium and precipitated just before binding to the plasma membrane. In contrast, derivative **80** with two substituents formed virtually non-fluorescent water-soluble aggregates. However, when bound to the plasma membrane, these aggregates decomposed to a molecular form with bright fluorescence (Φ_{fl} = 0.92). Such fluorogenic properties made it possible to visualize the plasma membrane using one- and two-photon excitation at low reporter concentrations (20 nM) with high signal-to-background fluorescence ratio.

3.2. Cytoplasm

Apparently, labelling of cellular objects localized in the cytoplasm is possible only with the water-soluble BODIPY derivatives. On the other hand, although the introduction of substituents with ionizable groups or bulky PEG groups into the BODIPY structure increases water solubility, it may also reduce their ability to penetrate cell membranes. One possible way to address this issue is through targeted labelling of proteins that are specific for cytoplasm (see the Section 4).

Another possible way is to fine tune the physicochemical properties of the fluorescent reporter. Kim and co-work-

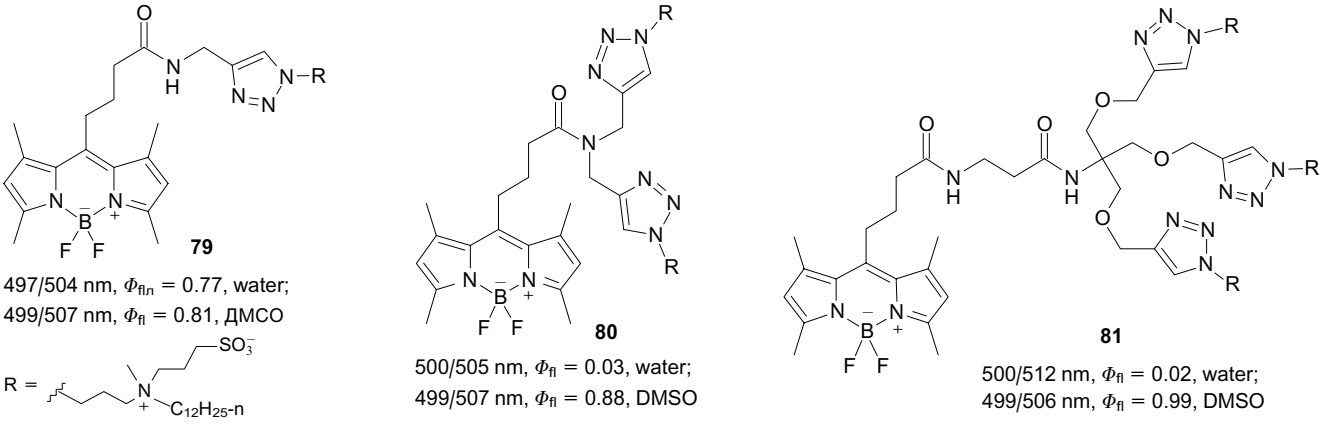
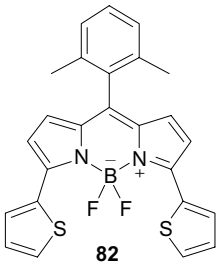


Figure 15. Zwitterionic and aliphatic BODIPY derivatives for plasma membrane labelling.[88]

Structure 82



82

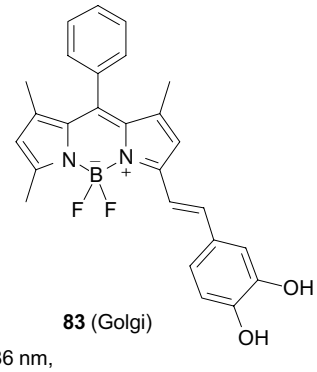
621/640 nm,
Φ_{fl} = 0.85,
dichloromethane

ers [100] synthesized a series of PEG-substituted BODIPY derivatives (see Fig. 8, compound **54**) and examined their properties. *meso*-Disubstituted PEG derivatives of BODIPY were prepareded in order to reduce aggregation tendency, The latter derivatives exhibited good solubility and high fluorescence quantum yields in aqueous solutions ($\Phi_{fl} \sim 0.5$). It was shown that the synthesized dyes penetrate the cell membrane and are concentrated in the cytoplasm of MCF-7 (Ref. 100) cells, which allows the use of these compounds as a cytoplasmic marker.

Yamada and co-workers [45] synthesized a number of BODIPY derivatives with absorption in the red and NIR regions (600 – 850 nm). These compounds contain a thiophene substituent and its derivatives at the 3- and 5-positions of BODIPY. Using fluorescence microscopy, it was shown that 3,5-dithienyl-substituted derivative BODIPY **82** penetrates the plasma membrane and is localized in the cytoplasmic space of eukaryotic cells.

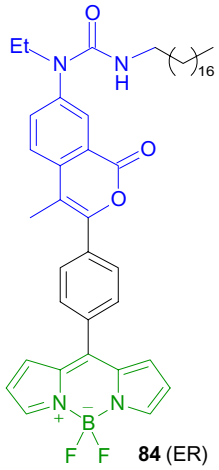
3.3. Golgi apparatus and endoplasmic reticulum

The Golgi apparatus is a membrane structure of eukaryotic cells, which generally performs a secretory function by transporting proteins synthesized in the endoplasmic reticulum (ER). In the Golgi apparatus, post-translational modifications of the newly synthesized proteins take place, which are catalyzed by various Golgi-associated enzymes. These modifications can install signal sequences into the synthesized proteins that target them to other cell compartments, for example, to lysosomes. The Golgi apparatus is connected to the ER. The latter represents a membrane structure composed of tubules and cisternae, which extends from the nuclear membrane into the cytoplasm.[127] Its main functions include the translation and transport of newly synthesized proteins to the Golgi apparatus and the synthesis and transport of various lipids and phospholipids. Currently, there are several techniques for targeted delivery of fluorophores into these cell structures. One of these is the inclusion of vector substituents into the fluorophore structure, which bind to proteins specifically expressed in Golgi/ER.[128, 129]



83 (Golgi)

550/586 nm,
$\Phi_{фл}$ = 0.0034, PBS buffer – acetonitrile,
$\Phi_{фл}$ = 0.116, in presence of HClO



84 (ER)

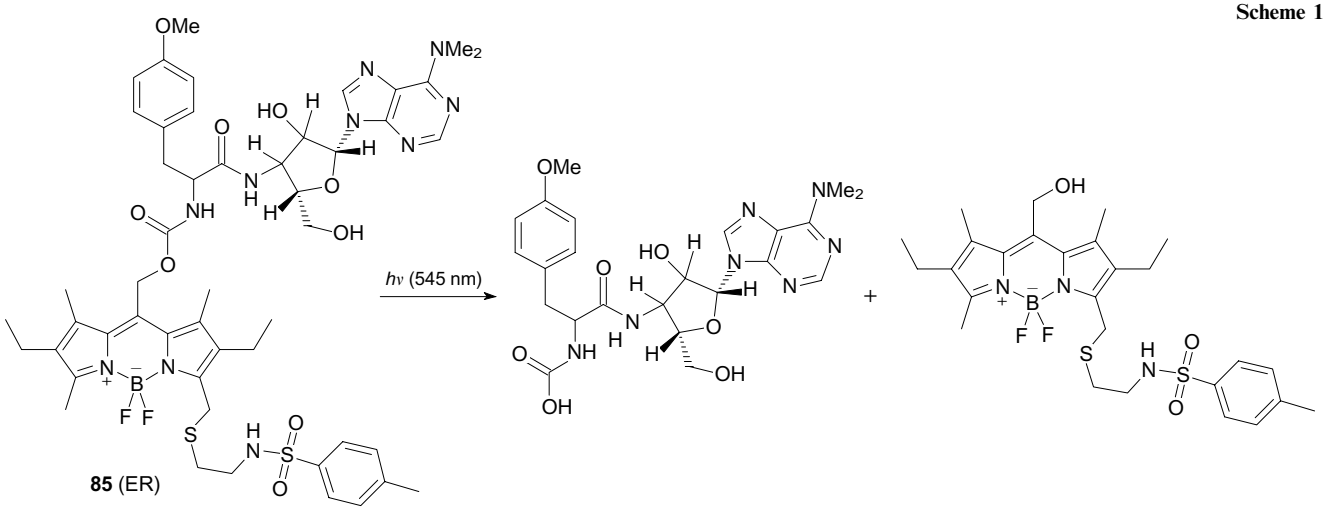
350, 500/439, 518 nm

Figure 16. BODIPY derivatives with localization in the Golgi and the endoplasmic reticulum.

The highly reactive hypochlorite anion ClO^- is formed in cell organelles by myeloperoxidase-catalyzed oxidation of Cl^- (see also Section 5.4.5). Das and co-workers [130] synthesized BODIPY derivative **83** (Fig. 16), which was characterized by weak emission at 586 nm (Φ_{fl} = 0.0034) upon excitation at 550 nm wavelength. However, a significant increase in the fluorescence emission was observed in the presence of HClO (Φ_{fl} = 0.116). Experiments on colocalization with the well-known commercial dyes showed that **83** is predominantly localized in the Golgi apparatus and lysosomes. Thus, compound **83** can be used as a specific HClO sensor in these cell compartments (see also Section 5.4.6).

Kim and co-workers [131] synthesized BODIPY conjugate **84** with the coumarin moiety carrying a long hydrocarbon chain (C_{18}) as a vector targeting this conjugate to

Scheme 1



85 (ER)

549/571 nm, acetonitrile – water

ER[132, 133] (Fig. 16). The resulting compound is selectively incorporated into the ER membrane and may be used as a ratiometric sensor for lipid membrane viscosity (see also Section 5.5), the values of which are determined by the ratio of the fluorescence intensities of two fluorophores. Compound **84** was used to study changes in the fluidity of the ER membrane in HeLa cells under the stress conditions.[131]

It was shown that sulfonamide substituents may serve as a vector targeting fluorophores to the endoplasmic reticulum.[134 – 136] Along with model compounds **72** – **74** (see Fig. 13), Weinstein and co-workers[123] used tolylsulfonamide-substituted BODIPY **85** for targeted delivery of fluorophore to ER. It was previously shown that the ester bond of various substituents with a hydroxymethyl group in the *meso* position of BODIPY is photolabile and is cleaved under green light illumination.[137 – 139] Such BODIPY compounds can be used as light-activated photocaging groups of biologically active compounds. In this work, using the sulfonamide derivative of BODIPY, it was shown that the protein biosynthesis inhibitor puromycin can be specifically targeted to and released into ER under visible light exposure (Scheme 1).[123]

3.4. Mitochondria

On the whole, mitochondria have a net negative charge; therefore, positively charged dyes are used for targeted delivery of fluorescent reporters to these organelles.[140] For example, the commercially available MitoTracker dye includes the cationic dye rhodamine, as a targeting to mitochondria vector.[141] As already mentioned, the core structure of BODIPY has a neutral charge. Therefore, for directed staining of mitochondria cationic substituents should be introduced into the BODIPY structure.

For targeted delivery to mitochondria, Belfield and co-workers[142] introduced two triphenylphosphonium groups into the BODIPY structure, and two PEG groups were additionally added to increase water solubility (Fig. 17, compound **86**). Besides, PEG groups restrain the rotational freedom of the phenyl ring, thereby reducing nonradiative relaxation and increasing the fluorescence quantum yield (Φ_{fl} = 0.59 in water). As a mitochondria-specific fluorescent reporter, compound **86** had a low pH sensitivity, high photostability and low cytotoxicity.

In another study,[143] triphenylphosphonium or triethylammonium groups were attached to the BODIPY core structure *via* a flexible hydrocarbon spacer (Fig. 17, compounds **87** and **88**). These derivatives selectively stained mitochondria and had high brightness, good photostability and low cytotoxicity. In addition, compared to commonly used mitochondrial dyes, derivative **88** has a smaller size and better biocompatibility.

3.5. Lysosomes and endosomes

As already mentioned, BODIPY has a net neutral charge and significant lipophilicity, which facilitates the penetration of these compounds through the cell membrane and the accumulation in the membranes of subcellular structures. While the extracellular and cytoplasmic pH values are close to neutral (pH = 7.2), the pH in endosomes and lysosomes may be significantly reduced (pH = 4.5 – 6.3). Since substituted morpholines have pK_a = 5 – 6 and can be protonated only in lysosomes, they are usually selected as vector substituents targeting the fluorescent reporter to lysosomes.[144] The positive charge of morpholine derivatives of

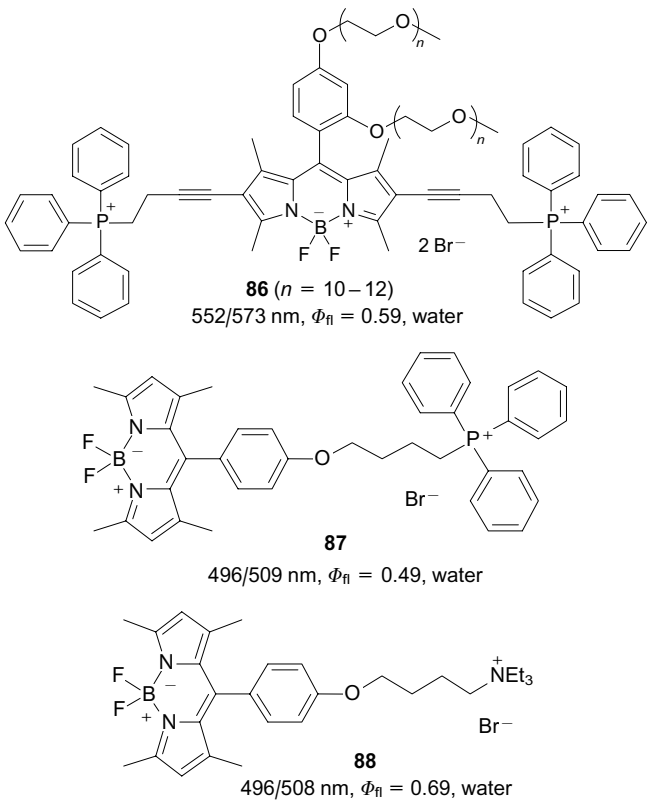


Figure 17. BODIPY derivatives for targeted delivery to mitochondria.[142, 143]

BODIPY within endosomes and lysosomes prevents the reverse release of the fluorophore through the membrane to the cytoplasm and favours the accumulation of fluorescent reporters in these organelles.

For targeted labelling of lysosomes, Zeng and co-workers[145] synthesized a number of photostable BODIPY derivatives, such as Lyso-Green (**89**), Lyso-Red (**90**) and Lyso-NIR (**91**) (Fig. 18) with fluorescence emission in the green, red and NIR regions. Experiments with live cells showed that these fluorescent dyes have excellent biocompatibility, low cytotoxicity and high resistance to photobleaching. These features are beneficial for the use of fluorescent reporters in the experiments on the lysosomal activities during diverse biological processes under long-term excitation.

Lu and co-workers[146] reported a series of lysosome-targeting derivatives **92** – **96** containing morpholine moieties in the *meso*-, 3-, and 3,5-positions of BODIPY, which showed fluorescence emission in the green, red and NIR regions. Electron-withdrawing *p*-nitrophenyl groups were introduced at the *meso* position of BODIPY (compounds **94**, **96**) in order to monitor the lysosomal functioning under hypoxia. Under normal conditions, in the presence of oxygen, reporter fluorescence is quenched due to an oxidative PET (for more details, see Section 5) from the BODIPY core towards the nitrophenyl substituent. After the reduction of the nitro group under hypoxic conditions, the fluorescence of the reporter is recovered. Compounds **94** and **96** were successfully used for imaging lysosomes in hypoxic HepG2 cancer cells by confocal microscopy. Thus, the synthesized hypoxic reporters may be useful in the future for cancer diagnosis and treatment.

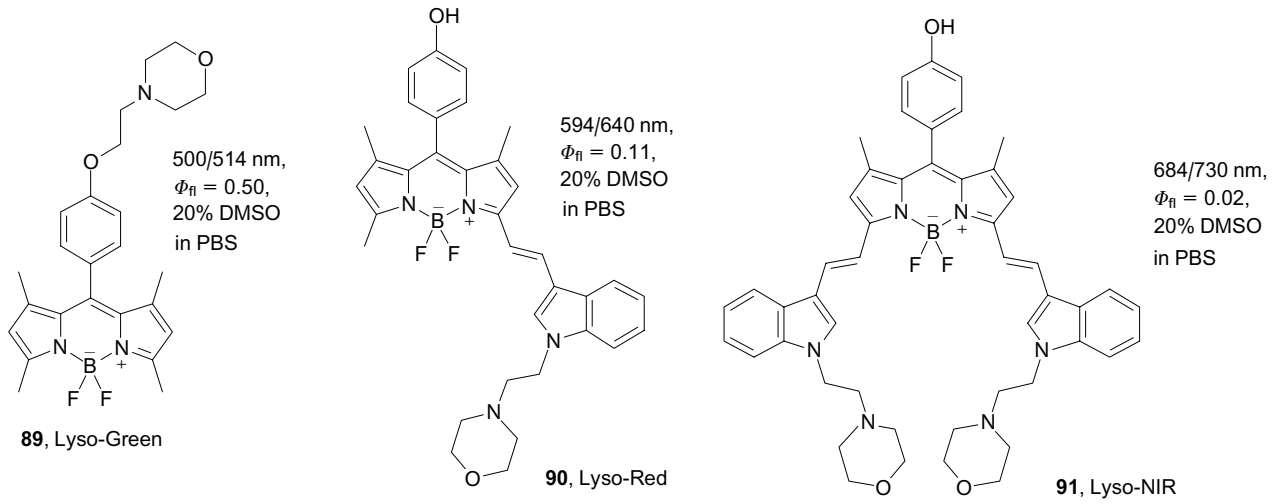
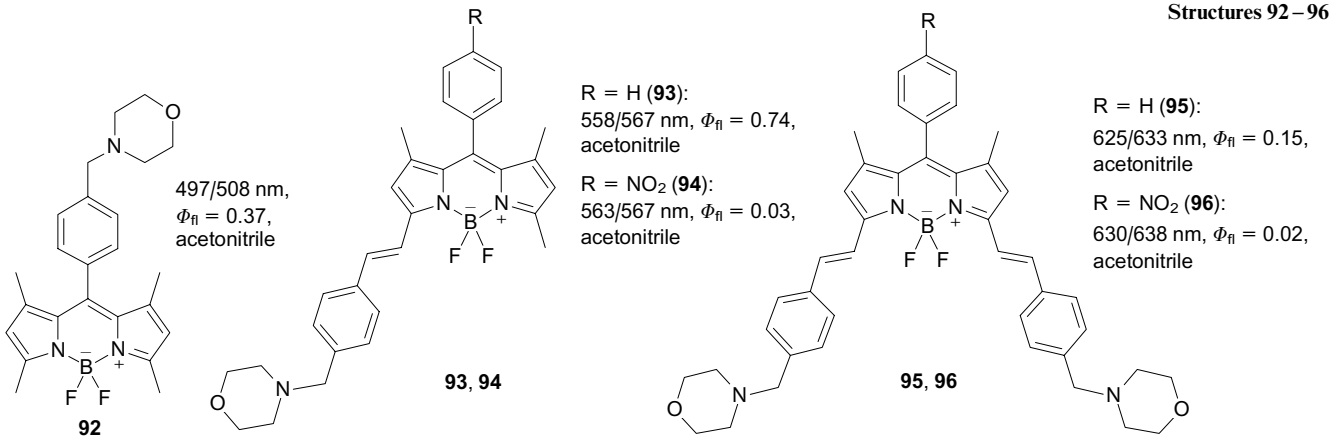


Figure 18. BODIPY-based fluorescent reporters with lysosomal localization.[145]

Structures 92 – 96



4. Targeted labelling of individual cellular proteins with BODIPY derivatives

Until the 1980s, fluorescent labelling of biomolecules was usually applied to fixed biological specimens. To this end, low-molecular-weight synthetic fluorophores were conjugated with antibodies specific for a protein of interest (POI).[147] To deliver antibodies to intracellular proteins, the cells were fixed and subjected to various manipulations in order to increase the cell membrane permeability.[148, 149] These manipulations usually led to the impairment of important physiological functions of the cell, which hampered the imaging of the activities of a normally functioning living cell. With the discovery of GFP-like† fluorescent proteins (FPs), the problem of noninvasive targeting of the fluorescent label to POI was resolved. Using genetic engineering methods , it became possible to intracellularly tag POI with FP, while ensuring the cell integrity. This generation of genetically encoded fluorophores made it possible to image the expression of POI, its movements, interactions with other cellular objects and its intracellular activity. However, as already noted, the use of FPs has its own limitations. In particular, the large size (about 25 kDa) and the formation of oligomeric FP structures can ultimately impair the physiological function of POI.

From this point of view, low-molecular-weight fluorophores, such as BODIPY, are advantageous due to their small size, a fairly easy core structure derivatization and the availability of derivatives with NIR fluorescence. In light of the foregoing, a key problem in the fluorescence imaging of biomolecules using synthetic fluorophores is the targeting of fluorophores to POI.[150] One way to resolve this problem is to use highly selective reactions, *e.g.*, so-called bioorthogonal chemistry [151, 152] and click chemistry.[153] According to this methodology, a small azido group is introduced into the POI structure by means of metabolic activities of the cell [154 – 156] or the POI enzymatic activity.[157, 158] The azido group is stable in an aqueous medium and has low reactivity towards functional groups of biological molecules. Moreover, the introduction of a small azido group leads only to minor structural perturbations of the biomolecule. On the other hand, these groups are highly reactive with alkynes and can participate in a highly selective azide-alkyne cycloaddition click reaction [159] (Fig. 19).

To investigate the structural basis of the gating mechanisms of voltage-dependent sodium channels, a genetically encoded lanthanide-binding site was introduced into the channel structure, which, after the addition of terbium ions (Tb^{3+}), served as a donor module in luminescence reso-

† GFP is green fluorescent protein from the jellyfish *Aequorea Victoria*.

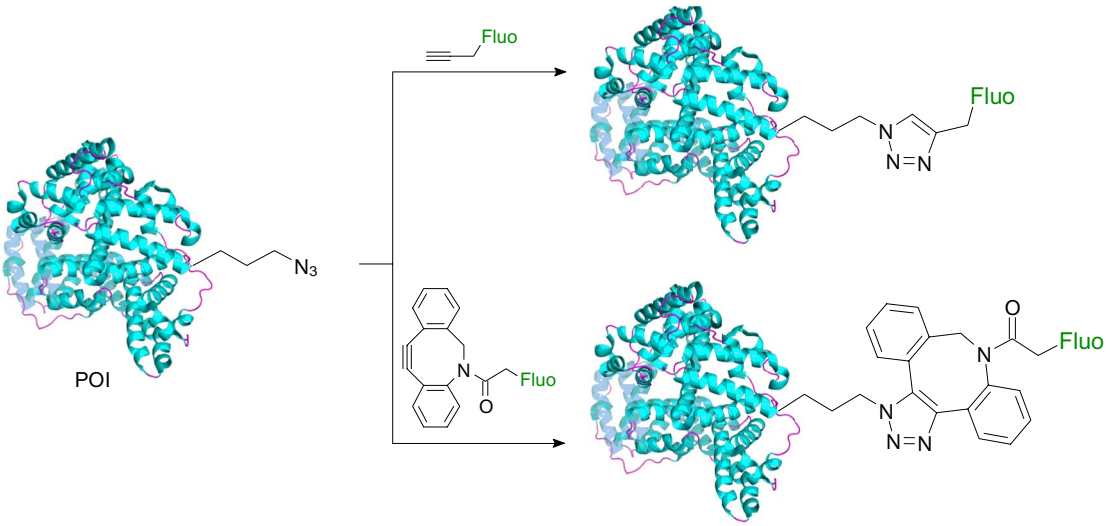


Figure 19. Attachment of a fluorescent dye (Fluo) to the target cellular protein (protein of interest, POI) by the azide-alkyne cycloaddition.

nance energy transfer (LRET).[160] Three different azide-modified peptide toxins conjugated to BODIPY-alkyne derivatives *via* a click reaction were used as an acceptor module of the construct. Changes in the resonance energy transfer between the donor and the acceptor provided a structural insight into the voltage-driven structural dynamics of the mammalian gating mechanism.

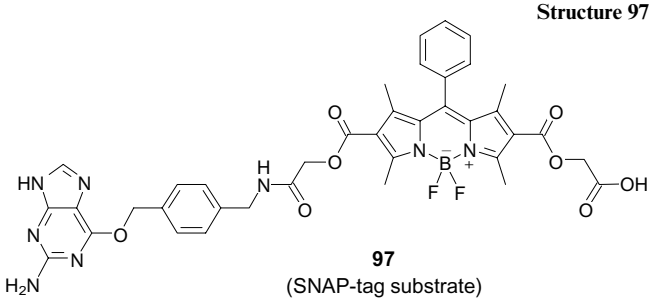
Another method for the targeted delivery to POI is based on enzymatic reactions.[161] This approach includes the so-called SNAP-tag,[162–164] CLIP-tag,[165] HaloTag[166–168] and TMP-tag[169–171] technologies (Fig. 20). The SNAP-tag technology uses O^6-alkyl guanine transferase (AGT), which is encoded in the same reading frame with POI, and thus covalently connecting AGT and POI. The enzyme AGT has a molecular weight of 20 kDa and transfers alkyl groups from the O^6 position of alkylated guanine to its own cysteine residue. The incubation of cells expressing the AGT–POI construct with an O^6-benzylguanine substrate carring a fluorophore in the *para* position of the benzyl group leads to the selective fluorescent labelling of AGT–POI at the active site cysteine of AGT (see Fig. 20).[162] The CLIP-tag method is similar to the SNAP-tag one, but it uses the mutant form of AGT, for which O^2-benzylcytosine analogues are used as fluorescent substrates (see Fig. 20).[165] It should be noted that since the SNAP-tag and CLIP-tag have different substrate specificity, these methods can be used to simultaneously visualize several POIs using different fluorophores.

The HaloTag technology uses a genetically engineered version of the haloalkane dehalogenase enzyme, which specifically reacts with halogen-substituted alkanes covalently bound to a fluorophore (see Fig. 20).[166] This reaction is also highly specific and allows the attachment of a fluorescent tag to proteins both *in vitro* and *in vivo*. Finally, the TMP-tag method uses the mutant of dihydrofolate reductase (eDGFR) from *Escherichia coli* (molecular weight ~18 kDa) as an enzyme fused to POI. As a result of the enzymatic reaction, fluorescently labelled 2,4-diamino-5-(3,4,5-trimethoxybenzyl)pyrimidine binds to the eDGFR-POI construct that is expressed in living cells (Fig. 20).[170]

For quantitative evaluations and in experiments with the prolonged light exposure, such as in protein dynamics studies, it is necessary to use photobleaching-resistant fluorophores. Nagano and co-workers[25] showed that more electron-deficient BODIPY compounds are less susceptible to photobleaching (see also Section 2.4). Compound **97**, after appropriate derivatization for its incorporation into the SNAP tag, was used to study the dynamics of the epidermal growth factor receptor (EGFR) in the green monkey fibroblast COS-7 cell line transformed with the SV40 virus. After binding of the fluorophore to EGFR–SNAP, the cells were washed from the unbound label. Repeated excitation by light in a confocal microscope showed that EGFR-SNAP labelled with compound **97** had much greater photostability compared to the standard SNAP-tag substrate based on fluorescein.

Urano and co-workers[172] also used the SNAP-tag technology to visualize the dynamics of EGFR in HeLa cells. However, this technology did not require the washing of the photoactivatable marker in order to remove the unbound fluorophore (Fig. 21). The selective labelling of EGFR-SNAP was performed using an O^6-benzylguanine substrate in which *meso*-phenol-substituted BODIPY was attached to the benzyl group (compound **98**, Scheme 2) and a 2,6-dinitrobenzyl (DNB) substituent was attached to the phenolic group *via* an ether bond. Since the DNB substituent has electron-withdrawing properties, the photoinduced electron transfer (PET) from the BODIPY core to the DNB group (for more detail about PET see Section 5) takes place, which competes with the fluorescence emission process and leads to fluorescence quenching ($\Phi_{fl} = 0.001$, pH 7.4). When exposed to UV light, the ether bond with the DNB substituent breaks down (uncaging, see Scheme 2) leading to fluorophore photoactivation, with 600-fold increase in

Structure 97



97
(SNAP-tag substrate)

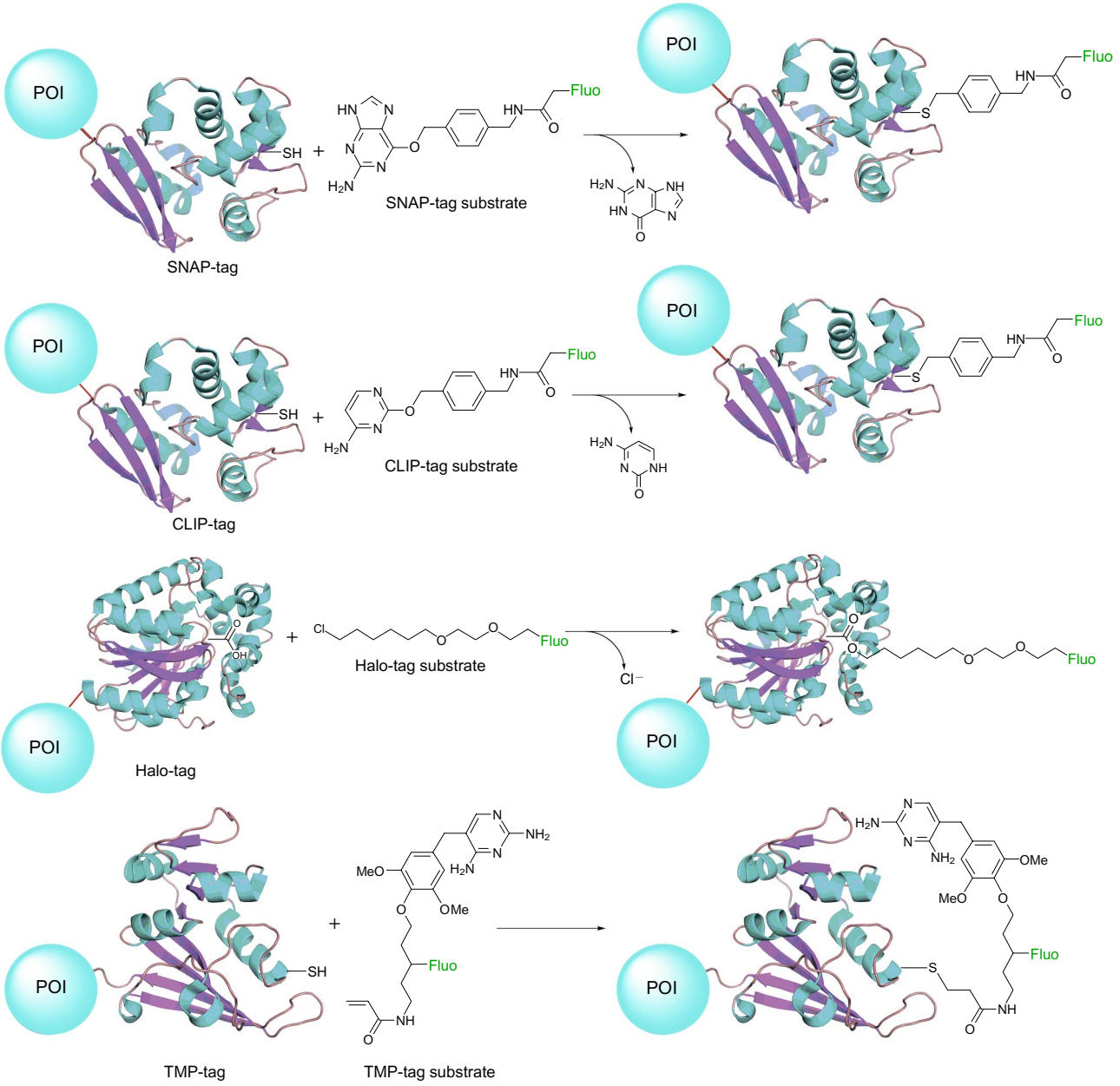


Figure 20. Attachment of a fluorescent dye to POI *via* enzymatic addition reactions to the protein domains of SNAP-tag, CLIP-tag, Halo-tag and TMP-tag.

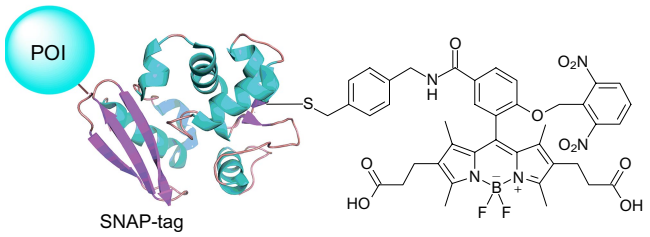
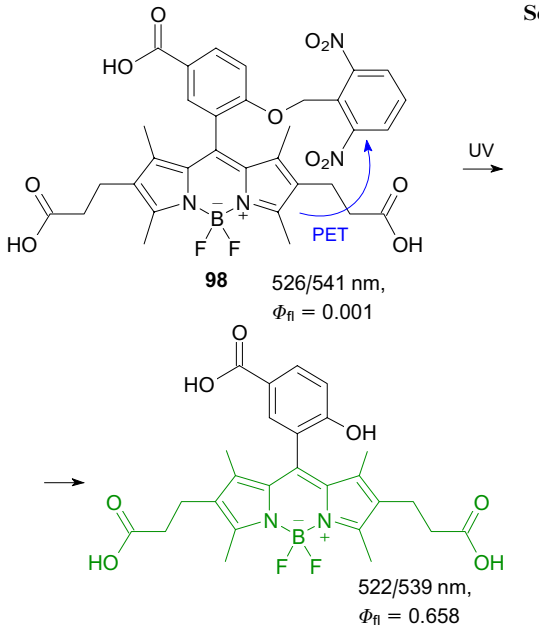


Figure 21. Photoactivatable BODIPY derivative bound to the hybrid SNAP-tag-POI protein.[172]

fluorescence intensity (Φ_{fl} = 0.658). The designed fluorogenic dye was used *in vitro* for spatiotemporal imaging of the EGFR-SNAP fusion in living cells and *in vivo* to visualize the dynamics of SNAP-tagged histone 2A in live zebrafish embryos.

A promising method for the POI targeting with synthetic fluorophores is based on the incorporation of a small amino acid sequence into POI *via* genetic manipulations. This sequence must have a sufficiently high affinity for the selected fluorescent reporter. For this purpose, cysteine-containing peptides are often used, since cysteine is less common than other amino acids in proteins. Due to the Pro-Gly insert, the sequence Cys-Cys-Pro-Gly-Cys-Cys forms a hairpin-like structure. Four cysteines form a cluster having a high affinity for organic arsenic compounds. In particular, the disubstituted arsenic derivative of fluorescein FlAsH forms a complex with this tetracysteine sequence with dissociation constants in the picomolar range.[173] In a similar approach, a small peptide Arg-Cys-X-X-Arg-Cys

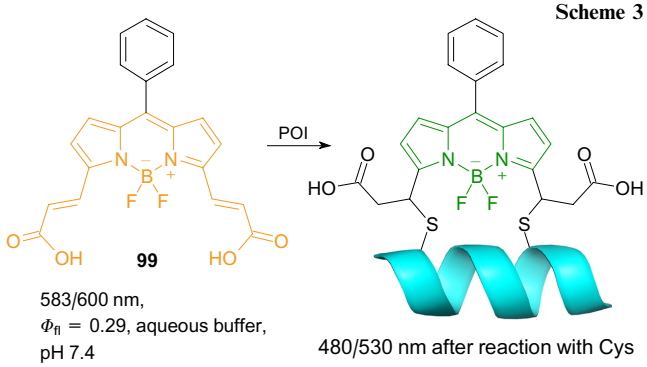
Scheme 2



98

was used for the labelling of intracellular proteins.[174] It was shown that this peptide covalently binds to BODIPY derivative **99** (Scheme 3) changing the fluorescence colour from orange to green due to a decrease in the π-electron extension upon the binding of cysteines to the acrylate double bonds (Fig. 22).

Scheme 3



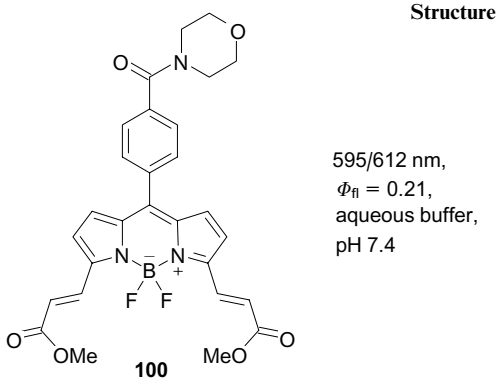
99



Figure 22. Fluorescence colour change of compound **99** in the absence (left) and in the presence (right) of the model peptide ···–Arg-Cys-Arg-Glu-Arg-Cys–··· upon excitation with UV light (365 nm).[174] Published with the permission from Royal Society of Chemistry.

Several derivatives with various substituents in the *meso* position of BODIPY were synthesized to increase cell permeability and decrease intracellular background fluorescence. It was shown that compound **100**[174] had the optimal properties and was further used for histone H2B labelling after the inclusion of the peptide with two cysteines into the N-terminal sequence of the histone and its expression in human embryonic kidney 293 cells (HEK293).

Structure 100



100

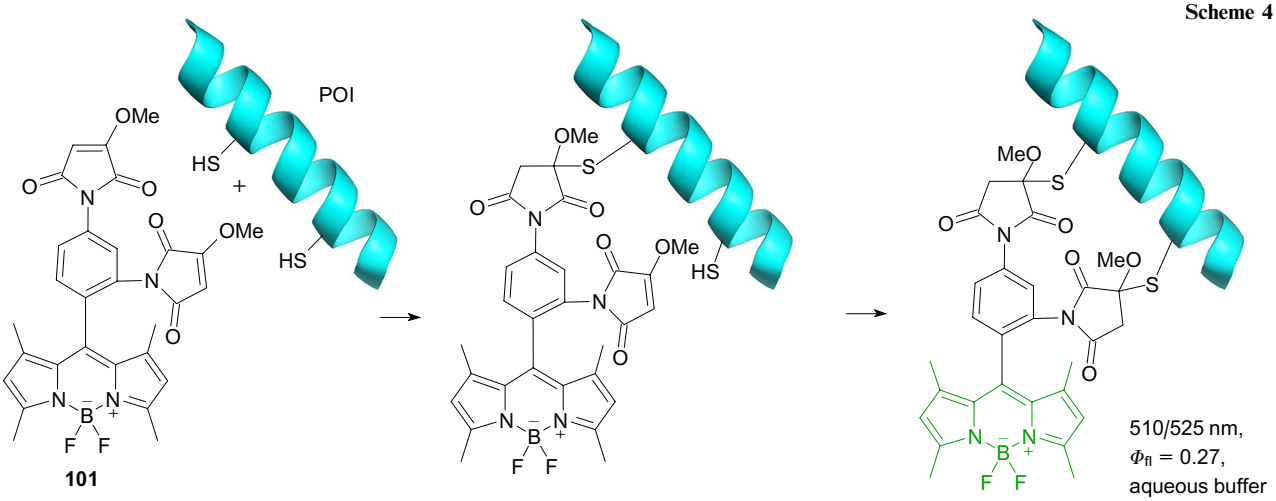
A similar approach was recently implemented by Keillor and co-workers.[175] The authors used a dimaleimide derivative of BODIPY **101** as a fluorogenic probe capable of specific binding to two cysteines within an α-helical region of a small peptide (Scheme 4, Fig. 23). These two cysteines are at a distance of ~ 10 Å from each other, which roughly corresponds to the distance between maleimide groups in compound **101**. In its free form, this compound is non-fluorescent, since maleimide groups are efficient quenchers due to the PET effect.[176] However, after covalent binding to the peptide within the POI (in Fig. 23, POI is the maltose-binding protein (MBP) containing an insert of a peptide with two cysteines [dC10α)], a ~800-fold increase in the fluorescence intensity at 525 nm is observed. To test the selectivity of fluorescent staining in live cells, histone H2B was chosen due to its clear localization in the nucleus. The peptide containing two cysteines was fused to the C-terminal sequence of the histone. Green fluorescent staining of the HeLa cell nuclei after addition of the fluorogenic probe confirms the specificity of the reaction of the dimaleimide derivative with the peptide-tagged histone.

It should be noted that along with the advantages of fluorogenic labelling at cysteine residues, there are some limitations that are mainly associated with side reactions with monothiols. Therefore, in experiments with cysteine-containing peptides, an excess of dithiothreitol is often used in order to get rid of nonspecific binding and background fluorescence. The SNAP-tag, CLIP-tag, HaloTag and TMP-tag technologies also have drawbacks, in particular, a significant size of the enzyme tag (about 20 kDa), which can affect the physiological functions of POI.

5. BODIPY derivatives as the basis for the design of cell sensors

Owing to the unique chemical and photophysical properties, BODIPY derivatives are frequently used as sensing molecules for imaging molecular activities of the cell accompanied by changes in intracellular metabolite concentration.[22] In this case, the key point is the ability of the BODIPY fluorophore to change its fluorescence characteristics in the

Scheme 4



101

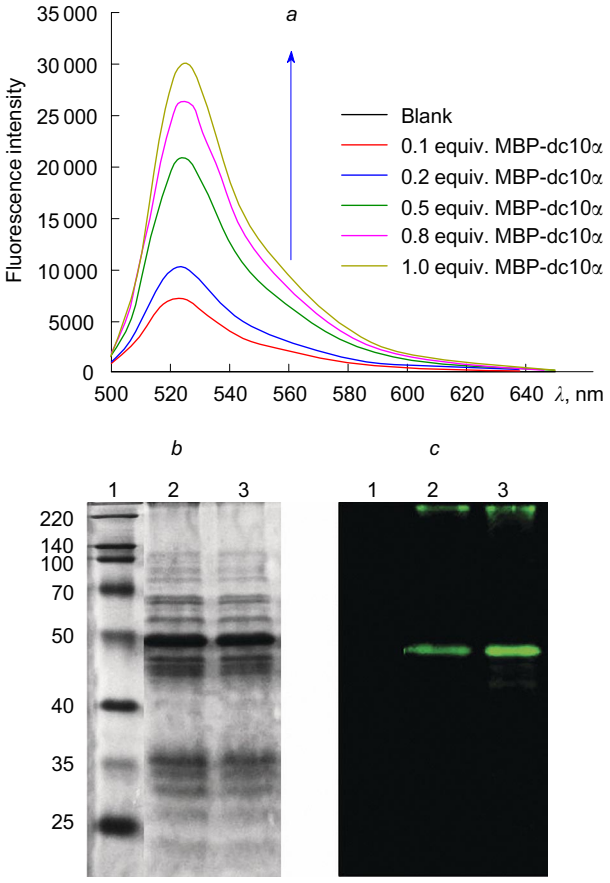
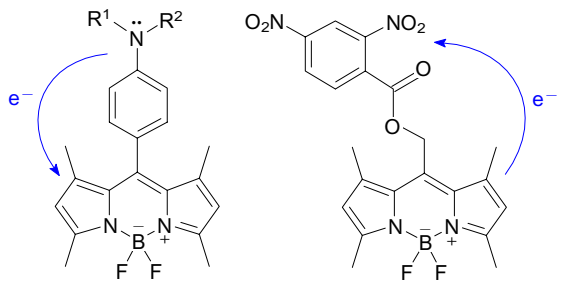


Figure 23. Change in the fluorescence intensity of a 25 μM solution of **101** (λ_{exc} = 480 nm) with increasing concentration of the maltose-binding protein (MBP) containing an insert of a peptide with two cysteines (dC10α) (*a*); gel electrophoresis of a water-soluble fraction of proteins from the lysate of *E. coli* bacteria expressing MBP-dC10α. Staining of the water-soluble total protein fraction with Coomassie blue; (*b*) selective fluorescent staining of MBP-dC10α with compound **101** (λ_{exc} = 491 nm, λ_{exc} = 508 nm) (*c*); lane 1 represents the molecular weight markers.[175] Published with the permission from Wiley.

presence of the tested intracellular component. This property can be based on various effects, such as photoinduced electron transfer (PET),[177,178] intramolecular charge transfer (ICT),[179] the influence of heavy metals,[180] the chelate effect,[181] FRET[182] and some others. Upon binding to the intracellular component, the fluorescence intensity of the BODIPY derivative can increase or decrease (on- and off-sensors), which is indicative of a relative increase or decrease in the concentration of the analyte. The absolute concentrations can be evaluated using ratiometric sensors, which have two excitation wavelengths or two emission maxima.[183,184] The binding of the cellular component leads to a change in the ratio of the intensities of two excitation (emission) peaks, and the absolute concentration of the analyte can be calculated from the intensities ratio.[185] Ratiometric sensors consist of either a single fluorophore molecule[186] or a pair of fluorescent molecules interconnected by a linker. In the latter case, one fluorophore is a non-ratiometric sensor, and another one is insensitive to concentration changes of the component and is used as a reference.[109]

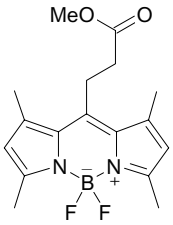
The construction of cell sensors is often based on the PET effect. Photoinduced electron transfer is usually observed between the π-electron non-conjugated parts of a fluorescent molecule and leads to fluorescence quenching. To activate this mechanism, it is necessary to introduce electron-donating (such as dimethylaniline) or electron-withdrawing (nitrophenyl) groups in the *meso* position of BODIPY[177] (Fig. 24, compounds **102**, **103**). In this case, the electron transfer process would compete with the fluorescence emission. In the case of electron-donating substituents, PET occurs towards the BODIPY core and has a reductive character (reductive PET); BODIPY with elec-



102 **103**

Figure 24. Photoinduced electron transfer effect in BODIPY derivatives (R^1, R^2 = Alk).

Structure 104



500/510 nm,
Φ_{fl} = 0.90,
acetonitrile

104

tron-withdrawing substituents are characterized by oxidative PET.

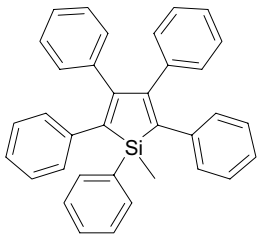
PET-based fluorescent sensors are often synthesized as fluorophore-chelating ligand constructs that are separated by a small spacer group. This group disconnects the π-electron systems of the fluorophore and the chelating group. Biosensors based on BODIPY derivatives are constructed by attaching a chelating group to the *meso* position of the fluorophore because the perpendicular orientation of the chelator with respect to the plane of the fluorophore leads to the separation of the π-electron systems. The design of BODIPY-based biosensors is most often based on the reductive PET effect when a free chelating group serves as an electron donor and the BODIPY core acts as an acceptor, resulting in non-radiative relaxation of the excited fluorophore and its quenching (*off*-state). The complexation of the intracellular component with a chelating group results in the suppression of PET, and the molecule undergoes transition to the fluorescence *on*-state.

If the electron-donating or and -withdrawing groups are in the same plane and participate in the overall conjugated π-electron system, the intramolecular charge transfer (ICT) can take place.[187] The photoexcitation and ICT cause significant changes in the dipole moment of the fluorophore. This effect largely depends on the solvent polarity. Thus, the fluorescence quantum yield is usually lower in polar solvents compared to nonpolar ones. The interaction of cations or protons with electron-donating groups lead to a decrease in the electron-donating ability and, as a result, to a decrease in the efficiency of ICT. Conversely, the interaction of cations with electron-withdrawing groups results in the enhancement of ICT, which ultimately affects the fluorescence quantum yield and lifetime. The main difference between PET- and ICT-based biosensors is that they cause different changes in the fluorescence spectra. The binding of the cellular component to PET sensors leads to an increase in the signal intensity or fluorescence quenching (on- and off-sensors) without any shift of the maximum. In contrast, the binding to ICT sensors causes a shift of the fluorescence maximum , thereby allowing ratiometric measurements of the absolute concentrations of the cellular component.[187]

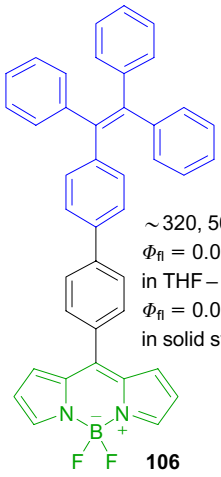
As noted above, most BODIPY derivatives have significant lipophilicity and form π – π stacking aggregates in polar solvents. Since these derivatives have a small Stokes shift, the formation of aggregates, in turn, leads to self-quenching of fluorescence (ACQ). In apolar solvents, aggregates are destroyed and fluorescence is restored. This solvatochromic behaviour of BODIPY derivatives was harnessed for instant staining of the cell membrane.[87] In this case, fluorogenic dye **104**, like compound **66** (Section 2.5), acquires fluorescent properties only after binding to the plasma membrane and does not require washing from an unbound label for further visualization using fluorescence microscopy and in flow cytometry experiments.[87]

Another effect employed in the design of cell sensors is the emission of fluorophore induced by its aggregation (aggregation-induced emission, AIE). In contrast to the ACQ phenomenon, the formation of aggregates of fluorophores with particular structures significantly increases their fluorescence intensity.[188] It was shown that the transfer of a 1-methyl-1,2,3,4,5-pentaphenyl derivative of silole (compound **105**) from ethanol to an aqueous medium leads to a more than 300-fold increase in its fluorescence quantum yield.[189] The authors attributed this effect to the rotational freedom of five phenyl rings about the bond with the silyl ring in a non-aggregated form, resulting in the activation of the nonradiative relaxation of the excited fluorophore. On the contrary, in the close-packed structures of fluorophore aggregates, such intramolecular rotation is impossible and the molecule acquires fluorescent properties. Later on, a series of tetraphenylethene-containing BODIPY derivatives with a similar AIE property were synthesized (compounds **106** – **108**).[190] The synthesized compounds had fluorescence emission from the visible to the NIR region and exhibited a significant Stokes shift of about 140 nm.

Structures 105 – 108

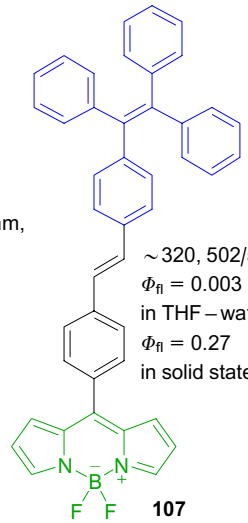


105



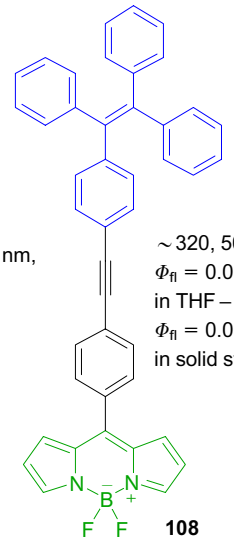
~320, 501/524, 650 nm,
Φ_{fl} = 0.002
in THF – water;
Φ_{fl} = 0.05
in solid state

106



~320, 502/533, 640 nm,
Φ_{fl} = 0.003
in THF – water;
Φ_{fl} = 0.27
in solid state

107



~320, 504/529, 600 nm,
Φ_{fl} = 0.001
in THF – water;
Φ_{fl} = 0.075
in solid state

108

Besides, cell sensors may be based on FRET between the two fluorophores connected by a small linker.[191] The key parameters responsible for efficient FRET are the donor quantum yield and the molar extinction coefficient of the acceptor. If these parameters vary with changing concentration of the cellular component, the FRET pair can be used as a ratiometric probe for this component.[192–196]

5.1. Cation sensors

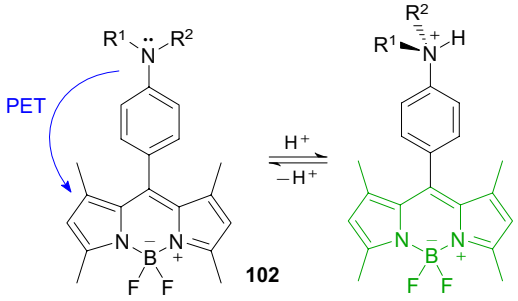
Maintaining ion homeostasis is crucial for the normal development of the cell. Homeostasis impairment can lead to significant changes in the cell functioning and may affect its growth and division. The concentration of intracellular ions is maintained by various ion-specific transport proteins (ATPases) and with the aid of membrane ion channels, the activity and permeability of which are regulated by the intracellular ion composition and various endogenous regulatory proteins. Given the important role of ions in the normal functioning of cells, significant recent efforts of synthetic chemists have been made to design and synthesize intracellular ion sensors.

5.1.1. pH indicators

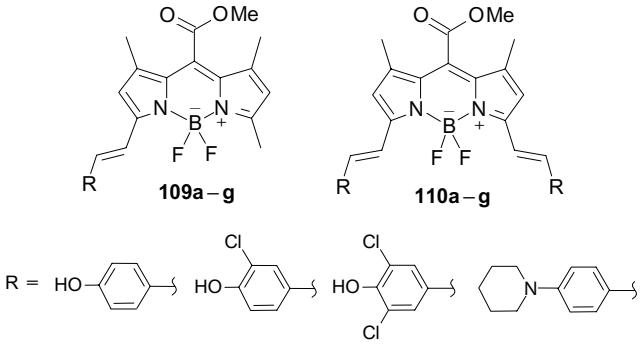
Different cellular compartments are characterized by different pH values. While pH in the cytoplasm and the endoplasmic reticulum is maintained close to neutral (7.4 and 7.0, respectively), mitochondria display a slightly basic pH (about 8.0). In the Golgi apparatus, pH is decreased to 6.5–6.7, and in endosomes and lysosomes, pH is significantly lower than neutral (5.5–6.3 and 4.5–5.5, respectively). Therefore, to target a specific cell compartment, it is necessary to employ pH sensors with appropriate pKa. The PET or ICT effects are often used in the design of BODIPY-based pH sensors. The protonation degree of the substituent usually changes with the pH change, which influences the efficiency of PET/ICT along with changes in the fluorescence quantum yield.[178] Scheme 5 illustrates pH-sensing properties of *meso*-aniline BODIPY derivative **102**.

Until recently, due to the similarity of the lysosomal and endosomal properties, researchers have experienced significant difficulties in targeting of synthetic reporters to endosomes. For selective staining of late endosomes, Chang and co-workers[197] synthesized a series of pH-sensitive mono- and 3,5-disubstituted BODIPY derivatives **109a–g** and **110a–g**. Among the fourteen synthesized derivatives, only compound **110f** with the pK_a of 5.1 allowed selective pH measurements in late endosomes. A decrease in pH from 7.3 to 5.0 resulted in a 79-fold increase in the fluorescence intensity of **110f** at 786 nm (Scheme 6). By fluorescence microscopy of three different cell lines, human osteosarcoma, cervical carcinoma and human lung adenocarcinoma (U2OS, HeLa and A549, respectively), it was demonstrated that **110f** can be used for real time imaging of the fusion late endosomes with lysosomes within live cells.

Scheme 5



Structures 109, 110



109a
650/– nm,
578/618 nm,
pK_a = 8.20,
Golgi

109b
631/– nm,
584/608 nm,
pK_a = 7.54,
Golgi

109c
629/– nm,
582/609 nm,
pK_a = 6.79,
Golgi

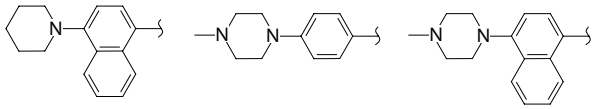
109d
620/– nm,
571/584 nm,
pK_a = 2.45,
lipid droplets

110a
750/– nm,
670/700 nm,
pK_a = 8.77,
Golgi

110b
745/– nm,
679/688 nm,
pK_a = 7.95,
Golgi

110c
740/816 nm,
708/803 nm,
pK_a = 6.33, 4.03,
lipid droplets

110d
752/– nm,
639/652 nm,
pK_a = 1.69,
lipid droplets



109e
630/– nm,
575/599 nm,
pK_a –,
lipid droplets

109f
593/– nm,
593/709 nm,
pK_a = 6.54,
lipid droplets

109g
593/– nm,
593/710 nm,
pK_a = 6.27,
lysosomes

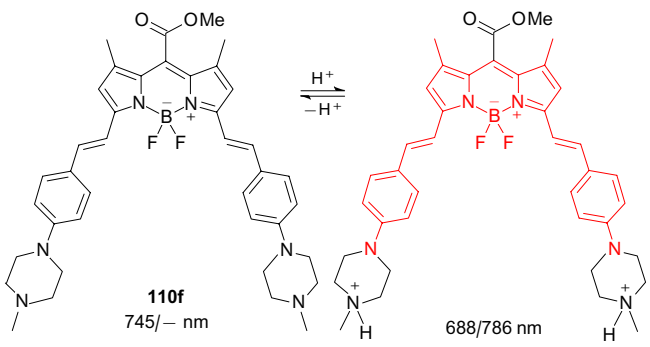
110e
712/– nm,
664/680 nm,
pK_a –,
lipid droplets

110f
745/– nm,
688/786 nm,
pK_a = 5.08,
late endosomes

110g
722/– нм,
688/757 nm,
pK_a = 4.62,
lysosomes

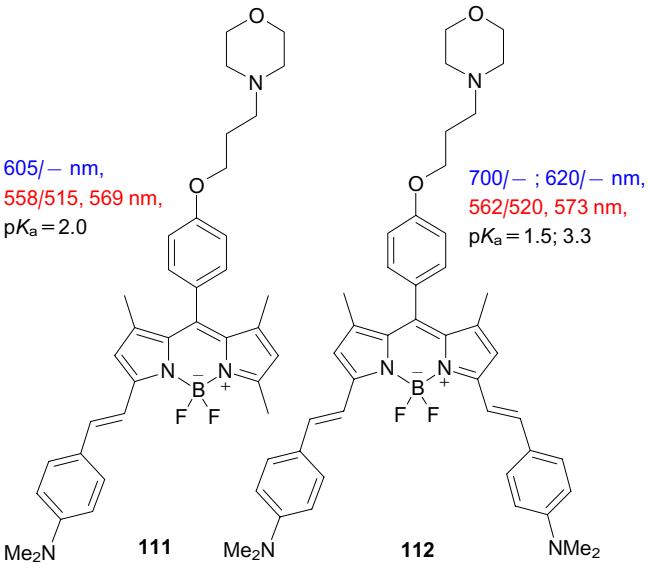
The fluorescence absorption/emission maxima of the fluorophore in the protonated and deprotonated forms (in red and blue, respectively), pK_a values and the sites of cellular localization are given under the structures.

Scheme 6



Jiang and co-workers[198] synthesized two ratiometric sensors for selective measurement of pH in lysosomes. In order to endow pH-sensing properties, one or two *p*-dimethylaminostyryl substituents were introduced at the 3- and 5-positions of the BODIPY structure. In an acidic medium, the dimethylamino moiety is protonated and the ICT is suppressed, thereby increasing the fluorescence intensity. Moreover, dimethylaminostyryl substituents cause a shift in the absorption and emission spectra to longer wavelengths. To target these derivatives to lysosomes, a morpholine moiety was introduced at the *meso* position of **111** and **112.** The lysosomal localization of these pH sensors was confirmed by the simultaneous staining of A549 cells with the lysosome-specific LysoTracker Blue DND-22.[198] One of the drawbacks of these pH sensors is too low pK_a (about 2.0) as compared to the pK_a values optimal for lysosomes (4.0 – 6.0).

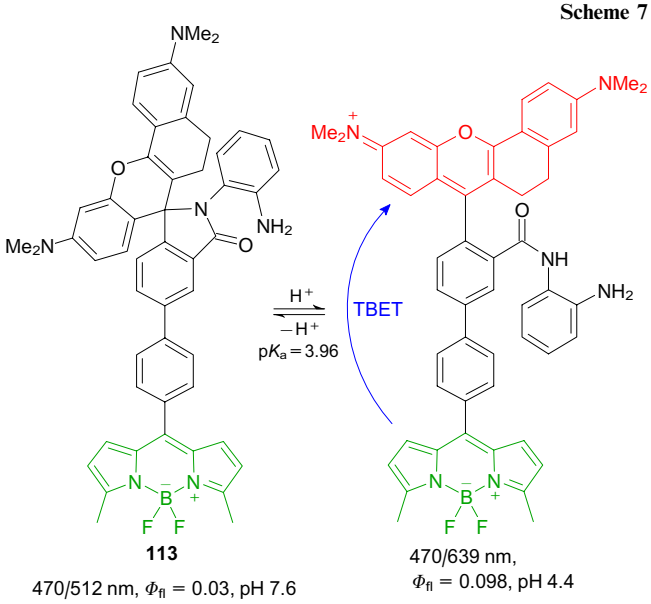
Structures 111, 112



In order to obtain ratiometric pH indicators with emission in the NIR region, Liu and co-workers[81] synthesized three donor-acceptor pairs consisting of different BODIPY derivatives (as donors) bound to rhodamine (Scheme 7, compound **113**) or merocyanine as acceptors. The synthesized compounds contained a morpholine moiety, which facilitated accumulation of pH sensors in lysosomes. It was shown that the donor – acceptor pair **113** comprising 3,5-dimethyl BODIPY and rhodamine modified with the *o*-phenylenediamine moiety (pK_a = 3.96) is optimal for measuring pH in lysosomes. At neutral and alkaline pH values, these compounds possess fluorescence exclusively due to the BODIPY donor, since rhodamine and merocyanine exist in the closed spirolactam form under these conditions. A decreas in pH leads to the the spirolactam ring opening and, due to the TBET effect, the fluorescence intensity of BODIPY decreases with a simultaneous increase in the fluorescence intensity of the acceptor groups of rhodamine and merocyanine (Scheme 7, Fig. 25). The synthesized pH sensor was used to determine pH fluctuations in HeLa cells under oxidative stress.

For real-time lysosomal pH imaging, O'Shea and co-workers[199] used the similar to Chang and co-workers[197] methodology, which was described above, for selective

Scheme 7



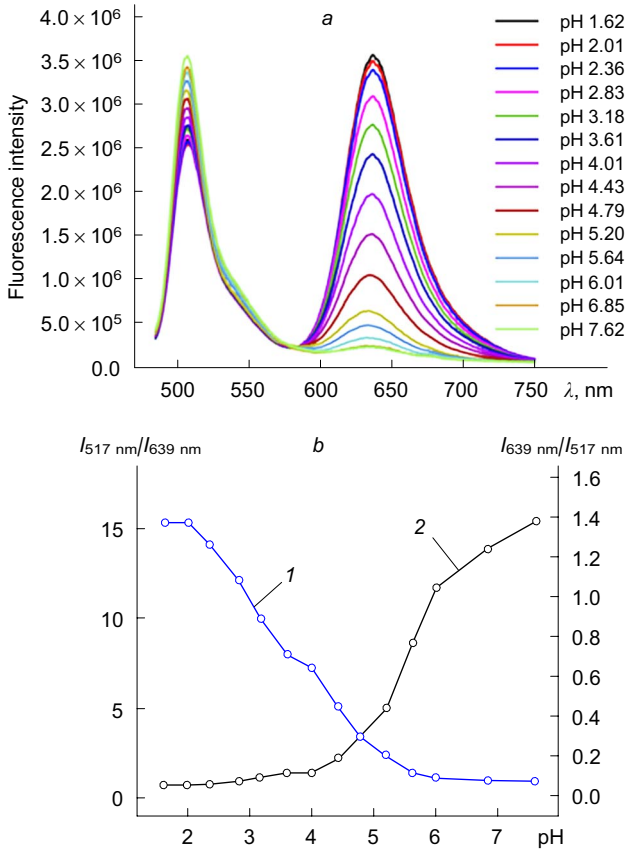
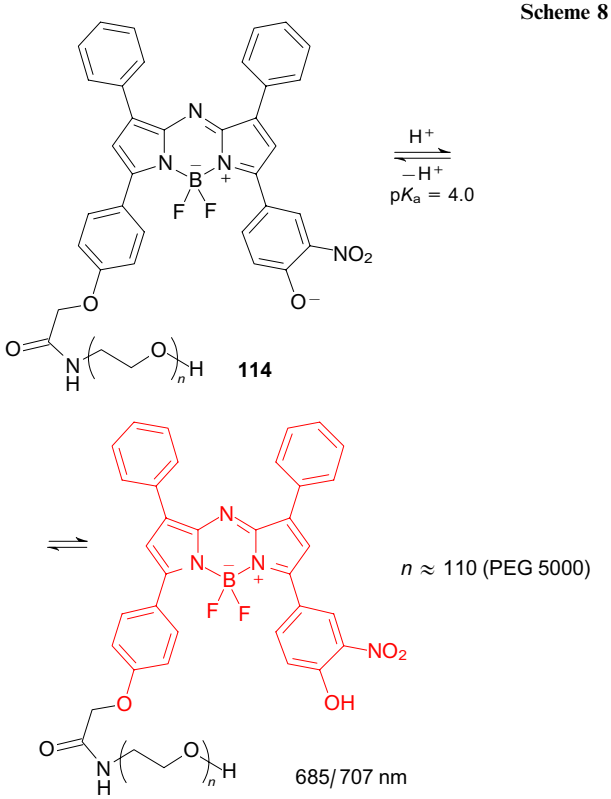


Figure 25. Fluorescence spectra of compound **113** at different pH (λ_{ex} = 470 nm) (*a*) and the pH dependence of the ratio of the fluorescence intensities of the donor and acceptor parts of **113**: $I_{517\ nm}/I_{639\ nm}$ (*1*), $I_{639\ nm}/I_{517\ nm}$ (*2*) (*b*).[81] Published with the permission from Elsevier.

staining of late endosomes. It is known that endocytosis causes significant changes in pH. Extracellular and cytoplasmic pH values are usually close to 7.2, while in early endosomes, pH decreases to 6.3, the late endosomes are

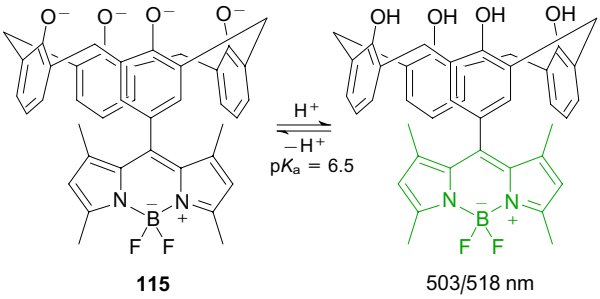
Scheme 8



characterized by even lower pH of 5.5, and the pH further drops to 4.5 in lysosomes.[200] O'Shea and co-workers used the nitrophenol substituent in the 5-position of BODIPY as the pH-sensitive module (Scheme 8, compound **114**). At pH = 7.4, this compound is virtually non-fluorescent; however, after conversion to the phenolic form in acidic pH, the fluorescence intensity at 707 nm significantly increases (pK_a = 4.0). Using a sensor-labelled lysosomal membrane protein, experiments with HeLa cells showed that fluorescent staining is characteristic only of lysosomes. This pH sensor is also localized outside lysosomes, but its fluorescence is turned off due to a higher pH. The synthesized sensor was successfully used to monitor lysosomal trafficking in real time. Furthermore, using the MDA-MB-231 subcutaneous breast cancer model,[199] it was demonstrated that NIR emission of the synthesized sensor allows its use for *in vivo* tumor imaging.

Han *et al.*[120] syntheised a pH indicator based on BODIPY with calix[4]arene in the *meso* position (Scheme 9, compound **115**). This indicator allows the measurement of pH values close to neutral (pK_a = 6.5). With a pH decrease from 7.2 to 6.3, the fluorescence intensity of the indicator at

Scheme 9



518 nm increases twofold. Due to the ability to penetrate through the cell membrane, this compound can be used as a specific cytosolic pH indicator. This indicator was used to monitor changes in intracellular pH during initial stages of cell apoptosis.

5.1.2. Calcium ions

Calcium ions play an extremely important role in biological systems, particularly, as intracellular secondary messengers, which regulate multiple physiological functions.[201] Nowadays, the most popular intracellular Ca^{2+} indicators are based on mutant forms of GFP-like proteins, such as Cameleon[202] and GCaMP2.[203] The advantage of these protein sensors is that they can be delivered to any desired cell compartment using genetically encoded signal sequences. However, as already mentioned, some of GFP-like proteins are characterized by a low maturation rate, an increased response times and lower sensitivity compared to synthetic indicators. The main difficulties in application of

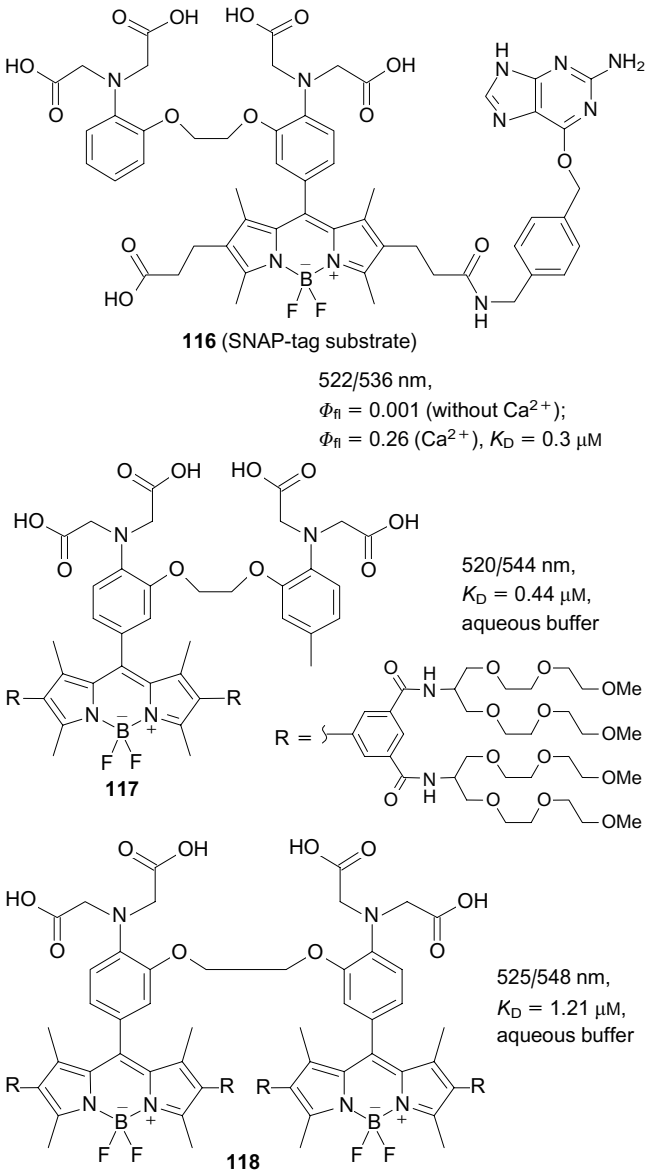


Figure 26. Chemical structures of intracellular Ca^{2+} sensors. K_D is the dissociation constant.

synthetic indicators are associated with targeted delivery to the desired location in the cell.

In 2010, Johnsson and Kamiya [204] suggested the application of the SNAP-tag technology for developing intracellular calcium indicators with predictable localization in the defined live cell compartment. To this end, O^6-benzylguanine derivative **116** (Fig. 26) was obtained, which specifically reacted with O^6-alkylguanine transferase (AGT), an enzyme covalently linked to POI with a definite intracellular localization. Using the chinese hamster ovary CHO-K1 cell line, it was demonstrated that after binding to AGT, **116** can be used as a highly sensitive indicator of calcium concentration in the cytosol and nuclei of living cells.

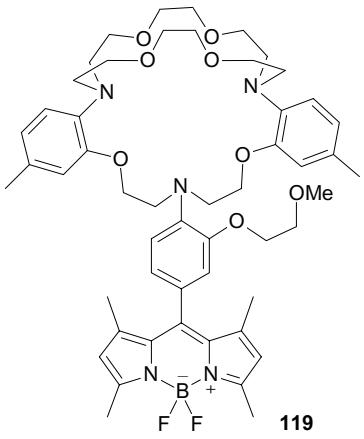
As indicated above, PEG derivatives of BODIPY are water-soluble and can be efficiently internalized by cells, accumulating in the cytoplasm. To obtain an intracellular Ca^{2+} sensor, Gao and co-workers [205] used PEG-substituted BODIPY fluorophore **117**, to which 1,2-bis(2-aminophenoxy)ethylene-*N*,*N*,*N*′,*N*′-tetraacetic acid (BAPTA) was attached at the *meso* position as a Ca^{2+}-sensitive module (see Fig. 26). Besides, related compound **118** with two PEG-substituted BODIPY fluorophores was synthesized . It was shown that **118** has a higher molar extinction coefficient compared to **117** (8.4×10^4 L mol^{-1} cm^{-1} at 525 nm) and higher sensitivity and selectivity for Ca^{2+} ions. Moreover, using the HeLa cell line, it was shown that **118** has a higher membrane permeability and can be used as a cytoplasmic indicator of Ca^{2+} ions, which exhibits higher fluorescence intensity with increasing concentration of this cation.

5.1.3. Potassium ions

Potassium ions perform a number of very important physiological functions, ensuring the excitability and conductivity of the cells of the nervous system, participating in the nervous regulation of heart contractions, the contraction of skeletal muscles and maintenance of the osmotic pressure in cells, tissues and biological fluids. In this regard, in recent years, extensive work has been carried out on the synthesis of new fluorescent sensors to determine the concentration of K^+ ions in the intracellular and extracellular space. Benzofuran isophthalate derivative (PBFI) is the most popular and commercially available fluorescent potassium sensor, which contains diaza-18-crown-6 as a K^+ sensitive module and a benzofuran derivative as a fluorophore.[206] However, PBFI is characterized by poor K^+ selectivity compared to Na^+.

In 2015, Belfield and co-workers [207] designed an improved method for the synthesis of *meso*-triazacryptand-substituted BODIPY. Complexation of potassium ions with **119** resulted in a significant increase in the fluorescence intensity with excellent selectivity for K^+ over other metal cations that are present in tissues (Fig. 27). The applicability of this compound for the intracellular potassium concentration measurements was demonstrated in the human glioma cell line (U87MG) using fluorescence microscopy.

Structure 119



119

–/512 nm,
Φ_{fl} = 0.03 (without K^+),
Φ_{fl} = 0.43 (150 mmol K^+),
C_{min} = 1.5 μM,
K_D = 65 μM,
acetonitrile – water buffer,
pH 7.2

C_{min} is the minimum detectable concentration

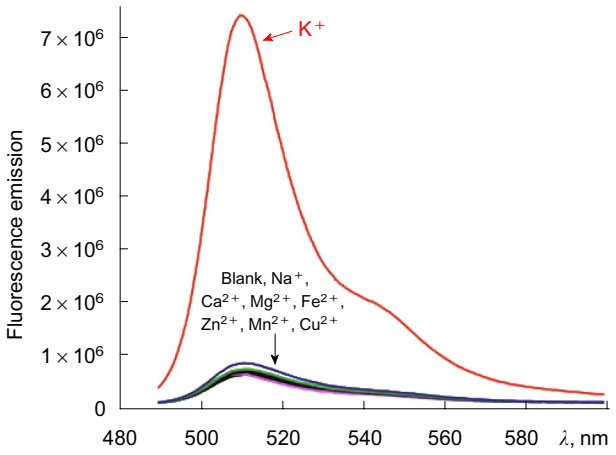
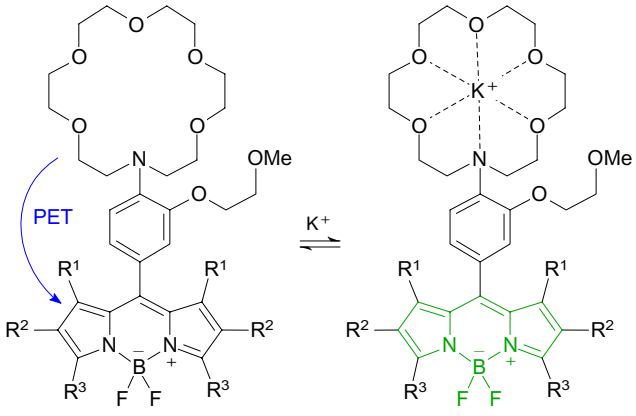


Figure 27. Fluorescence spectra of **119** (10 μM) upon addition of solutions of various cations at the physiological concentrations, mM: Na^+ (150), K^+ (150), Ca^{2+} (0.5), Mg^{2+} (2.5), Fe^{3+} (18), Zn^{2+} (45), Mn^{2+} (0.9), Cu^{2+} (16).[207] Published with the permission from Wiley.

In 2016, Borisov and co-workers [208] synthesized a K^+ ion sensor based on the aza-crown ether as the sensor module bound to the BODIPY fluorophore (Scheme 10, compound **120**). Complexation with K^+ ions caused fluorescence enhancement due to the reduction of the PET effect. A number of similar indicators were obtained with optical properties that are easily tuned to the desired spectral range (with fluorescence excitation in the green to red region and fluorescence emission in the red to NIR region). These sensors exhibit high brightness with quantum

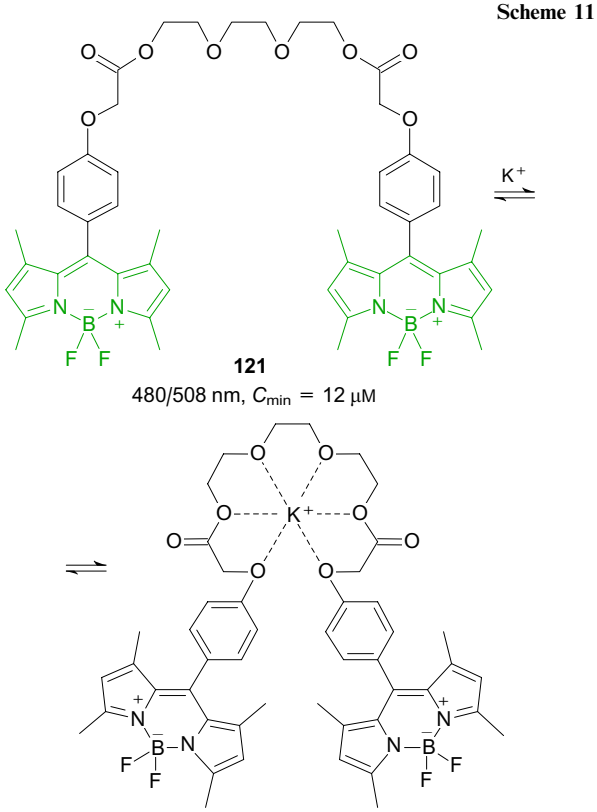
Scheme 10



120

R^2 = H: R^1 = R^2 = Me; R^1 = Ph, R^3 = 4-Pr^{n}C$_6$H$_3$;
R^1 = Ph: R^2 – R^3 — 5-chloro-1,4-dihydroindeno[1,2-*b*],
6-methoxy-5,6-dihydronaphtho[1,2-*d*];
R^1 = Ph, R^2 – R^3 — 5-(3-chloro-4-methoxyphenyl)furo[1,2-*b*]

Scheme 11



yields between 0.20 and 0.47 and molar absorption coefficients between 30 000 and 290 000 L mol^{-1} cm^{-1}. All synthesized indicators show high K^+ selectivity; moreover, the pH changes in the physiological range have no effect on sensor readout.

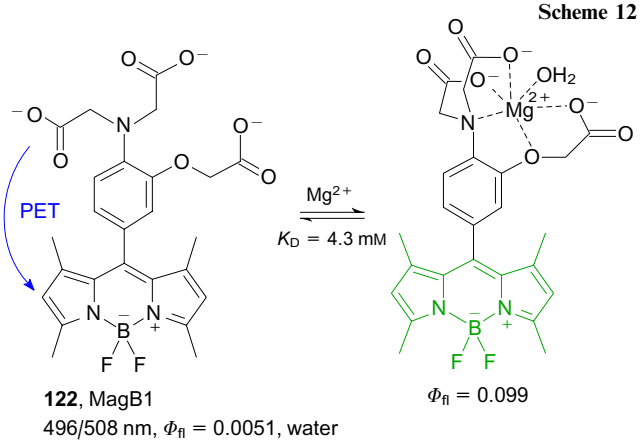
While the functioning of sensors based on BODIPY and crown ethers is due to PET effects with the fluorescence switching upon potassium ion complexation, the K^+ sensor prepared by Yang and co-workers [209] is based on a completely different mechanism. These authors synthesized *bis*-BODIPY derivatives connected by a polyethylene glycol chains of different lengths and showed that among many metal ions tested, compound **121** has a pronounced selectivity for K^+. In contrast to the K^+ sensors described above, the fluorescence intensity of *bis*-BODIPY derivative **121** significantly decreased with increasing concentration of potassium ions. The authors attributed the observed effect to the formation of pseudo-crown ether during complexation of **121** with K^+ ions (Scheme 11), which should lead to the closer distance between two BODIPY units and, as a result, to fluorescence quenching due to the ACQ effect.

5.1.4. Manganese cations

The proper regulation of the Mg^{2+} concentration in cells and cellular compartments is essential for maintaining biological processes, including the functioning of various Mg^{2+}-dependent enzymes, the regulation of K^+ and Ca^{2+} ion transport. Not so long ago, it was shown that Mg^{2+} can serve as a secondary messenger associated with T-cell receptors that activate a number of intracellular effectors in lymphocytes.[210] Nevertheless, the role of Mg^{2+} in signaling mechanisms and regulation of cell functioning is poorly understood, and the published data are often contradictory. This is primarily due to the lack of sensors that selectively detect intracellular Mg^{2+} concentrations without interference of other divalent cations, in particular Ca^{2+}.

Buccella and co-workers [211] synthesized two molecular sensors for the determination of intracellular Mg^{2+} concentration. These sensors consist of *o*-aminophenol-*N*,*N*,*O*-triacetic acid as the sensor module connected to two different BODIPY fluorophores (Scheme 12, compound **122**; Fig. 28, compound **123**). Both sensors are characterized by fluorescence absorption and emission in the visible region. With increasing Mg^{2+} concentration, the fluorescence intensity of these compounds significantly increases due to inhibition of PET (Fig. 28). Compound **123** with a styryl substituent in the 3-position of BODIPY shows fluorescence emission in the red spectral range (602 nm, $\Phi_{fl} = 0.274$), with a 58-fold increase in the fluorescence intensity upon Mg^{2+} binding and a dissociation constant in the millimolar range, which corresponds to physiological concentrations of this cation. To measure the intracellular Mg^{2+} concentration, **123** was introduced into HeLa cells in the free acid form by means of pinocytosis.

Scheme 12



In addition to *o*-aminophenol-N,N,O-triacetic acid, other groups selectively chelating Mg^{2+} were also used. In particular, Levy and co-workers [214] suggested the use of 4-oxo-4*H*-quinolizine-3-carboxylic acid conjugated with fluorescein as a fluorescent indicator of Mg^{2+}. However, fluorescein restricted membrane permeability limits the use of this sensor as the intracellular indicator. Later, Vendrell and co-workers [212] synthesized BODIPY derivative **124** with 4-oxo-4*H*-quinolizine-3-carboxylic acid as a substituent in the *meso* position. An increase in the Mg^{2+} concentration within the physiological range (up to 1 mM) led to an increase in the fluorescence intensity of **124** at 520 nm. The complexation with Mg^{2+} leads to a 4 times higher increase in the fluorescence intensity compared to that with Ca^{2+} at the same concentration. Colocalization experiments with other known fluorescent dyes (LysoTrackerRed and MitoTracker Red) using the human adenocarcinoma cell line (A549) showed that the synthesized sensor is predominantly localized in the cytoplasm, mitochondria and lysosomes.[212]

Lin and Buccella [213] also synthesized two BODIPY derivatives **125a**,**b** with 4-oxo-4*H*-quinolizine-3-carboxylic acid as a sensor module. The alkoxystyryl groups in the 3-position of BODIPY shifted the absorption and emission spectra of the compounds to the red region (above 600 nm) and had a significant effect on their membrane permeability and retention within the cells. The complexation with Mg^{2+}

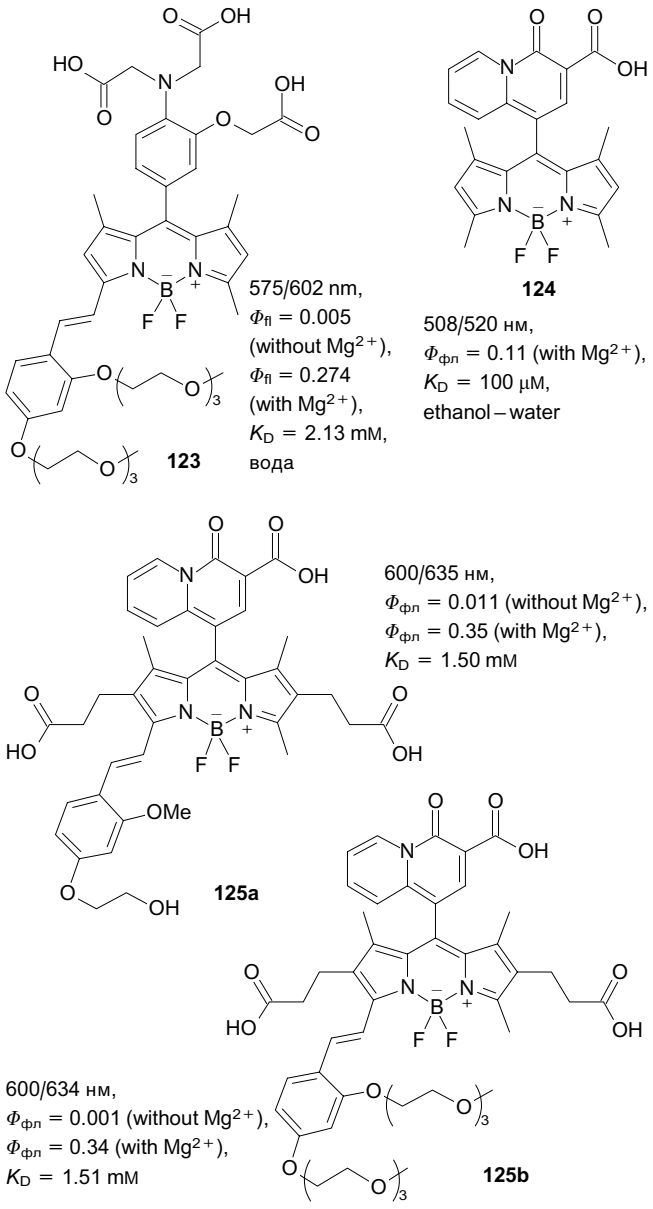


Figure 28. Mg^{2+} sensors based on BODIPY.

led to a 29-fold increase in the fluorescence intensity in aqueous solutions with quantum yields $\Phi_{fl} > 0.3$. Using the HeLa cell line, it was shown that, compared to **125a**, derivative **125b** containing a triethylene glycol residue has an extended retention time within the cell, which allows application of this compound for visualizing intracellular Mg^{2+} concentration changes by fluorescence microscopy.

5.1.5. Intracellular sensors for zinc cations

Zn^{2+} ions are involved in many fundamental physiological processes as cofactors of metalloproteins, regulators of the activity of many enzymes, in particular, those involved in the transmission of nerve impulses and gene expression. Disorders of zinc homeostasis are directly related to various neurological disorders, such as cerebral ischemia, Alzheimer's disease, and Parkinson's disease and epilepsy.[215–217] To date, a substantial number of zinc ion indicators have been synthesized based on various fluorophores, such as BODIPY,[218] quinoline,[219] dansyl,[220] acridine,[221] cyanines,[222] *etc*. However, most of them are of limited use due to poor water solubility and the need of short-wavelength excitation.

Liu and co-workers[223] synthesized three water-soluble (with a solubility higher than 50 mg ml^{-1}) dipicolylamino derivatives of BODIPY **126**–**128** with attached thriethylene glycol chains (Fig. 29) In its free form, fluorescent sensor **128** has two emission maxima, at 661 nm and a smaller one at 521 nm. With increasing Zn^{2+} concentration, the fluorescence intensity at 661 nm decreases, while the intensity at 521 nm increases, which makes it possible to perform ratiometric measurements of Zn^{2+} concentrations in live cells.

To enhance water solubility, Akkaya and co-workers[224] synthesized 3,5-distyryl-substituted BODIPY derivative **129**, with the inclusion of several triethylene glycol groups as the substituents (see Fig. 29). The incorporation of aromatic substituents in the BODIPY structure gave rise to a sensor with fluorescence in the NIR region. In addition, the resulting compound contained a dipicolylamino group as a Zn^{2+} chelating ligand. An increase in the Zn^{2+} concentration causes a hypsochromic shift of the emission maximum from 730 to 680 nm with the simultaneous increase in the fluorescence intensity. This effect is probably due to the blockage of ICT from the dipicolylamino group as a result of complexation with zinc ions. Thus, compound **129** can be used as a ratiometric sensor allowing the determination of the exact Zn^{2+} concentration from the ratio of fluorescence intensities at two wavelengths.

Recently, Volkova and co-workers[225] synthesized BODIPY derivative **130** with a dipicolylamino group in the *meso* position (see Fig. 29). In the Zn^{2+} non-bound form, this compound has a low fluorescence quantum yield (0.06 in $MeCN/H_2O$) due to PET between the electron-donating amino group and the BODIPY core structure. An increase in the concentration and the formation of Zn^{2+} complexes leads to a bathochromic shift of the emission maximum from 548 nm to 610 nm with a 21-fold increase in the quantum yield. In this work, **130** was used to study the dynamics of Zn^{2+} concentration changes in the cells of the roots of the rape plants *Brassica napus* L.

Tanasova and co-workers[226] developed BODIPY-based Zn^{2+} ratiometric sensor **131** with *N*,*N*-di-(2-picolyl)ethylenediamine as a substituent in the 5-position and methylcarboxylate in the 6-position, which form a chelate complex with zinc (see Fig. 29). This sensor allows monitoring the changes in the intracellular Zn^{2+} concentration with high selectivity and sensitivity. In its free form, fluorophore **131** has a maximum fluorescence emission at 540 nm. With increase in the Zn^{2+} concentration, the emission maximum shifts by 40 nm to the red region of the spectrum, which allows for ratiometric measurements.

5.2. Anion sensors

For the most part, anions ensure buffering properties in the intracellular and extracellular spaces. For example, the phosphate buffer system maintains pH in the cytoplasmic space within 6.9–7.4. In the extracellular space, pH 7.4 is maintained mainly due to the bicarbonate buffer system. Using Cl^- ion channels located in the cell membranes, ion homeostasis, regulation of cell volume, transepithelial transport and regulation of electrical excitability are maintained.[227] Also, some anions have significant toxicity to cells, tissues and organisms. This necessitates the develop-

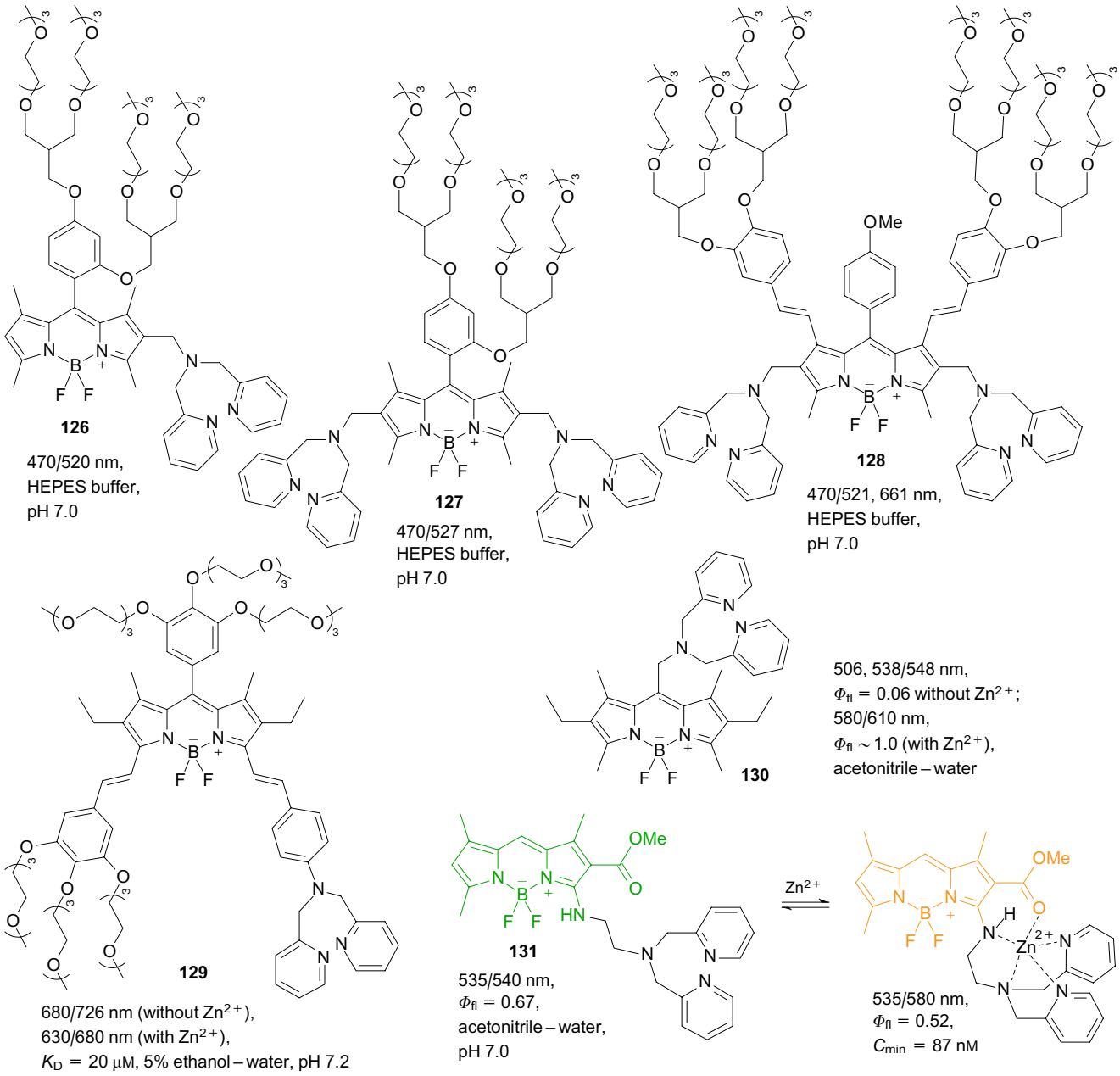


Figure 29. Intracellular Zn^{2+} sensors. (HEPES is 2-[4-(2-hydroxyethyl)piperazin-1-yl]ethanesulfonic acid).

ment of sensitive and efficient methods for their detection.[17, 228]

5.2.1. Chloride ions

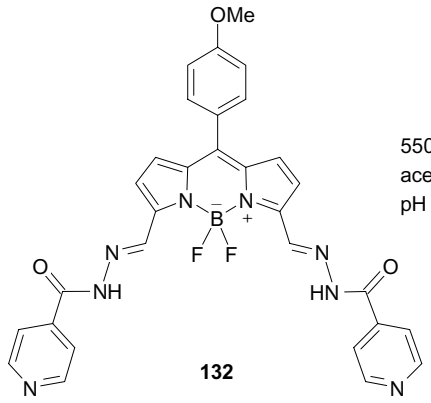
As noted above, chloride ions play an important role in the body as an electrolyte and are transported in and out of the cell through chloride ion channels. Improper regulation of chloride transport across the cell membrane can cause cystic fibrosis.[229] Reports on the synthesis of chloride sensors are quite rare in the literature, which is probably due to problems with the selectivity of these sensors.

Ravinkanth and co-workers[230] synthesized two *N*-acylhydrazone-substituted BODIPYs (**132** and **133**), which, when titrated with Hg^{2+}, form 1 : 1 mercury complexes. Compounds **132**-Hg^{2+} and **133**-Hg^{2+} are virtually non-fluorescent ; however, in the presence of Cl^-, these complexes are destroyed with the release of initial **132** and **133** and with the concomitant 22-fold and 16-fold increase in the fluorescence intensity, respectively (λ_{ex} = 550 nm). Experiments on the competitive binding in the presence of various anions showed that the resulting mercury complexes specifically and reversibly react with chloride ions. However, the use of the synthesized sensors in experiments with live cells is complicated due to the toxicity of Hg^{2+}-containing compounds. Therefore, in the work cited, chloride anions were detected in fixed human breast adenocarcinoma cells (MDA-MB-231). Compound **132** was shown to be able to penetrate the cell membrane of fixed cells, which made it possible to use it as an intracellular chloride sensor.

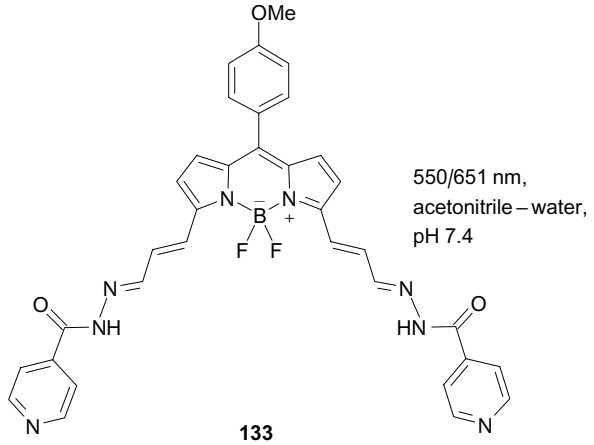
5.2.2. Carbonate ions

To date, several fluorescent sensors for CO_3^{2-} based on small organic molecules have been obtained,[231 – 234] but most of them are unsuitable for use in living systems due

Structures 132, 133



132



133

to poor solubility in water, the complex synthesis or low selectivity.

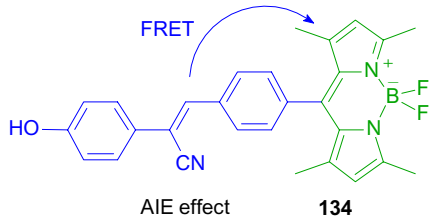
Yang and co-workers [192] synthesized *meso*-cyanodiphenylethylene derivative of BODIPY **134**, which exhibits bright fluorescence due to the AIE effect and a significant pseudo-Stokes shift (160 nm) due to FRET between the cyanodiphenylethylene moiety and the BODIPY core. Owing to the presence of the phenol group, the intensity of fluorescence of **134** depends on pH (pK_a = 9.79). Moreover, the fluorescence intensity is significantly reduced at CO_3^{2-} concentrations above 20 μM, and complete fluorescence quenching is observed at a concentration of 40 μM. Fluorescence quenching is selective in the presence of carbonate anions, which allows **134** to be used as a carbonate sensor. Using the MTT assay, it was shown that 90% of MCF-7 cells remain viable upon 24 h incubation in a 10 μM solution of this compound.

5.2.3. Cyanide ions

Among other inorganic anions, cyanide ion is one of the most toxic to living organisms. Recently, several reviews have been published that comprehensively summarize the information on the synthesis and application of optical chemosensors for cyanide ions.[235, 236] Nucleophilic addition reactions, complexation with metal ions and interactions with ligands involved in hydrogen bonding with the cyanide ion [236] are used as the main approaches for creating selective sensors for this anion. To date, a number of fluorescent sensors for CN^- have been obtained, but most of them are unsuitable for use in living systems due to poor solubility in aqueous solutions or because of the need of UV-light excitation of the sensor.

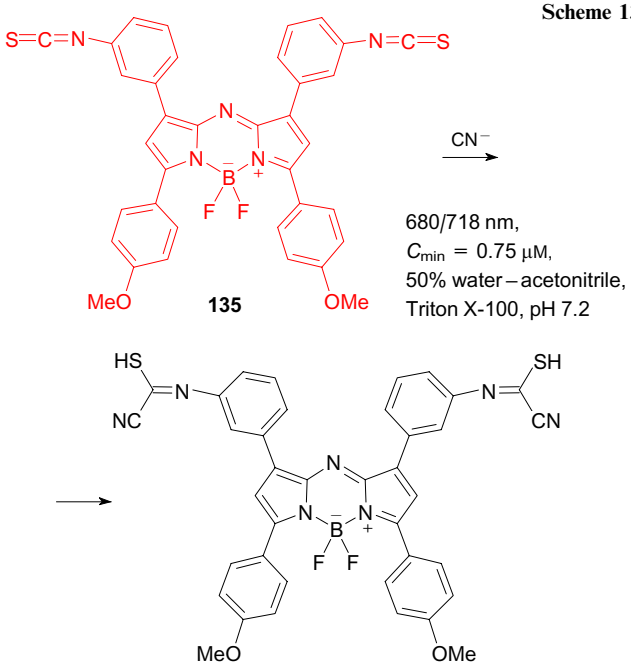
Recently, water-soluble CN^- sensor **135** (Scheme 13) with excitation and emission in the NIR region was obtained.[237] This compound includes two isothiocyanate groups, which undergo a nucleophilic addition reaction with CN^- and represent the sensor module, while aza-BODIPY embodies the fluorescent reporter constituent. The fluorescence intensity of **135** at 718 nm decreases with increasing CN^- concentration.[237] Compound **135** has a high sensitivity (C_{min} = 0.75 μM) and selectivity for CN^- compared to other anions. The applicability of compound **135** as an intracellular sensor was tested with 4T1 human breast cancer cells (the murine mammary carcinoma cell line widely used as a syngeneic tumor model for human breast cancer) using confocal laser scanning microscopy. It was shown that the red fluorescence associated with **135** is localized mainly in the cytoplasm; however, after addition of 100 μM KCN to the cells, this fluorescence signal disappears.

Structure 134



134

Scheme 13



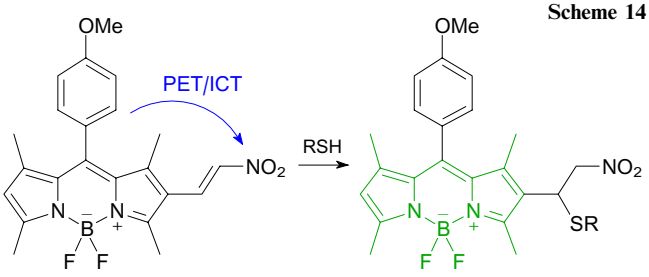
5.3. Thiols

Low-molecular-weight thiols, such as cysteine (Cys), homocysteine (Hcy) and glutathione (GSH), play an important role in physiological and pathological processes.[238-240] Despite the similar chemical structures, these compounds have different physiological functions and are associated with various related diseases.[241] For a more complete understanding of the role of thiols in complex biological systems, the efforts of many researchers are focused on the

development of new highly sensitive sensors for their detection.[242, 243]

Fluorescent indicators of thiols are often prepared using the Michael nucleophilic addition. To this end, alkene or alkyne groups with electron-withdrawing substituents are bound to fluorogenic groups. In particular, water-soluble nitroolefin-based BODIPY **136** with ratiometric properties (Scheme 14) was prepared.[244]

Scheme 14



136

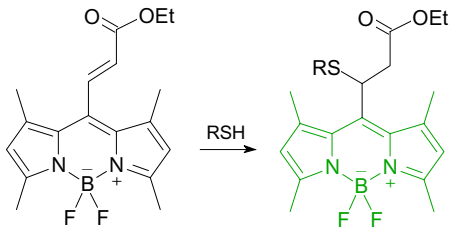
480/517, 573 nm,
PBS, pH 7.4

RSH = Cys, Hcy, GSH

The reaction of **136** with thiols results in an increase in the fluorescence intensity at 517 nm and its decrease at 573 nm, making it possible to determine the exact concentration of thiols from the intensity ratio. Sensor **136** is more sensitive to GSH and Hcy compared to Cys. The mechanism of action of this sensor is apparently associated with PET and ICT effects, which lead to fluorescence quenching at 573 nm. These processes are inhibited as a result of the thiol reaction with the double bond of the nitroolefin group, with an increase in the fluorescence intensity at 517 nm. The applicability of sensor **136** for measuring the intracellular concentration of thiols was shown using human adenocarcinoma cells (A549). It should be noted here the possible drawbacks of intracellular indicators based on the Michael reaction, since the nature of the nucleophilic reagent undergoing this reaction can greatly vary. In particular, amino groups in proteins and water as a source of hydroxide anions can compete as nucleophiles, affecting the overall readouts of the indicator.

Another mechanism involves the transition to the fluorescent state of *meso*-acrylate-BODIPY **137** (Scheme 15). As in the case of *meso*-vinyl derivatives of BODIPY (see compound **3** in Fig. 1), compound **137** has an almost zero fluorescence quantum yield due to a predominantly nonradiative transition to the ground state *via* vibrational relaxation.[48] In the presence of thiol, a significant increase in the brightness of this compound is observed due to the disappearance of the double bond in the *meso* position and fluorescence quenching mediated by this bond.[49]

Scheme 15



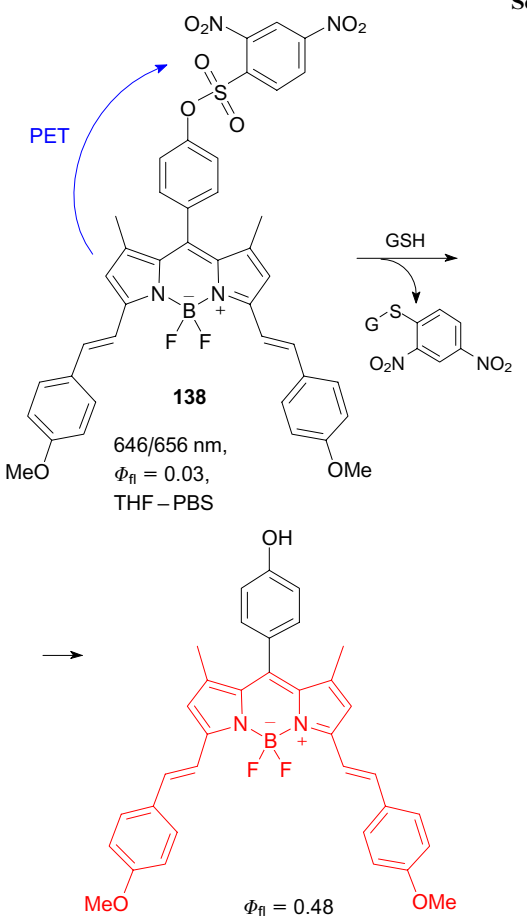
137

505/– nm

500/508 nm,
Φ_{fl} = 0.9, ethanol

Wang *et al.*[245] synthesized 3,5-distyryl BODIPY derivative **138** containing a 2,4-dinitrobenzenesulfonyl group as a fluorescence quencher (Scheme 16) for the selective detection of GSH. In the absence of thiols, this sensor does not fluoresce but acquires fluorescence in the NIR range after addition of thiols. It was shown that this sensor is 2 – 4 times more sensitive towards GSH compared with Cys and Hcy. Also, using the breast cancer cell line (MCF-7), compound **138** was shown to be applicable for the determination of endogenous and exogenous GSH in living cells.[245]

Scheme 16



138

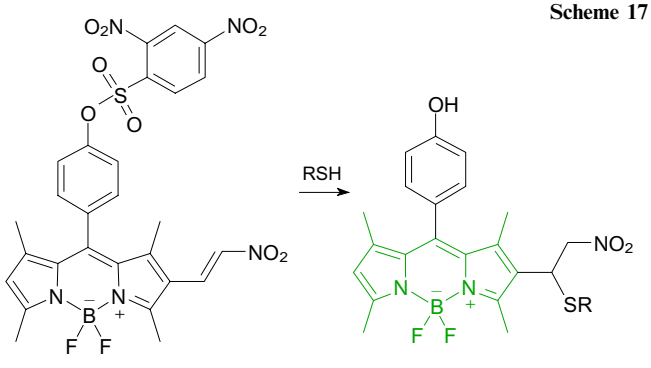
646/656 nm,
Φ_{fl} = 0.03,
THF – PBS

Φ_{fl} = 0.48

Liu and co-workers[246] synthesized BODIPY derivative **139** with two groups reacting with thiols, which increase the sensitivity and selectivity of the sensor (Scheme 17). In the free form, **139** shows almost no fluorescence (λ_{ex} = 543 nm, Φ_{fl} = 0.012); however, the addition of thiols leads to a significant increase in the fluorescence intensity at 517 nm: 106-fold for Hcy, 77-fold for GSH and 56-fold for Cys. The low background fluorescence level of this sensor make it possible to conduct experiments with live cells without intermediate washing out the unbound dye; therefore intracellular thiol concentrations can measured in fairly short periods of time (about 10 min). It was also shown with the HeLa cell line that sensor **139** specifically accumulates in mitochondria.

Thiol-sensitive fluorescent sensors **140** and **141** were also prepared on the basis of 1,7-dimethyl-3,5-diaryl-substituted BODIPY with an arylmercapto group in the *meso* posi-

Scheme 17



139

522/543 nm, acetonitrile – water, pH 7.4

504/517 nm

RSH = Cys, Hcy, GSH

tion.[247] Prior to the reaction with thiols, the original compounds shows almost no fluorescence. However, a significant increase in the fluorescence intensity at 562 nm was observed for **140** within the 15 min incubation with thiols. This compound has an enhanced sensitivity and higher reaction rates with cysteine. Mono- and disubstituted morpholine derivatives **142** and **143** were synthesized for targeted delivery of the sensor to lysosomes. It was shown that these compounds are indeed localized in the HeLa cell lysosomes, making it possible to determine the cysteine concentration in these organelles with a minimum detectable concentration of 46 and 76 nM for **142** and **143**, respectively.

5.4. Sensors of reactive oxygen and nitrogen species

Reactive oxygen and nitrogen species (RONS) play an important role in metabolism in terms of physiology and pathology.[248] At low concentrations, they perform a regulatory role, participating in intracellular signaling processes as chemical mediators,[249] regulating gene expression [250] and post-translational modification of proteins[251] and exhibit protective functions against various microbial infections.[252] Besides, an increase in the RONS concentration causes oxidative stress,[253] leading to an impairment of the genetic apparatus, mitochondria or the plasma membrane by free radicals, with the subsequent initiation of apoptosis and necrosis. Oxidative stress may also cause mutational process in the cell, which ultimately manifests itself as pathological changes such as neurodegenerative, cardiovascular and cancer diseases. RONS are a group of highly reactive and short-lived compounds, including ions, free radicals and peroxides: hydrogen peroxide (H_2O_2), singlet oxygen ($^1O_2$), superoxide anion radical ($O_2^{-\bullet}$), hydroxyl radical ($HO^\bullet$), hypochlorous acid (HClO), peroxynitrite ($ONOO^-$), nitric(II) oxide (NO) and some others. Given the significant role of RONS in physiology, the real-time monitoring of the processes associated with these species seems to be challenge, which is closely associated with theranostics of various diseases.

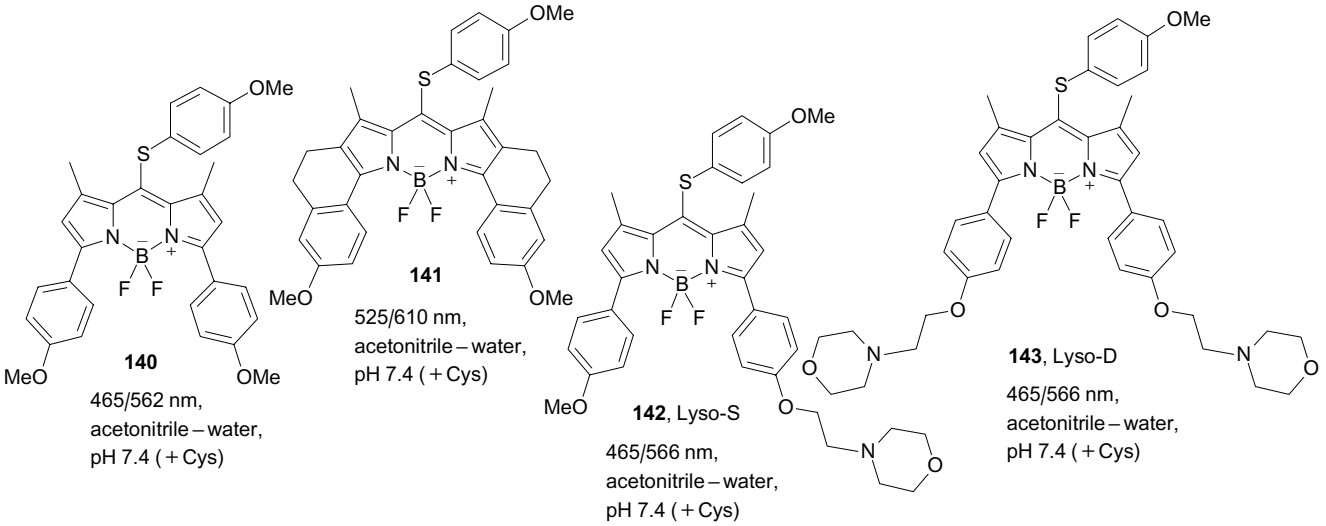
5.4.1. Hydrogen peroxide

It is now established that eukaryotic cells produce hydrogen peroxide as a mediator of various physiological processes, such as cell proliferation, differentiation and migration.[254] Furthermore, hydrogen peroxide is involved in processes related to the immune system, aging and cancer.[255] The direct participation in many physiological and pathological processes necessitates the development of new highly sensitive and efficient methods for the H_2O_2 detection.

Lin and co-workers [256] synthesized *meso*-phenyl derivatives of BODIPY **144a**,**b** with a 3-bithiophene-tetrazol-5-yl moiety in the *para* and *meta* positions of the benzene ring. Upon illumination with 365 or 405 nm light, these compounds undergo a light-dependent reaction with dimethyl fumarate to form BODIPY pyrazoline derivatives **145a**,**b** (Scheme 18). Pyrazoline cycloadducts **145** exhibit almost no fluorescence due to intramolecular PET. However, the fluorescence is recovered when **145** is oxidized back to pyrazole in the presence of hydrogen peroxide ($\lambda_{em} \sim 510$ nm). It was shown that this property of switching on the fluorescence of BODIPY pyrazoline derivatives **145a**,**b** can be used for the detection of H_2O_2 in HeLa cells.

Purdey *et al.*[257] also studied two systems **146** and **147** based on *meso*-phenyl-substituted BODIPY as sensors for the detection of H_2O_2 (Scheme 19). The sensitivity and selectivity of these two sensors were compared. The reaction of **146** with H_2O_2 yields the phenol-substituted BODIPY (Scheme 19), with a significantly decreased fluorescence intensity. On the contrary, the fluorescence intensity of sensor **147** increases with increasing H_2O_2 concentrations.

Structures 140 – 143



140

465/562 nm, acetonitrile – water, pH 7.4 (+ Cys)

141

525/610 nm, acetonitrile – water, pH 7.4 (+ Cys)

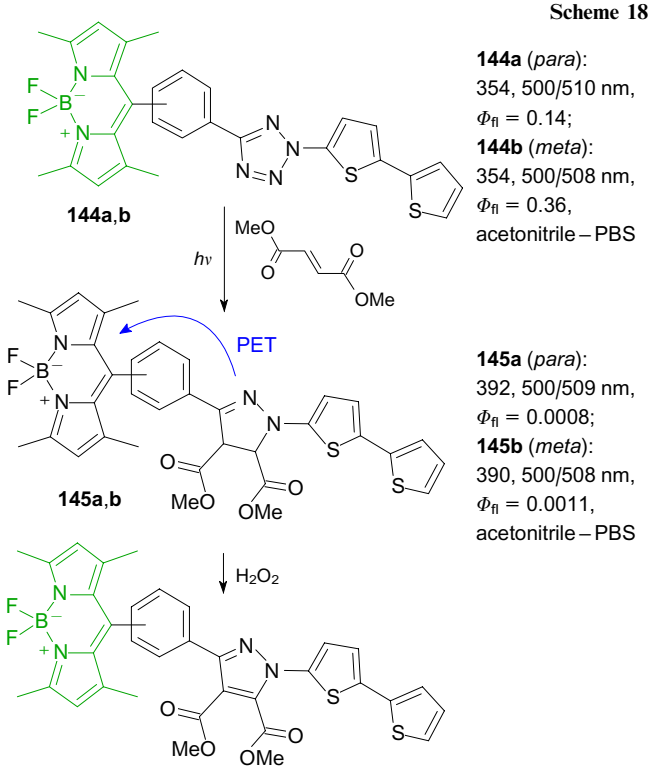
142, Lyso-S

465/566 nm, acetonitrile – water, pH 7.4 (+ Cys)

143, Lyso-D

465/566 nm, acetonitrile – water, pH 7.4 (+ Cys)

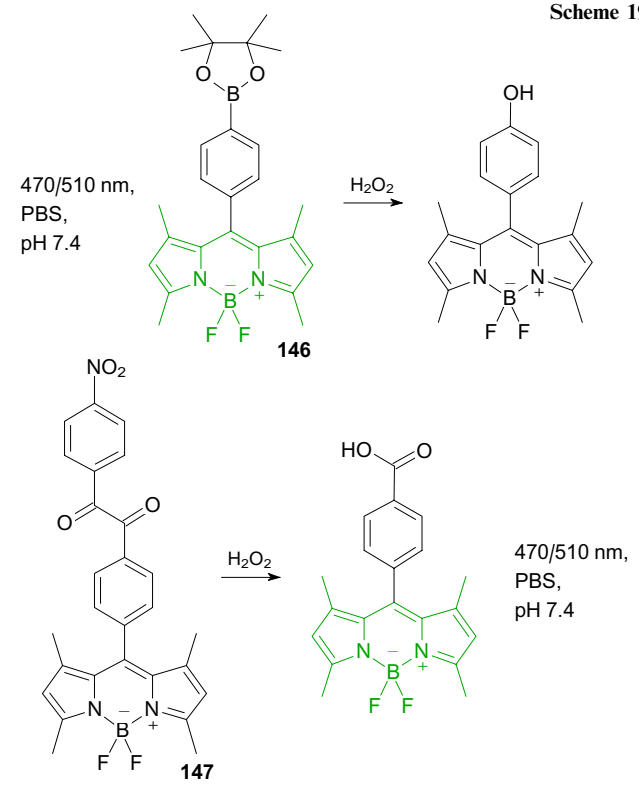
Scheme 18



144a (*para*): 354, 500/510 nm, Φ_{fl} = 0.14;
144b (*meta*): 354, 500/508 nm, Φ_{fl} = 0.36, acetonitrile – PBS

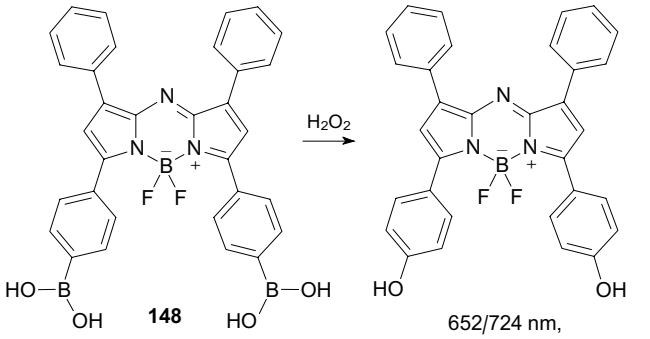
145a (*para*): 392, 500/509 nm, Φ_{fl} = 0.0008;
145b (*meta*): 390, 500/508 nm, Φ_{fl} = 0.0011, acetonitrile – PBS

Scheme 19



Compound **146** is characterized by the largest changes in the fluorescence intensity in the presence of H_2O_2, while **147** has the best selectivity compared to other RONS. Both sensors show the ability to penetrate the cell membrane. With the human embryonic kidney cell line HEK 293, it was shown that both sensors do not significantly affect cell proliferation at concentrations of up to 5 μM during 48 h of incubation. Also, the possibility of using these sensors *in vitro* was shown with bovine oocytes.

Scheme 20



652/682 nm, HEPES buffer, pH 7.4

652/724 nm, HEPES buffer, pH 7.4

Aza-BODIPY derivative **148** (Scheme 20) with two phenylboronic acid moieties at the 3,5-positions was synthesized as a sensor for the hydrogen peroxide detection.[258] The reaction with H_2O_2 resulted in the transformation of the phenylboronic groups of the sensor to phenolic groups. Increasing peroxide concentrations lead to a decrease in the fluorescence intensity at 682 nm and an increase in the intensity at 724 nm (Fig. 30). Therefore, compound **148** is a ratiometric sensor that allows real-time measurement of H_2O_2 concentrations. The possibility of using compound **148** as an intracellular sensor was investigated with the HeLa cell line. It was shown that this compound has sufficient cell permeability, excellent photostability and high selectivity compared to other RONS. Analysis of the fluorescence intensity ratio at 682 and 724 nm allows obtaining quantitative data on the intracellular concentration of H_2O_2.

5.4.2. Hydroxyl radical

In biological systems, the hydroxyl radical is one of the most reactive forms of RONS. The half-life of HO$^{\bullet}$ is only about 2 ns, and this radical participates in various redox processes in living systems. The hydroxyl radical was shown

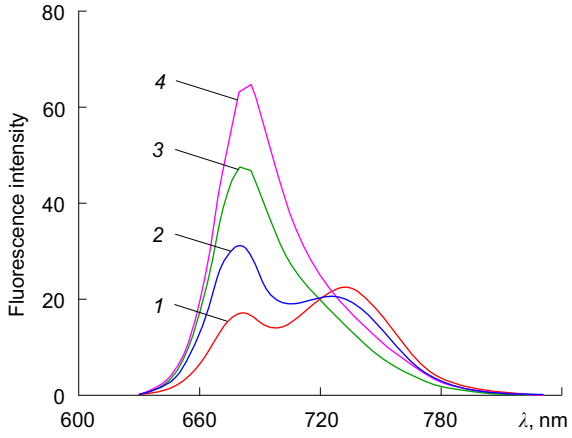
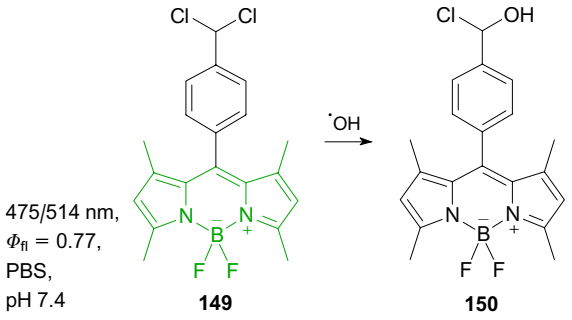


Figure 30. Changes in fluorescence spectra of aza-BODIPY **148** in live HeLa cells in the presence of H_2O_2 at a concentration of 10^{-2} M (*1*), 10^{-3} M (*2*) and 10^{-4} M (*3*) as compared with the control in the absence of H_2O_2 (*4*).[258] Published with permission from the Royal Society of Chemistry.

to be involved in oxidative damage of DNA,[259] proteins and lipids[260] and is a mediator in the regulation of the redox status of transmembrane Ca^{2+} channels.[261] Due to the difficulties in detecting such a short-lived form, new highly selective and sensitive sensors of intracellular HO$^{\bullet}$ concentration are currently being developed.

Sensor **149** for the detection of HO$^{\bullet}$ was synthesized based on a BODIPY fluorophore and *gem*-dichlorotoluene as a reaction centre.[262] Compound **149** is readily soluble in water and has a sufficiently high fluorescence quantum yield. However, after the reaction with hydroxyl radicals (Scheme 21), fluorescence of resultant **150** is quenched. Sensor **149** penetrates the cell membrane, which allows measurements of the intracellular HO$^{\bullet}$ concentration of up to 11 nM. It was shown that in MCF-7 cells, sensor **149** is localized in the cytoplasm (but not in the nucleus), has low cytotoxicity and high specificity for HO$^{\bullet}$.

Scheme 21

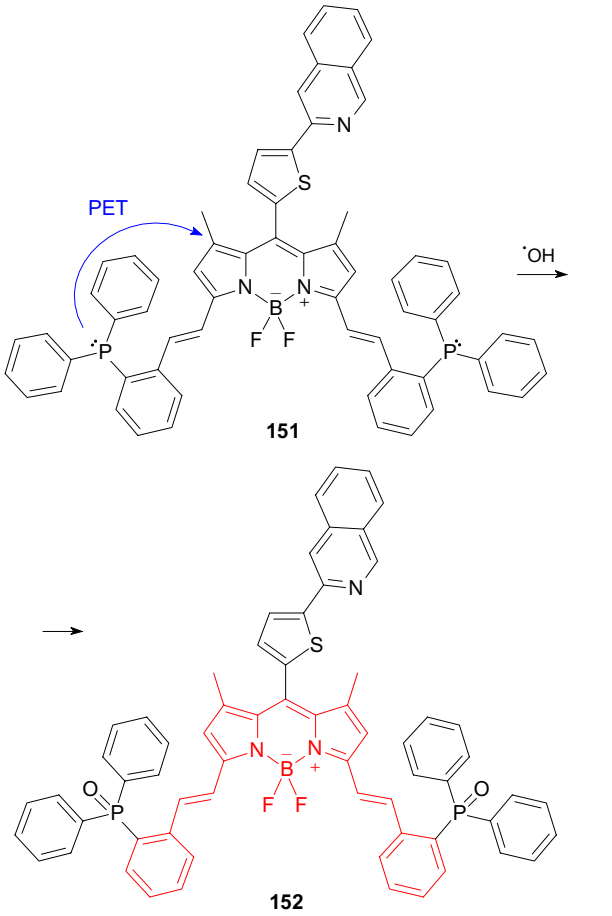


For the highly selective detection of hydroxyl radicals, NIR fluorescent sensor **151** consisting of the 2-(isoquinolin-3-yl)thienyl moiety as an electron donor and 3,5-bis(2-diphenylphosphino)styryl-substituted BODIPY as an acceptor was also synthesized.[263] Triphenylphosphine groups serve as a reaction centre, undergoing an oxidation reaction in the presence of HO$^{\bullet}$ (Scheme 22, compound **152**). An increase in the HO$^{\bullet}$ concentration triggers the reaction to form triphenylphosphine oxide accompanied by the inhibition of PET from the P(III) atom to the BODIPY fluorophore and a significant increase in the fluorescence intensity at 665 nm with the minimum detectable concentration of about 10 μM.

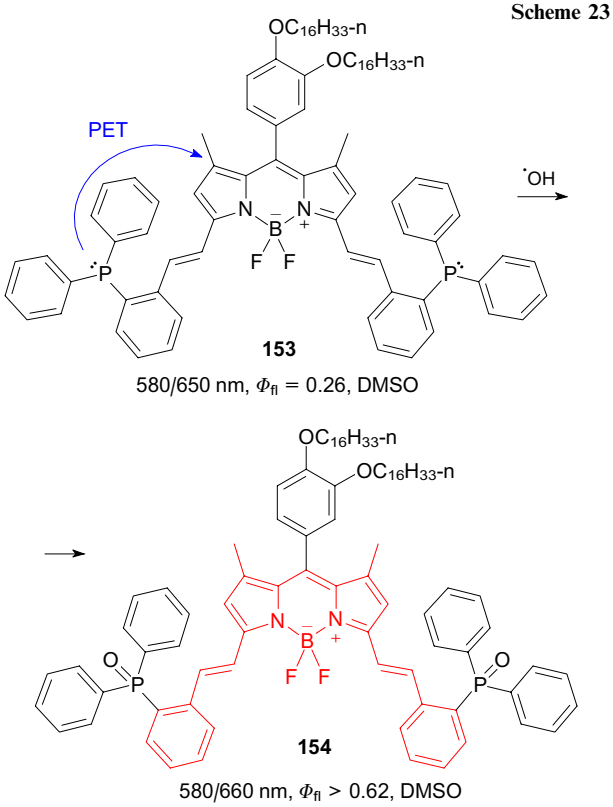
It was shown that sensor **151** is selective for hydroxyl radicals, and in the presence of other RONS, there is no noticeable increase in the fluorescence intensity of the sensor. Also, using the MTT assay, it was shown that compound **151** has almost no cytotoxicity, since more than 80% of the cells turned out to be viable after incubation with this compound in a wide range of concentrations (5 – 50 μM) for 24 h. The *in vitro* applicability of the synthesized sensor was demonstrated in HeLa cells.

Later on, analogous hydroxyl radical sensor **153** was synthesized on the basis of 3,5-bis(2-diphenylphosphino)-styryl-substituted BODIPY (Scheme 23).[264] When excited at 580 nm, compound **153** emits at 650 nm. Reaction product **154** has similar photophysical characteristics. However, **153** has a fluorescence quantum yield of 0.26 in DMSO, while compound **154** shows Φ_{fl} of more than 0.62. Therefore, compound **153** can be used as an HO$^{\bullet}$ sensor with switching on fluorescence in the presence of hydroxyl radicals. This compound is selective for hydroxyl radicals

Scheme 22



Scheme 23



and, in the presence of other RONS, there is no noticeable increase in the fluorescence intensity of the sensor.

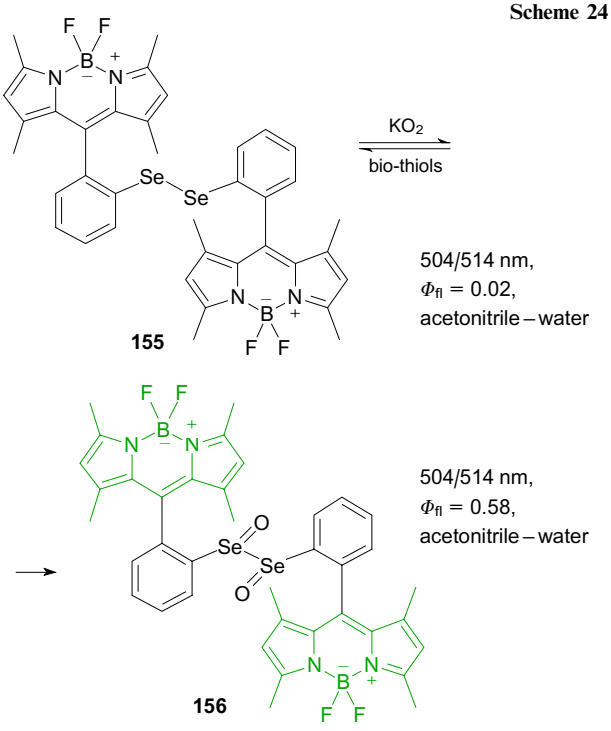
5.4.3. Superoxide anion radical

In large quantities, superoxide anion radicals (superoxide radicals, superoxide) are produced as an oxidative defense mechanism against external pathogens in phagocytic cells by the enzyme NADPH oxidase (NADP is nicotinamide adenine dinucleotide phosphate). Mutations in the gene encoding NADPH oxidase lead to immunodeficiency syndrome, the chronic granulomatous disease. The respiratory chain of mitochondria can also be a source of superoxide as a by-product. Since superoxide is toxic, its normal concentrations in the cell are maintained by the enzyme superoxide dismutase, which catalyzes the disproportionation reaction to form hydrogen peroxide and oxygen.

To date, several fluorescent sensors of superoxide radical based on selenium-containing organic compounds have been synthesized. Selenium exhibits strong antioxidant properties. Therefore, many synthetic sensors are based on the ability to mimic redox processes in the active sites enzymes.[265, 266] In particular, in the presence of $O_2^{-\bullet}$ bis(BODIPY) diselenide **155** undergoes selective oxidation to selenium oxide **156** accompanied by an increase in the fluorescence intensity at 514 nm (Scheme 24).[267] This reaction is reversible in the presence of various biothiols, such as glutathione and cysteine, which makes it possible to detect the dynamics of changes in superoxide concentration in living systems. The applicability of **155** as an intracellular sensor was confirmed using human breast cancer MCF-7/ADR cells.

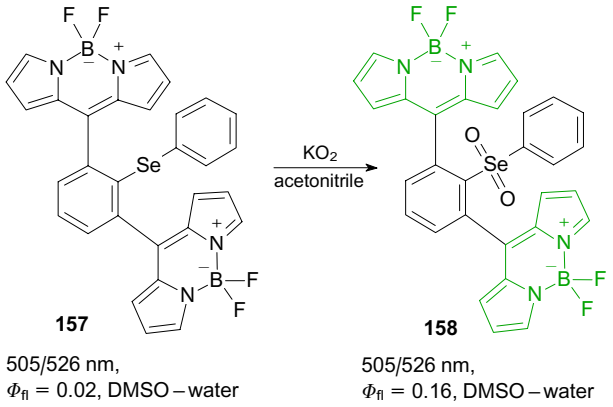
A highly sensitive and selective $O_2^{-\bullet}$ sensor based on selenium monosubstituted bis-BODIPY **157** (Scheme 25)[268] was synthesized. The excitation of original structure **157** with light causes reductive PET from the selenium atom to the BODIPY core, and thus compound **157** is virtually non-fluorescent. However, after the reaction with $O_2^{-\bullet}$, the resulting compound **158** shows an 11-fold increase in the fluorescence intensity at 526 nm. It was shown with MCF-7 cells that this derivative has satisfactory membrane permeability and can serve as an intracellular sensor of superoxide radicals with the lowest detectable concentration of 4.42 μM.

Scheme 24

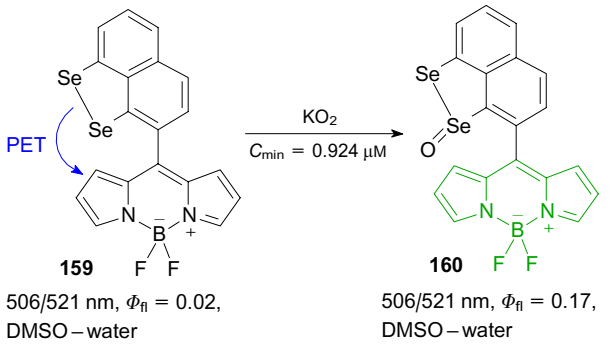


Another superoxide sensor is based on cyclic diselenide substituted BODIPY **159** (Scheme 26).[269] The reaction of **159** with the superoxide radical leads to a 9-fold increase in the fluorescence with the lowest detectable superoxide concentration of 0.924 μM. The reported quantum yield of oxidized product **160** is 0.17. The applicability of this sensor was demonstrated in the MCF-7 cell line. It was shown that compound **159** at concentrations of up to 100 μM is efficiently internalized by cells without losing their vital functions.

Scheme 25



Scheme 26

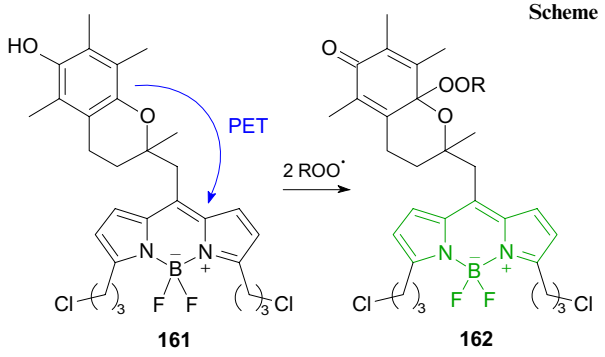


5.4.4. Peroxyl radical

The peroxyl radical ($HO_2^{\bullet}$), like its conjugated base superoxide, performs important biochemical functions, participating, in particular, in oxidation reactions with the antioxidant tocopherol (vitamin E), as well as in the oxidation reactions of polyunsaturated fatty acids that constitute the lipid bilayer of the cell membrane.[270] The lipid peroxidation affords lipid peroxyl radicals $ROO^{\bullet}$, which affects the properties of cell membranes and which ultimately can cause cell death.[271]

To monitor the real-time formation of lipid peroxyl radicals in the membrane, fluorogenic analogues of α-tocopherol were synthesized,[272, 273] which include the BODIPY substituent as a lipophilic site. As a result, the sensor molecule mimics the oxidation reaction of tocopherol with a simultaneous increase in the fluorescence intensity. Highly sensitive sensor **161** was recently synthesized to detect trace

Scheme 27



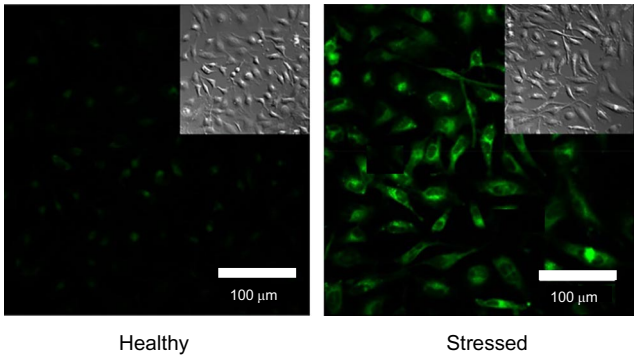
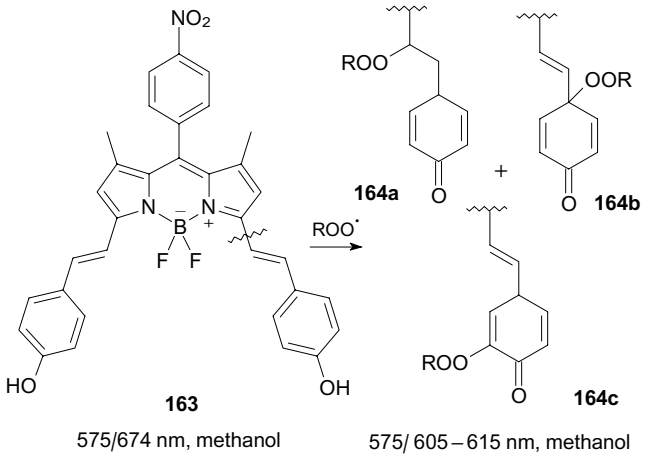


Figure 31. HeLa cells after incubation with compound **161**.[274] Fluorescence microscopy images were obtained upon excitation at 488 nm. The inset shows the scaled-down images of cells in the transmitted light for the same area. Adapted with permission from the American Chemical Society. Copyright (2017) [L.E.Greene, R.Lincoln, G.Cosa. *J. Am. Chem. Soc.*, **139**, 15801 (2017)].

Scheme 28



amounts of lipid peroxyl radicals.[274] The reaction with ROO$^{\bullet}$ yields compound **162** (Scheme 27) characterized by a 1000-fold higher fluorescence intensity, which makes it possible to use this sensor both under conditions of oxidative stress (Fig. 31) and under normal cellular homeostasis. Experiments with the HeLa cell line under normal conditions showed that the cells produce about 33 nM of lipid peroxyl radicals per hour.

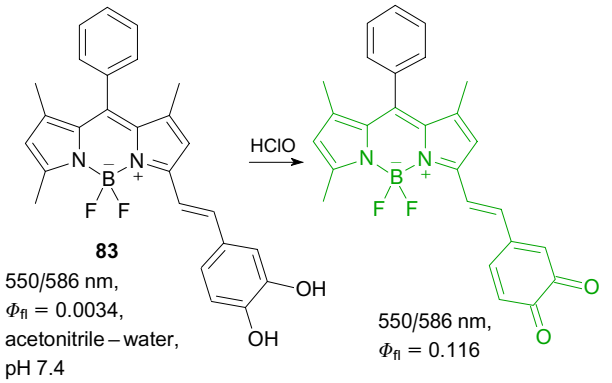
Recently, sensor **163** (Scheme 28) was synthesized.[275] The reaction with peroxyl radicals yields three isomeric addition products **164a – c** (Scheme 28). These compounds exhibit a 14-fold higher fluorescence intensity in methanol and a 4-fold higher intensity in artificial micelles.

5.4.5. Hypochlorous acid

A highly reactive short-lived hypochlorite ClO^- anion (HClO, hypochlorous acid) is produced in neutrophils by myeloperoxidase-catalyzed Cl^- oxidation.[276,277] This anion is involved in protecting the body, shows antibacterial and anti-inflammatory properties and serves as an adjuvant in adaptive immunity. On the other hand, excessive concentrations of hypochlorite ion can cause various diseases, such as arthritis, cancer, cardiovascular and neurodegenerative diseases and some others.[278] Therefore, the design of highly selective and sensitive sensors for the detection of hypochlorite anions is considered to be a key challenge for studying the role of ROS in these diseases.[279]

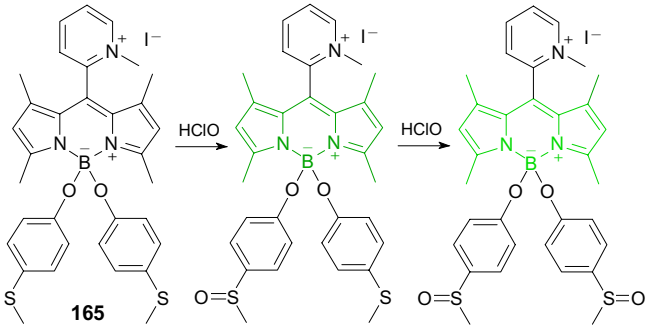
Hypochlorous acid is a strong oxidizing agent. Therefore, redox reactions can provide the basis for the sensing mechanism of HClO indicators. It was shown that the dihydroxystyryl substituent at the 5-position of BODIPY (compound **83**) can serve as the sensing group of HClO (Scheme 29).[130] In its free form, **83** shows almost no fluorescence at 586 nm; however, a significant rise of the fluorescence intensity is observed with increasing HClO concentrations due to oxidation of hydroxyl groups. In this work, it was demonstrated that **83** is selective for HClO in comparison with other RONS representatives. Also, by means of sub-diffraction microscopy using the transformed mouse macrophage cell line RAW 264.7, it was shown that **83** mainly accumulates in lysosomes and the Golgi apparatus (see also Section 3.3).

Scheme 29



In the study,[280] two methylmercaptophenoxy groups bound to the BODIPY boron atom were used as an HClO sensor (compound **165**). Due to the presence of the a quaternized pyridinium nitrogen atom in the *meso* position, this derivative has significant solubility in water. In the initial form, it virtually non-fluorescent (Φ_{fl} = 0.0013) due to PET between methylmercaptophenoxy groups and the BODIPY core. An increase in the HClO concentration leads to the stepwise oxidation of the thioether groups to mono- and then disulfoxide derivatives (Scheme 30). This is accompanied by an increase in the fluorescence intensity first at 545 nm and then at 562 nm, which makes it possible to detect HClO in wide concentration ranges. The possibility of using the synthesized sensor in living cells has been

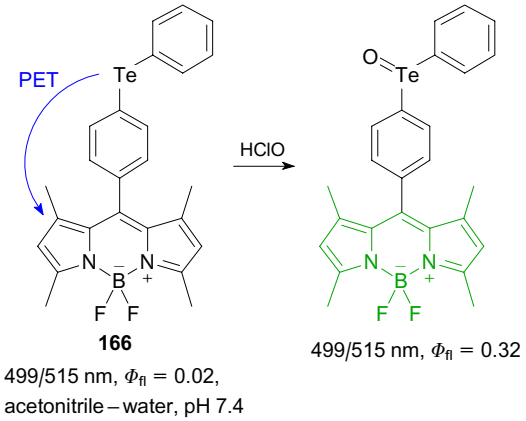
Scheme 30



successfully demonstrated in the cervical cancer HeLa cell line.

In a recent work,[281] tellurium BODIPY derivative **166** was used as a selective fluorescent HClO sensor. In an unoxidized form, compound **166** is virtually non-fluorescent, but with an increase in ClO^- concentration, it acquires bright-green fluorescence as a result of inhibition of PET between the tellurium atom and the BODIPY core (Scheme 31). The applicability of **166** as an intracellular HClO sensor was demonstrated by confocal microscopy of RAW264.7 and the human liver cancer cell line HepG2.

Scheme 31

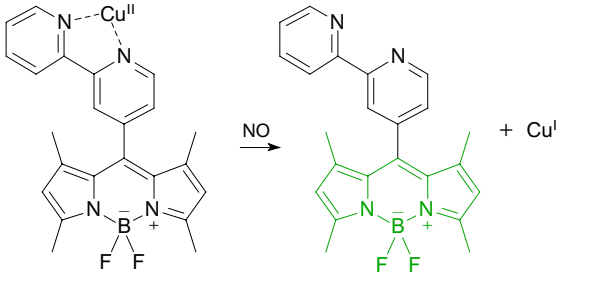


5.4.6. Nitrogen(II) oxide

Nitric(II) oxide is an important regulator and mediator in various processes of nervous, immune and cardiovascular systems [282] and its synthesis in the body is catalyzed by the specific enzyme, NO synthase.[283] Three isoforms of this enzyme were characterized: endothelial, neuronal and inducible. Dysregulation of NO synthesis can cause various diseases, such as neurodegenerative disorders and cancer.[284] Nitric(II) oxide possesses the properties of a free radical and has a high reactivity, undergoing both oxidation and reduction reactions. Therefore, the NO detection is complicated due to instability and its low concentrations in living cells.

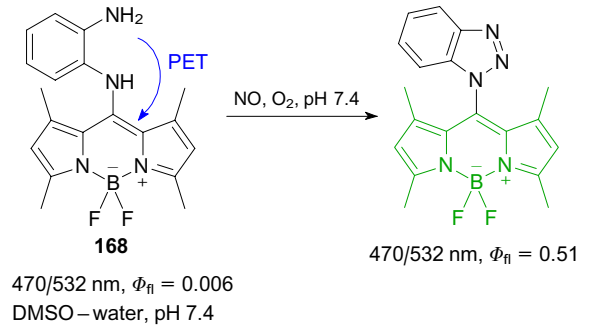
Several BODIPY-fluorophore based sensors for the determination of the intracellular NO concentration were synthesized. The activity of these sensors is based on either the NO-induced cyclization of *o*-phenylenediamine, yielding benzotriazole,[74, 285] or on the formation of NO complexes with metals. Costero and co-workers [286] synthesized a complex of divalent copper with BODIPY bipyridine derivative **167** (Scheme 32). In the presence of NO, divalent copper is reduced to the monovalent state accompanied by the decomposition of the complex with the metal and a significant increase in the fluorescence intensity at 520 nm. The possibility of the application of the sensor in *in vitro* experiments was demonstrated using RAW 264.7 cells.

Scheme 32



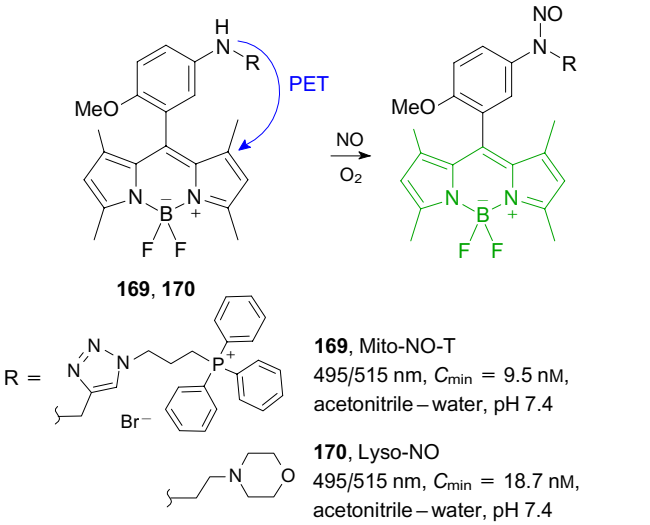
The addition of *o*-phenylenediamine *via* one of its amino groups to the BODIPY core in the *meso* position gave fluorogenic sensor **168** (Scheme 33).[287] In contrast to neutral pH, under strongly acidic conditions (pH = 0 – 1), this sensor allows the selective detection of nitrite ions. At neutral pH, in its original form, **168** is virtually non-fluorescent as a result of PET from *o*-phenylenediamine to the BODIPY core; however, an increase in the NO concentration leads to a significant rise of the fluorescence intensity at 532 nm. The possibility of using this derivative as an intracellular NO sensor has been demonstrated in HepG2 cells.

Scheme 33



Earlier studies have shown that NO is directly involved in physiological and pathological processes in mitochondria and lysosomes.[288,289] It is known that it is in mitochondria where nitric(II) oxide is produced by the inducible NO synthase.[290] In a recent work,[291] highly sensitive and selective fluorescent sensors with a minimum detectable NO concentration reaching 5.7 nM were created on the basis of meso-5-amino-2-methoxyphenyl BODIPY. For targeted delivery to mitochondria and lysosomes, triphenylphosphonium or morpholine moieties were introduced into the sensor structure, respectively (Scheme 34). In their original state, both **169** and **170** sensors do not exhibit fluorescence; however, after the reaction with NO, a significant increase

Scheme 34



in the fluorescence intensity is observed at 515 nm in a wide pH range. Using the MTT assay and flow cytometry, these compounds were shown to have low toxicity, which allows them to be used in experiments with living cells. The possibility of using **169** and **170** as intracellular NO sensors was demonstrated in HeLa cells.

5.4.7. Nitroxyl

Nitroxyl (HNO) is a reduced and protonated analogue of nitric oxide. However, unlike nitric oxide, there is currently no experimental evidence for the biosynthesis of HNO *in vivo* as an endogenous signaling molecule.[292] Only a few studies reported evidence of the possible role of NO synthases, which can participate in the HNO synthesis under certain conditions, especially at low concentrations of the cofactor.[293] Probably, the shortage of information on the biological role of nitroxyl is associated with the lack of highly selective and sensitive sensors of HNO.[294, 295]

Previously, a number of HNO sensors based on copper-containing compounds were created.[296, 297] However, the detection of nitroxyl using these sensors is complicated by the presence of reducing agents in living cells, such as glutathione and ascorbate. Later, NIR metal-free sensor **171** was synthesized for the *in vitro* and *in vivo* detection of nitroxyl.[298] The sensor consists of two components: aza-BODIPY as a fluorescent module and an HNO sensing module composed of two diphenylphosphine benzoyl groups. The proposed mechanism of the reaction of sensor **171** with HNO is presented in Scheme 35.[298]

Compound **171** is highly sensitive and selective for nitroxyl. With increasing HNO concentrations, the fluorescence intensity at 734 nm significantly increases with the minimum detectable concentration of 30 nM. During the reaction with HNO, the fluorescence quantum yield of the sensor increases from 0.02 to 0.35. The MTT assay showed that more than 90% of RAW 264.7 cells remain viable during incubation in 100 μM sensor solution for 24 h. Using confocal laser scanning microscopy, it was shown that sensor **171** is predominantly localized in the cytoplasm of RAW 264.7 cells, which makes it possible to quantitatively and qualitatively detect HNO in the intracellular space. The *in vivo* applicability of the sensor was also demonstrated in living mice (Fig. 32).

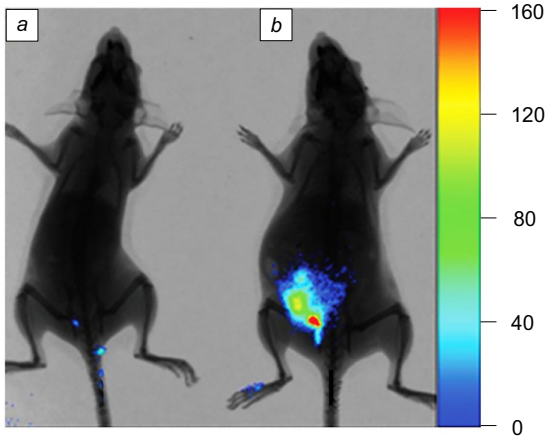
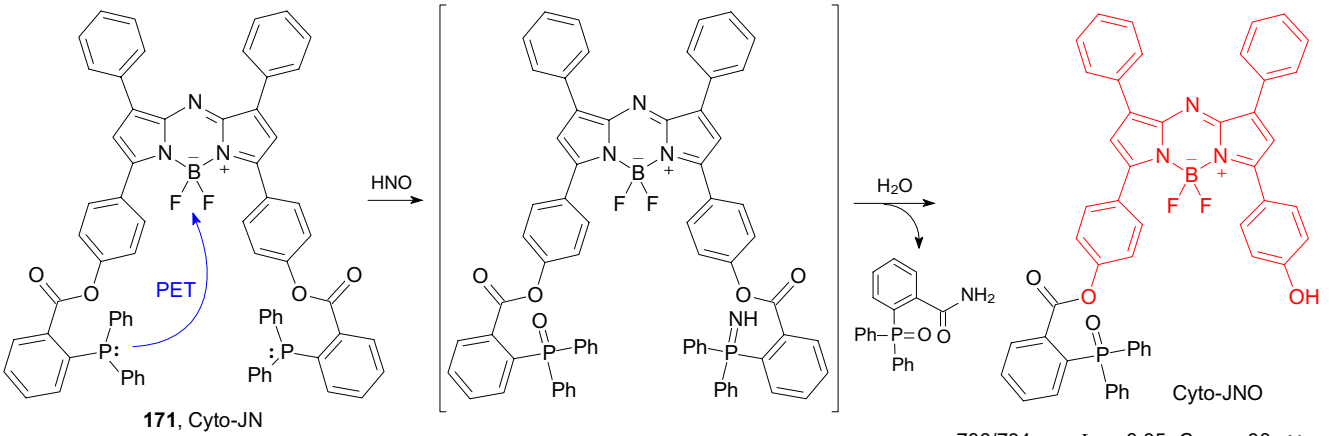
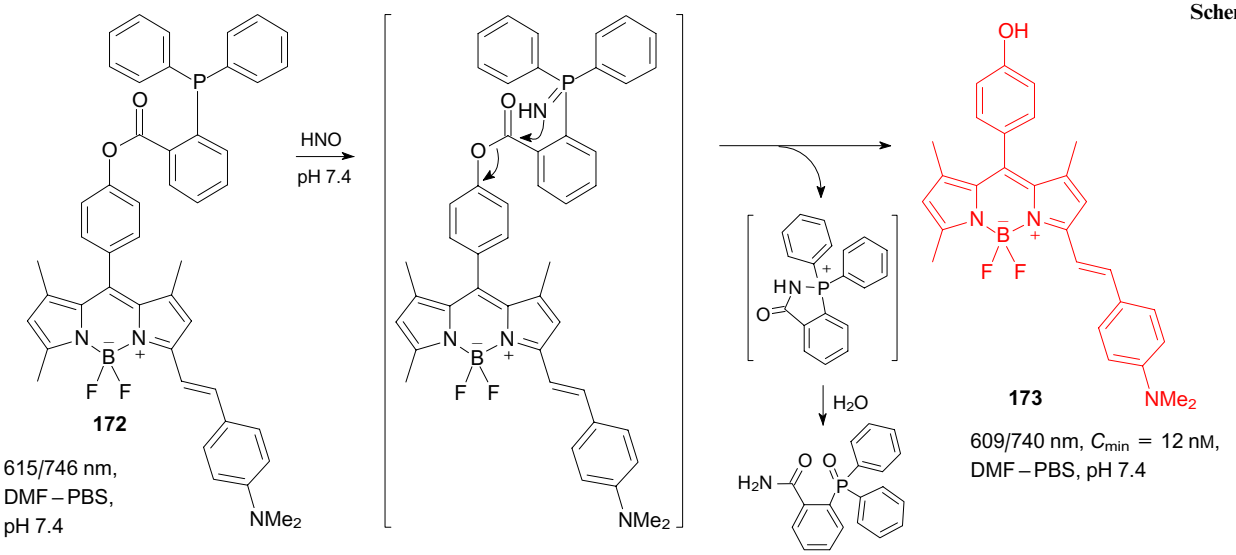


Figure 32. Visualization of HNO levels in living BALB/c mice using compound **171**. Fluorescence/X-ray images of the mice after intraperitoneal injection of compound **171** (*a*) and after the subsequent injection of compound **171** with Angeli's salt ($Na_2(ONNO_2)$) as a source of HNO (*b*). Excitation at 680 nm; the images were taken from the 700 nm fluorescence window.[298] Published with the permission from Royal Society of Chemistry.

Scheme 35

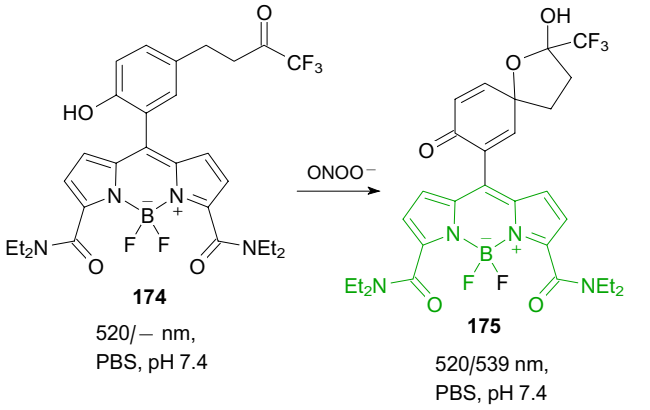


Scheme 36



In a recent work,[299] a highly selective and sensitive NIR fluorescent probe for HNO (Scheme 36) was synthesized. Compound **172** contains the 2-(diphenylphosphino)benzoate moiety in the *meso* position as a sensing part, which selectively reacts with HNO. Since diphenylphosphinobenzoate has electron-donating properties, fluorescence quenching of **172** occurs due to the PET effect. As a result of the reaction of **172** with HNO, phosphine oxide is released to give compound **173**, which has a fluorescence intensity at 740 nm 2.5 times higher than that of initial compound **172**. Meanwhile, only a slight change in fluorescence is observed in the presence of other forms of RONS in the pH range of 4 – 10. Experiments in the HeLa cell line revealed insignificant cytotoxicity of compound **172** (IC_{50} > 50 μM) and, consequently, this compound can be used as a highly sensitive intracellular HNO sensor.

Scheme 37

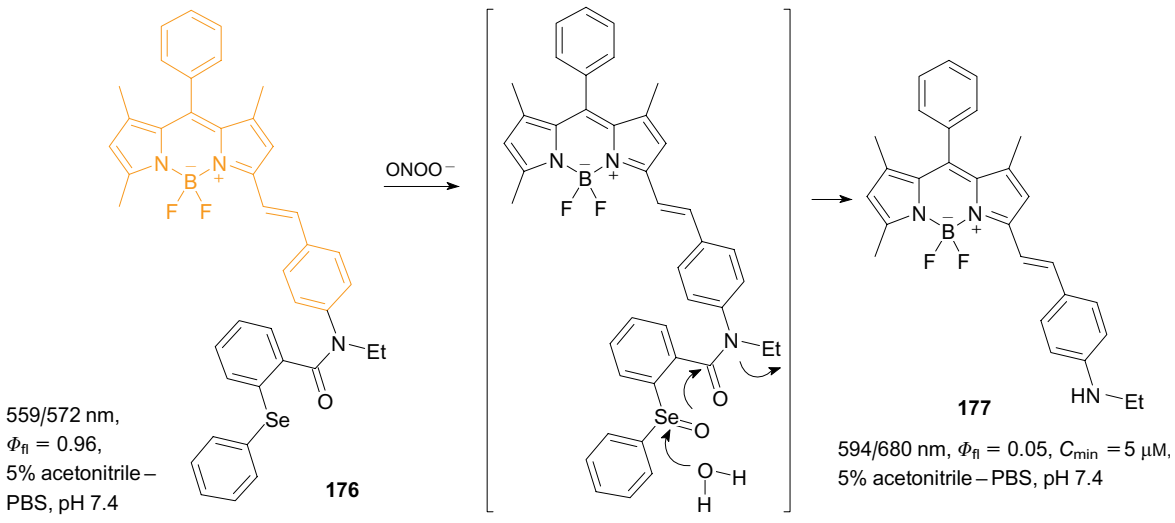


5.4.8. Peroxynitrite

In living organisms, peroxynitrite ($ONOO^-$) is produced by the reaction between nitric(II) oxide and superoxide.[300, 301] In a normally functioning organism, the $ONOO^-$ level is precisely controlled. However, elevated concentrations of peroxynitrite can cause a variety of pathologies such as cardiovascular and neurodegenerative diseases.[302]

Yang and co-workers[303] synthesized sensitive and selective sensor **174** for the intracellular $ONOO^-$ detection (Scheme 37). This sensor is based on intramolecular cyclization in the presence of peroxynitrite. This reaction results in the blocking of PET and a significant increase in the fluorescence intensity (69-fold increase in the presence of 7 equivalents of $ONOO^-$) of **175** at 539 nm. The synthe-

Scheme 38



sized sensor was successfully used for the intracellular detection of $ONOO^-$ in the J774.1 cell line (murine macrophages from BALB/c females).

In a study,[304] the spirocyclization of the intermediate selenium oxide was used for the peroxynitrite detection. Compound **176** (Scheme 38) shows bright fluorescence at 572 nm; however, the absorption maximum of compound **177** shifts to 594 nm as a result of the reaction with $ONOO^-$, and fluorescence quenching is observed due to the ICT effect. Using confocal microscopy and the RAW264.7 cell line, it was shown that this compound can be used for the determination of intracellular peroxynitrite concentrations.

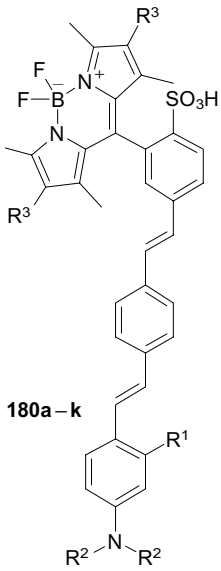
Zhao *et al.*[305] synthesized two compounds based on BODIPY with minimal structural differences in their sensing parts. It was shown that compound **178a** with a 4-hydroxyaniline substituent selectively reacts with $ONOO^-$ and does not react with HClO and other RONS. On the contrary, compound **178b** with a 4-methoxyaniline substituent has high selectivity towards HClO. In the original form, **178a** and **178b** (Scheme 39) are virtually non-fluorescent due to the PET effect. In the presence of 7 μM $ONOO^-$, a significant increase in the fluorescence of **179a** at 530 nm (λ_{ex} = 519 nm) is observed with a 150-fold increase in Φ_{fl} and with a minimum detectable concentration of 8.2 nM. In contrast to **179a**, product **179b** is characterized by insignificant changes in the emission spectra in the presence of $ONOO^-$. On the contrary, in the presence of HClO, its maximum in the absorption spectrum undergoes a hypsochromic shift from 575 to 519 nm with a significant increase in the fluorescence intensity at 528 nm. The minimum detectable concentration of HClO is 6.8 nM. The applicability of **178a**,**b** as intracellular sensors was demonstrated in the RAW264.7 cell line.

5.5. Membrane potential sensor

Fluorescent dyes are important tools for visualizing the electrical activity of neurons.[306] Synthetic sensors of the cell membrane potential are usually based on the photoinduced electron transfer from the electron-donating part of the molecule *via* a membrane-spanning molecular wire, consisting of a conjugated *para*-phenylenevinylene chain, to the fluorophore. A necessary condition for the functioning of the sensor is the hydrophilicity of the fluorophore, which should be located on the surface of the plasma membrane, directing the lipophilic molecular wire with an electron-donating substituent into the lipid bilayer. During membrane depolarization, PET is suppressed with a simultaneous increase in the fluorescence intensity of the sensor.

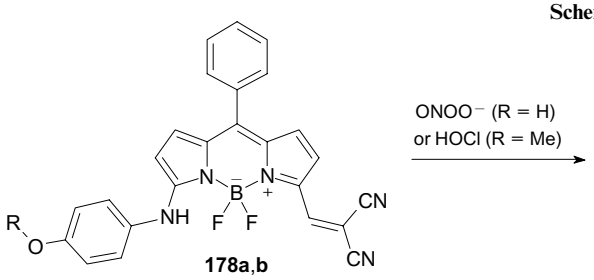
This principle of the sensor construction was applied in a number of BODIPY derivatives with hydrophilic sulfonated aromatic groups in the *meso* position and various substituents in the 2- and 6-positions (compounds **180a**–**k**).[307] An *p*-phenylenevinylene chain with a terminal tertiary amino group as an electron donor was used as a conductor (Fig. 33). The potential sensitivity of the synthesized sensors correlates with the electron-withdrawing force of the substituents in the 2- and 6-positions: stronger electron-withdrawing groups impart greater sensitivity to the sensor [Et < H < CO_2H < C(O)NHR > CN]. It was demonstrated that the sensor can be used to monitor the dynamics of the action potential in mammalian neurons and human cardiomyocytes. Among the synthesized sensors, compound **180e** showed the highest brightness, compound **180j** had the greatest response to changes in the membrane potential, and compound **180i** showed the best balance between brightness and sensitivity.

Structures 180



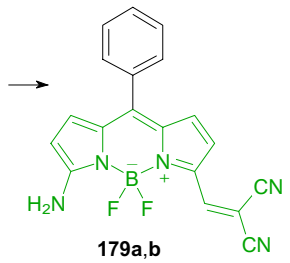
Compound	R^1	R^2	R^3
180a	H	Me	Et
180b	OMe	Me	Et
180c	H	Me	H
180d	Me	Me	H
180e	OMe	Et	H
180f	H	Me	CN
180g	H	Me	CO_2H
180h	Me	Me	CO_2H
180i	OMe	Et	CO_2H
180j	H	Me	$C(O)NHCH_2CO_2Me$
180k	Me	Me	$C(O)NHCH_2CO_2Me$

Scheme 39



R = H (**178a**): 577/530 nm, Φ_{fl} = 0.0002

R = Me (**178b**): 575/528 nm, Φ_{fl} = 0.0005, 1 mM CTAB, PBS, pH 7.4



R = H (**179a**): 519/528 nm, Φ_{fl} = 0.03, C_{min} = 8.2 nM;

R = Me (**179b**): 519/528 nm, Φ_{fl} = 0.05, C_{min} = 6.8 nM, 1 mM CTAB, PBS, pH 7.4

CTAB is cetyltrimethylammonium bromide

5.6. Viscosity and temperature sensors

Viscosity is one of the key parameters of the medium that has a noticeable impact on the diffusion rate of various substances, including biologically important ones. Changes in the mobility of intracellular mediators can lead to malfunctions in cellular processes, such as cell signaling involving short-lived intermediates, such as ROS. In living systems, a change in viscosity can lead to various cell dysfunctions and cause a number of diseases.[308]

Currently, fluorescent molecular rotors are used to measure intracellular viscosity. These fluorophores are characterized by non-radiative relaxation of the excited

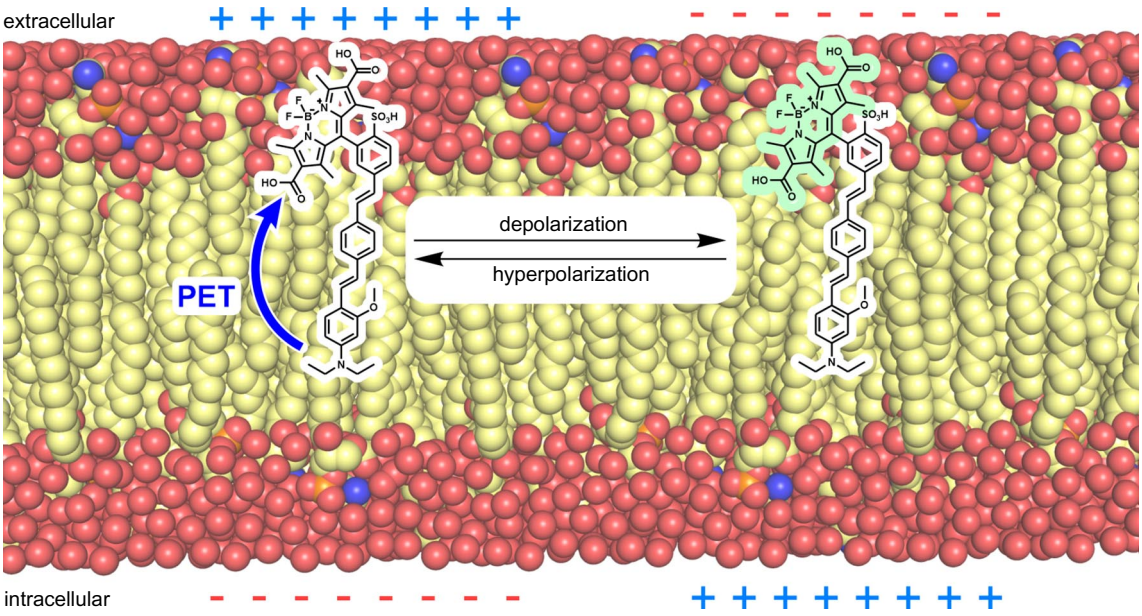


Figure 33. Fluorescence turn-on and turn-off of compound **180i** during membrane depolarization – hyperpolarization. Membrane atoms are represented by yellow (carbon), blue (nitrogen) and red (oxygen) balls. The figure was created by the authors on the basis of the Ref. 307.

state, which is typical of the free rotation of aryl groups attached, in particular, at the BODIPY *meso* position (Fig. 34 *a*), and results in lower quantum yields ($\Phi_{\text{fl}} \sim 0.06$) and fluorescence lifetimes (τ) (~ 500 ps).[309] The restriction of the rotational freedom of the molecular rotor in a viscous medium suppresses the non-radiative relaxation of the excited S_1 state, resulting in an increase in Φ_{fl} and τ.[125, 310] However, measurements of intracellular viscosity based on changes in the fluorescence intensity are not always correct, since they depend on the sensor concentration. To cope with this drawback, fluorescence lifetime imaging microscopy is used, since the concentration of the dye virtually does not affect the detected fluorescence lifetimes.[311] Moreover, the higher the concentration, the faster it is possible to accumulate data and minimize the contribution of cellular autofluorescence.

In recent years, a number of fluorescent molecular rotors based on BODIPY derivatives were synthesized.[312] To measure the local intracellular viscosity, Kuimova *et al.*[125] synthesized BODIPY derivative **75** (see Fig. 34 and also Section 3.1) bearing a *para*-alkoxy-substituted phenyl group in the *meso* position. Measurements in living cells were performed using FLIM. The reported data indicate that sensor **75** in SKOV-3 cells is localized in the environment about 2 times more viscous than water or the cytoplasmic milieu of the cell. The intracellular localization of this sensor is probably determined by the presence of a hydrophobic C_{12} hydrocarbon chain, which may facilitate its inclusion into intracellular organelles, where the viscosity is increased.[313]

Previously, Yang *et al.*[315] prepared sensors specifically bound to the lipid membrane for viscosity measurements of the lipid bilayer. However, the application of these sensors for measuring viscosity of the cytoplasmic membrane was complicated by their active endocytosis in living cells.[125, 316] As a result, compounds like **75** with a C_{12}-hydrocarbon chain accumulate predominantly in the membranes of intracellular organelles. To prevent endocytosis, molecular rotor

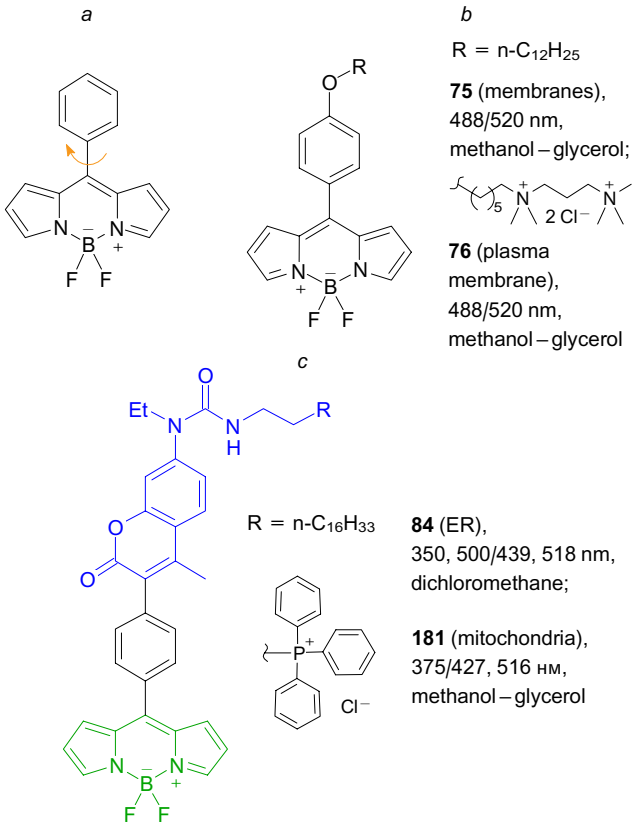


Figure 34. BODIPY-based viscosity sensors: the general structure of the rotor for measuring intracellular viscosity (*a*); viscosity sensors with localization in membrane structures (*b*) in ER and mitochondria (*c*).[115, 126, 131, 315]

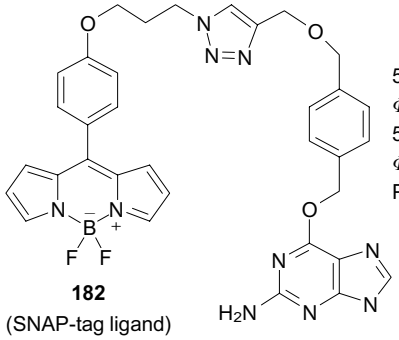
76 with a hydrocarbon chain including two positively charged ammonium groups was created[126] (see Fig. 34 and

also Section 3.1). This sensor selectively binds to the plasma membrane in SK-OV-3 cells. The most selective staining of the plasma membrane was observed during incubation of SK-OV-3 cells with the dye at 4 °C for less than 30 min in the medium deficient in Mg^{2+} and Ca^{2+}.

BODIPY–coumarin conjugates enable viscosity measurements from the ratio of the fluorescence intensities of two fluorophores. Compounds **84**, **181** (see Fig. 34) were used for the ratiometric determination of viscosity in various cell compartments. Thus, the introduction of a long aliphatic substituent C_{18} (compound **84**) into the probe led to the localization of the compound in the ER membrane,[131] while the triphenylphosphonium substituent (compound **181**) targeted the dye to mitochondria[314] (see also Sections 3.3 and 3.4)

To study the local viscosity in the microenvironment of a particular protein, a hybrid sensor was created consisting of a molecular rotor based on BODIPY, which is bound to O^6-benzylguanine as a substrate for SNAP-tag (compound **182**).[317] Using compound **182**, specific labelling of the histone H2B and the mitochondrial protein COX8A was performed in cells expressing SNAP-tag constructs of these proteins. Measurements of the fluorescence lifetime upon two-photon excitation showed that viscosity of the medium in the microenvironment of these proteins is different.

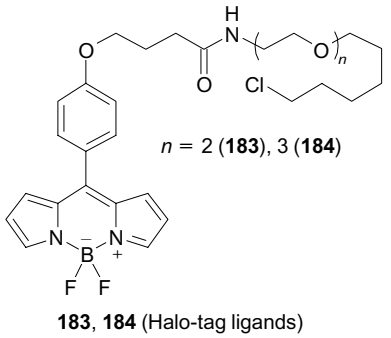
Structure 182



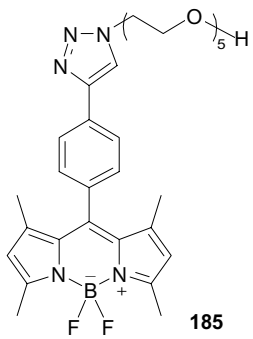
182
(SNAP-tag ligand)

A similar approach was applied using the HaloTag technology.[318] Two BODIPY derivatives **183** and **184** were synthesized with a molecular rotor containing a chlorine atom at the end and acting as a substrate of the haloalkane dehalogenase enzyme. It was shown that both compounds penetrate the cell membrane, which allows labelling of proteins with intracellular localization and the measurement of the viscosity of the environment using FLIM. It was also shown that the Halo-tag constructs of proteins labelled by the sensor with a longer rotor chain undergo photoinduced fluorophore degradation during prolonged exposure to light, whereas the shorter-chain construct is more photostable.

Structures 183–185



183, **184** (Halo-tag ligands)



185

Some BODIPY-based molecular rotors are sensitive not only to viscosity but also to temperature. In order to impart temperature sensitivity to the compound, the 1,3,5,7-tetramethyl-*meso*-phenyl derivative of BODIPY was modified by the addition of a polyethylene glycol chain.[319] With increasing temperature, the degree of non-radiative relaxation of the fluorophore **185** increases with a simultaneous decrease in its lifetime. The change in the lifetime is associated with both the changes in temperature and viscosity at low values of the latter parameter. In a high viscosity medium, the lifetime depends only on temperature. Since PEG-modified BODIPY penetrates the cell membrane, the probe can be used as an intracellular temperature sensor in the FLIM method.

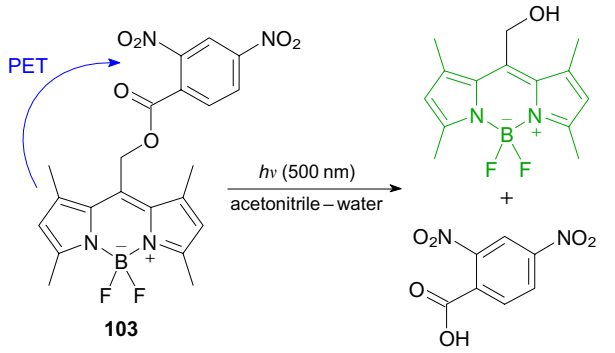
BODIPY derivatives were also used to create molecular viscosimeters for determining the viscosity in cellular organelles, such as lysosomes,[320, 321] the endoplasmic reticulum[322] and mitochondria.[323]

6. BODIPY phototransformable reporters

Live cell fluorescent reporters can be divided into two groups: stable and phototransformable.[324–326] The main requirement for stable reporters is invariability of photophysical properties, which should not significantly change under different external conditions. In contrast, phototransformable reporters are fluorescent molecules whose optical properties can be controlled by light of a specific wavelength, with a specific intensity and pulse duration. Phototransformable reporters can be further divided into photoactivatable, photoswitchable and photoconvertible ones. The former undergo an irreversible transformation from a non-fluorescent to fluorescent state when irradiated with light. The second turn on and off fluorescence when irradiated with light of two specific wavelengths. Photoconvertible reporters irreversibly change the colour of fluorescence upon exposure to light of a certain wavelength. Using phototransformable reporters, it is possible to track spatiotemporally specified cell populations, individual intracellular organelles and molecules of interest. In addition, phototransformable probes are used for the visualization of intracellular structures using sub-diffraction microscopy, which allows visualization of these structures with nanometer resolution.[327–330]

One way to create photoactivatable BODIPY derivatives is to use the photoinduced covalent bond cleavage between a fluorophore and a quencher.[128, 172, 331, 332] To switch-on the fluorescence of fluorophores of this type, preliminary irradiation at the wavelength that promotes photolysis is required, and afterwards, the fluorophore is exposed to light of an appropriate wavelength to excite fluorescence. Typically, quenchers are electron-donating or electron-withdrawing groups involved in PET with the BODIPY core. An ester group linked to the BODIPY core *via* a methylene unit in the *meso* position is usually employed as the bond susceptible to photolytic cleavage.[138, 139] In particular, 2,4-dinitrobenzoic acid is used as a quencher.[138] In its original form, compound **103** is almost non-fluorescent, but when irradiated with light of 500 nm, a photolysis reaction occurs with the release of the quencher and a subsequent increase in the fluorescence intensity

Scheme 40



(Scheme 40). The applicability of compound **103** as an intracellular photoactivatable reporter was demonstrated using *S*2 *Drosophila melanogaster* cells (Fig. 35).

Photoswitchable reporters can also be prepared by combining a photochromic component and a fluorescent module in the same molecule. The photochromic component usually undergoes reversible light-dependent photoisomerization to form an isomer with absorption spectra different from that of the initial state, which ultimately affects the properties of the fluorescent component. In 2005, Neckers and co-workers[333] synthesized BODIPY derivatives, in which the dithienyl derivative (DTE) of hexafluorocyclopentene **186** was used as the photochromic moiety. Compound **186** exhibits bright fluorescence in the ring-opened state, while in the case of isomerization to the ring-closed state, fluorescence quenching is observed (Scheme 41). It was proposed that fluorescence quenching is a consequence of intramolecular energy transfer from the excited fluorophore to the dithienylethene ring-closed form. The fluorescence on/off switching cycles can be repeated many times without significant loss of fluorescence intensity.

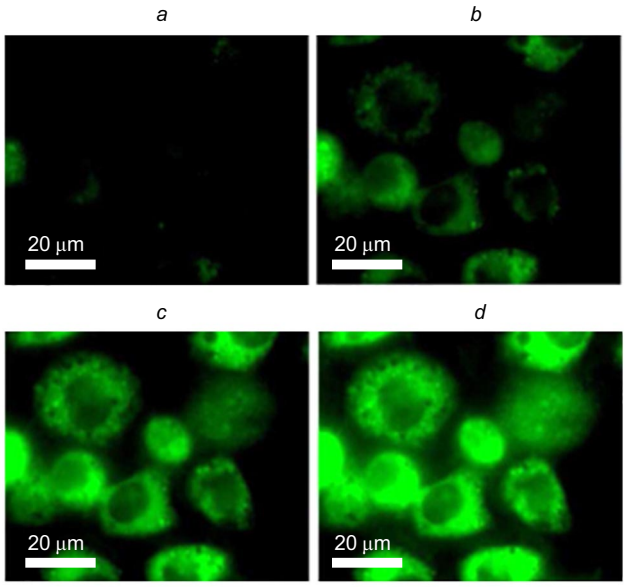
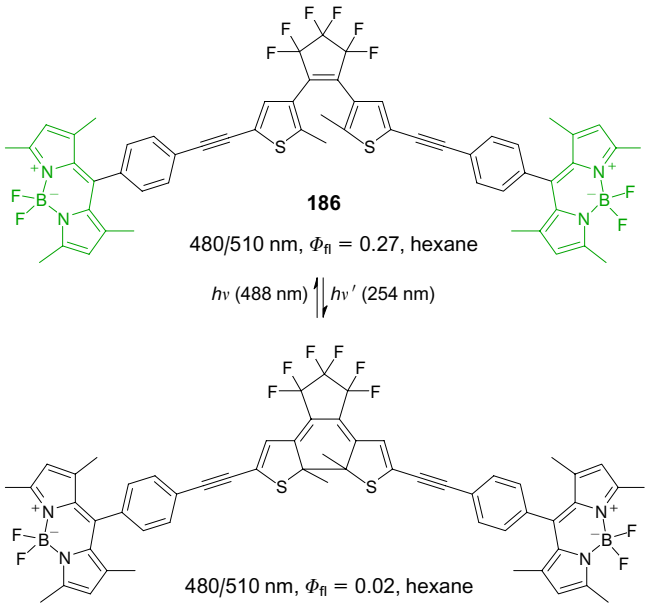


Figure 35. Changes in the fluorescence intensity of *S*2 cells after incubation with compound **103** as a function of the illumination time with 500 nm light. Images were taken after the exposition for 0 (*a*) 0.5 (*b*), 1 (*c*) and 2 s (*d*).[138]

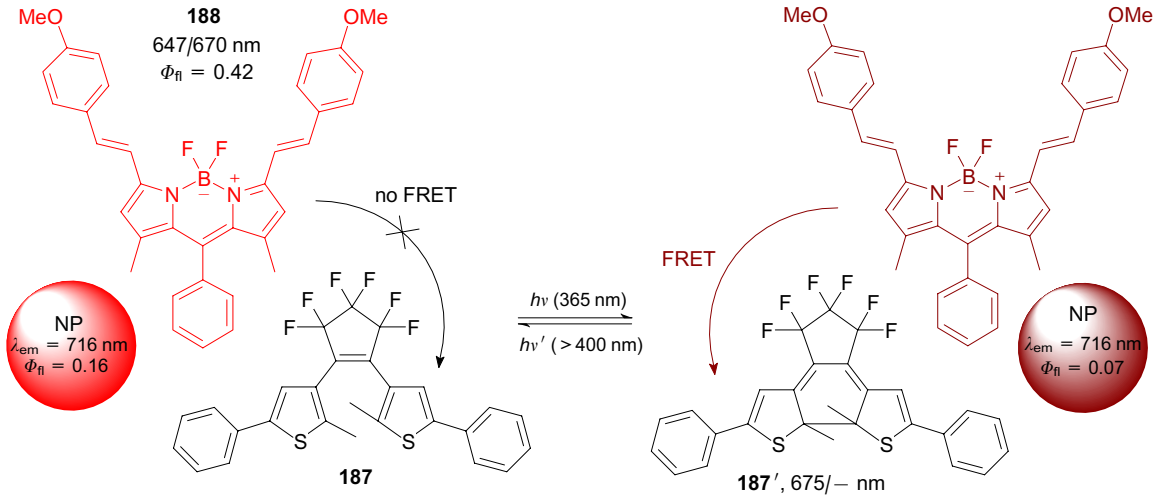
Scheme 41



Han and co-workers[334] synthesized photoswitchable nanoparticles with encapsulated DTE (**187**) and distyryl derivatives of BODIPY (**188**) as the fluorophore.When nanoparticles are irradiated with UV light, the closed state of DTE **187** is formed with an absorption maximum facilitating efficient FRET from the BODIPY fluorophore to DTE (Scheme 42), which results in fluorescence quenching. Upon visible light exposure, the DTE switches to its ring-opened state, the absorption maximum of which does not overlap with the emission of the fluorophore, and the fluorescence is restored. Nanoparticles were synthesized from a copolymer (styrene – maleic anhydride) and contained PEG chains on their surface (Fig. 36 *a*) to improve biocompatibility. Due to the presence of styryl derivative of BODIPY **188**, the particles exhibit emission spectra in the NIR region. Upon UV lamp irradiation, efficient quenching of fluorescence is observed ($\Phi_{fl} = 0.07$). However, after visible light exposure, the fluorescence is almost completely restored (see Fig. 36 *b*). Using the HeLa cell line, it was shown that these nanoparticles have insignificant cytotoxicity (45 μg ml^{-1}) and good membrane permeability with bright intracellular fluorescent staining. After 5 min irradiation of cells with UV light the fluorescent staining of cells was significantly reduced and it was restored after illumination with visible light (see Fig. 36 *c*).

Photoswitchable reporters were also synthesized based on 2*H*,3*H*-indole-2*H*,4*H*-benzo[1,3]oxazines as photochromic substituents in the BODIPY structure (Scheme 43).[335] Upon the excitation of **189** with visible light ($\lambda = 437$ nm), fluorescence at 541 nm is observed, which is characteristic of the BODIPY fluorophore. However, upon irradiation with light of 355 nm (λ_{OFF}), the [1,3]oxazine ring of the photochrome opens to form a 3*H*-indolinium cation within less than 6 ns. The resulting cation is capable of accepting an electron or energy from the fluorophore core, resulting in fluorescence quenching of BODIPY. After that, the resulting isomer, which has a lifetime of 1 – 3 s, returns to its original state. This photochromic system can withstand hundreds of on/off switching cycles without any noticeable signs of photodegradation.

Scheme 42



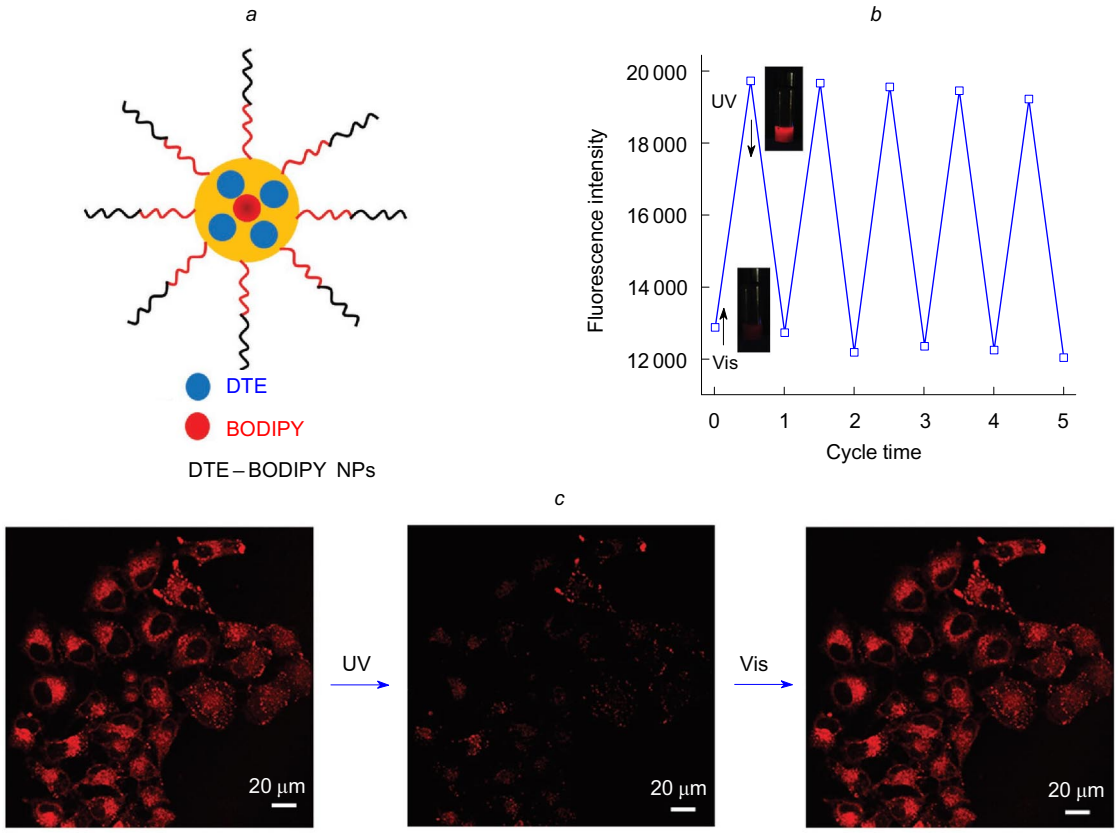
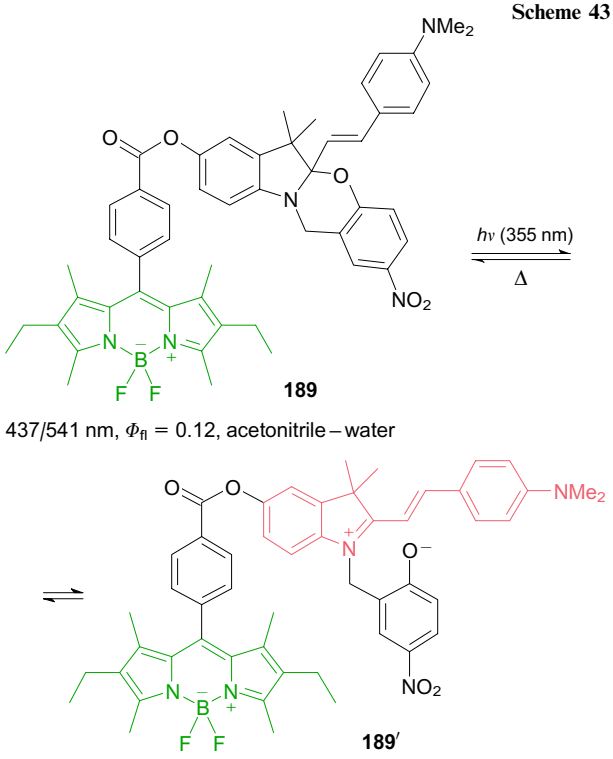


Figure 36. Structure of photoswitchable nanoparticles based on dithienyl derivative **187** and BODIPY **188** (*a*); fluorescence on/off switching in nanoparticles under illumination with visible (Vis) and ultraviolet light (*b*); fluorescence changes in nanoparticle-containing HeLa cells upon irradiation with UV/Vis light (*c*).[334] Published with the permission of Wiley Publishing house.

In the above example, the nitro group of the photochrome is located in the *para* position to the oxygen atom of the oxazine ring, resulting in a reversible photoreaction giving the 3H-indolinium cation. However, when the nitro group is transferred to the *meta* position of the benzene ring (compounds **190** – **192**), the photoreaction accompanied by the oxazine ring opening proceeds irreversibly with the release of 2-hydroxy-6-nitrosobenzaldehyde (Scheme 44).[336] Unlike fluorescence quenching upon formation of the 3*H*-indolinium cation, irradiation of compounds **190** and **191** with light at 350 nm results in photoreaction followed by the conjugation of π-electron systems of the indole heterocycle and BODIPY. This structural transformation irreversibly leads to a bathochromic shift in the absorption and emission spectra of BODIPY and to an increased quantum yield.

Some other photoconvertible reporters were also synthesized based on BODIPY and the oxazine system as an auxochrome,[337 – 339] in particular, compound **192**. Upon exposure to the activating light of 405 nm, compound **192**

Scheme 43



undergoes the irreversible oxazine ring opening followed by photoconversion yielding a product with fluorescence emission in the far-red and NIR regions (600 – 850 nm).[337] These reporters were used to obtain high-contrast images of the developing blastoderm embryo of *Drosophila melanogaster* with almost no background autofluorescence of the biological sample. In addition, sequential images acquired at certain time intervals made it possible to trace the movement of individual cells in the embryo in real time. Thus, the synthesized photoconvertible compounds can be used as molecular reporters for studying cellular dynamics *in vivo*.

7. Conclusion

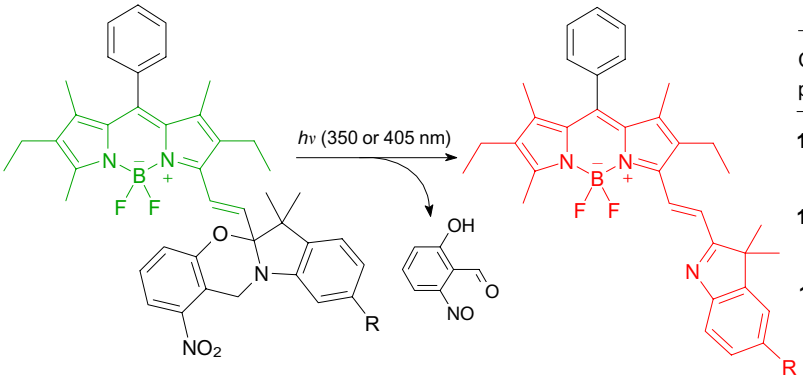
BODIPY-based fluorescent reporters are steadily turning into one of the indispensable tools for monitoring molecular processes in the living cell. These compounds display a high fluorescence quantum yield and photostability, narrow absorption and emission bands, neutral charge and low cytotoxicity. In this review, we provide an overview and a summary of recent advances in the area of fluorescent cellular reporters based on the BODIPY scaffold made mainly in 2015 – 2020. During this time, significant progress has been achieved in the synthesis of derivatives with photophysical properties necessary for bioimaging. In particular, BODIPY derivatives with an extended π-electron system of the fluorophore were synthesized by the incorporation of aromatic substituents into the central core of indacene. These derivatives exhibit fluorescence excitation and emission maxima in the far-red and NIR regions, which reduces phototoxicity, lowers the contribution of background autofluorescence and significantly decreases light scattering under fluorescence microscopy. However, BODIPY derivatives with the extended π-system suffer from a number of drawbacks, which are associated with the increased photodegradation, insufficient water solubility, aggregation in polar solvents and aggregation-caused quenching (ACQ). In this regard, attempts have recently been made to synthesize water-soluble BODIPY derivatives by attaching polyethylene glycol or oligosaccharide chains or by the incorporation of charged substituents. Furthermore, the encapsulation of these compounds into amphiphilic nanoparticles appears to be a promising way to prepare water-soluble BODIPY derivatives.

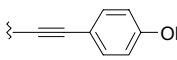
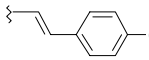
By the introduction of electron donating or electron withdrawing substituents, which can participate in PET, a series of sensors reporting on concentration changes of various intracellular components have recently been synthesized. A further introduction of specific functionalities into the BODIPY structure enables targeted delivery of these sensors to various intracellular compartments. Unfortunately, most of the BODIPY-based sensors are not suitable for quantitative measurements of concentrations. For this purpose, sensors based on the ICT or FRET effects enabling ratiometric measurements are in great demand.

The living cell is a complex biological system, the proper functioning of which is highly dependent on coordinated intracellular processes that are strictly arranged in time and space. Currently, multicolour intracellular reporters based mostly on FPs are being developed that allow the simultaneous monitoring of multiple intracellular activities or concentration measurements of several intracellular components. The application of BODIPY reporters with the diverse spectral properties is a prerequisite for these so-called multiparameter imaging experiments.

The use of phototransformable reporters in super-resolution microscopy opens up new possibilities for imaging processes in a living cell with a nanometre resolution. Further progress in this area is associated, in particular, with the synthesis of BODIPY derivatives with high brightness, significant photostability, high phototransformation contrast, low phototoxicity and sufficient cell membrane

Scheme 44



Compound	R	Before phototransformation	After phototransformation
190	H	548/562 nm, Φ_{fl} = 0.07	588/602 nm, Φ_{fl} = 0.50
191		548/560 nm, Φ_{fl} = 0.03	600/618 nm, Φ_{fl} = 0.19
192		548/581 nm, Φ_{fl} = 0.004	605/652 nm, Φ_{fl} = 0.04

permeability. New phototransformable reporters should also carry groups allowing the specific and high affinity binding to the target cell molecule without affecting its biological properties.

The targeted labelling of biomolecules by synthetic fluorophores in a living cell is still a challenge. In this regard, the application of enzymatic systems, such as SNAP-tag, CLIP-tag or HALO-tag, together with far-red or NIR BODIPY fluorophores will eventually allow the visualization of biological processes with deep tissue penetration and will facilitate the whole-body imaging. The latter task of *in vivo* bioimaging with BODIPY-based fluorophores should be attributed to the most urgent, since it is straightforwardly related to the diagnosis of various diseases.

This review was written with the financial support of the Russian Science Foundation (Project No. 19-73-20194).

8. List of acronyms

ε — molar extinction coefficient,
Φ_{fl} — fluorescence quantum yield,
C_{min} — minimum detectable concentration,
ACQ — aggregation-caused quenching,
AGT — O^6-alkylguanine-DNA alkytransferase,
AIE — aggregation-induced emission,
BAPTA — 1,2-bis(2-aminophenoxy)ethane-*N*,*N*,*N*′*N*′-tetraacetic acid,
BODIPY — 4,4-difluoro-4-bora-3a,4a-diaza-*s*-indacene,
Cys — cysteine,
DFT — density functional theory,
DNB — 2,6-dinitrobenzene,
DTE — dithienyl,
eDHFR — dihydrofolate reductase,
EGFR — epidermal growth factor receptor,
ER — endoplasmic reticulum,
FCS — fluorescence correlation spectroscopy,
FLIM — fluorescence lifetime imaging microscopy
FP — fluorescent protein,
FRET — Firster resonance energy transfer,
GFP — green fluorescent protein from the jellyfish *Aequorea Victoria*,
GSH — glutathione,
Hcy — homocysteine,
HOMO — highest occupied molecular orbital,
ICT — intramolecular charge transfer,
IC_{50} — half-maximal inhibitory concentration
LOMO — lowest occupied molecular orbital,
MBP — maltose-binding protein,
MCF-7 — human breast cancer cell line,
NADP — nicotinamide adenine dinucleotide phosphate,
NIR — near-infrared,
PBFI — benzofuran isophthalate,
PBS — phosphate buffered saline,
PEG — polyethylene glycol,
PET — photoinduced electron transfer,
POI — protein of interest,
PS — photosensitizer,
RONS — reactive oxygen and nitrogen species,
TBET — through-bond energy transfer,
UV — ultraviolet light,
Vis — visible light.

References

1. M.V.Matz, A.F.Fradkov, Y.A.Labas, A.P.Savitsky, A.G.Zaraisky, M.L.Markelov, S.A.Lukyanov. *Nat. Biotechnol.*, **17**, 969 (1999)
2. G.S.Baird, D.A.Zacharias, R.Y.Tsien. Proc. *Natl. Acad. Sci. USA*, **97**, 11984 (2000)
3. N.Pletneva, S.Pletnev, T.Tikhonova, V.Popov, V.Martynov, V.Pletnev. *Acta Crystallogr., Sect. D*, **62**, 527 (2006)
4. A.A.Pakhomov, V.I.Martynov. *Biochemistry*, **46**, 11528 (2007)
5. R.E.Campbell, O.Tour, A.E.Palmer, P.A.Steinbach, G.S.Baird, D.A.Zacharias, R.Y.Tsien. *Proc. Natl. Acad. Sci. USA*, **99**, 7877 (2002)
6. V.F.Traven, D.A.Cheptsov. *Russ. Chem. Rev.*, **89**, 713 (2020)
7. M.V.Fomina, A.S.Nikiforov, S.P.Gromov. *Russ. Chem. Rev.*, **85**, 684 (2016)
8. L.M.Wysocki, L.D.Lavis. *Curr. Opin. Chem. Biol.*, **15**, 752 (2011)
9. L.D.Lavis, R.T.Raines. *ACS Chem. Biol.*, **9**, 855 (2014)
10. V.I.Martynov, A.A.Pakhomov, N.V.Popova, I.E.Deyev, A.G.Petrenko. *Acta Naturae*, **8**, 33 (2016)
11. A.Loudet, K.Burgess. *Chem. Rev.*, **107**, 4891 (2007)
12. N.Boens, V.Leen, W.Dehaen. *Chem. Soc. Rev.*, **41**, 1130 (2012)
13. T.Kowada, H.Maeda, K.Kikuchi. *Chem. Soc. Rev.*, **44**, 4953 (2015)
14. S.Kolemen, E.U.Akkaya. *Coord. Chem. Rev.*, **354**, 121 (2018)
15. Z.Shi, X.Han, W.Hu, H.Bai, B.Peng, L.Ji, Q.Fan, L.Li, W.Huang. *Chem. Soc. Rev.*, **49**, 7533 (2020)
16. Y.Qin, X.Liu, P.P.Jia, L.Xu, H.B.Yang. *Chem. Soc. Rev.*, **49**, 5678 (2020)
17. L.Y.Wang, H.Ding, X.G.Ran, H.Tang, D.R.Cao. *Dyes Pigm.*, **172**, 107857 (2020)
18. A.Barattucci, S.Campagna, T.Papalia, M.Galletta, A.Santoro, F.Puntoriero, P.Bonaccorsi. *ChemPhotoChem*, **4**, 647 (2020)
19. A.V.Solomonov, Y.S.Marfin, E.V.Rumyantsev. *Dyes Pigm.*, **162**, 517 (2019)
20. E.Bodio, F.Denat, C.Goze. *J. Porphyrins Phthalocyanines*, **23**, 1159 (2019)
21. Z.P.Liu, Z.Y.Jiang, M.Yan, X.Q.Wang. *Front. Chem.*, **7**, 712 (2019)
22. P.Kaur, K.Singh. *J. Mater. Chem. C*, **7**, 11361 (2019)
23. Y.Ni, J.Wu. *Org. Biomol. Chem.*, **12**, 3774 (2014)
24. L.Jean-Gerard, W.Vasseur, F.Scherninski, B.Andrioletti. *Chem. Commun.*, **54**, 12914 (2018)
25. T.Komatsu, D.Oushiki, A.Takeda, M.Miyamura, T.Ueno, T.Terai, K.Hanaoka, Y.Urano, T.Mineno, T.Nagano. *Chem. Commun.*, **47**, 10055 (2011)
26. E.Sezgin, G.Chwastek, G.Aydogan, I.Levental, K.Simons, P.Schwille. *ChemBioChem*, **14**, 695 (2013)
27. S.Jantra, P.Butta, P.Jithavech, P.Rojsitthisak, T.Palaga, P.Rashatasakhon, M.Sukwattanasinitt, S.Wacharasindhu. *Dyes Pigm.*, **162**, 189 (2019)
28. X.L.Zhao, C.Gao, N.Li, F.Y.Liu, S.H.Huo, J.Z.Li, X.L.Guan, N.Yan. *Tetrahedron Lett.*, **60**, 1452 (2019)
29. I.A.Boldyrev, X.H.Zhai, M.M.Momsen, H.L.Brockman, R.E.Brown, J.G.Molotkovsky. *J. Lipid Res.*, **48**, 1518 (2007)

30. A.Panniello, M.Trapani, M.Cordaro, C.N.Dibenedetto, R.Tommasi, C.Ingrosso, E.Fanizza, R.Grisorio, E.Collini, A.Agostiano, M.L.Curri, M.A.Castriciano, M.Striccoli. *Chem. – Eur. J.*, **27**, 2371 (2021)
31. M.C.Dos Santos, W.R.Algar, I.L.Medintz, N.Hildebrandt. *Trac. Trends Anal. Chem.*, **125**, 115819 (2020)
32. H.Zong, X.Wang, X.Mu, J.Wang, M.Sun. *Chem. Rec.*, **19**, 818 (2019)
33. P.P.P.Kumar, A.Rahman, T.Goswami, H.N.Ghosh, P.P.Neelakandan. *ChemPlusChem*, **86**, 87 (2021)
34. A.S.Kashirina, I.Lopez-Duarte, M.Kubankova, A.A.Gulin, V.V.Dudenkova, S.A.Rodimova, H.G.Torgomyan, E.V.Zagaynova, A.V.Meleshina, M.K.Kuimova. *Sci. Rep.*, **10**, 14063 (2020)
35. R.Brodwolf, P.Volz-Rakebrand, J.Stellmacher, C.Wolff, M.Unbehauen, R.Haag, M.Schafer-Korting, C.Zoschke, U.Alexiev. *Theranostics*, **10**, 6322 (2020)
36. M.V.Shirmanova, L.E.Shimolina, M.M.Lukina, E.V.Zagaynova, M.K.Kuimova. *Adv. Exp. Med. Biol.*, **1035**, 143 (2017)
37. Q.D.Zheng, G.X.Xu, P.N.Prasad. *Chem. – Eur. J.*, **14**, 5812 (2008)
38. G.Ulrich, R.Ziessel, A.Harriman. *Angew. Chem., Int. Ed.*, **47**, 1184 (2008)
39. A.Treibs, F.-H.Kreuzer. *Justus Liebigs Ann. Chem.*, **718**, 208 (1968)
40. I.J.Arroyo, R.R.Hu, G.Merino, B.Z.Tang, E.Pena-Cabrera. *J. Org. Chem.*, **74**, 5719 (2009)
41. K.Tram, H.B.Yan, H.A.Jenkins, S.Vassiliev, D.Brucec. *Dyes Pigm.*, **82**, 392 (2009)
42. H.J.Wei, R.Feng, Y.Fang, L.Wang, C.Chen, L.Zhang, H.Y.Cui, X.P.Wang. *Chem. – Eur. J.*, **24**, 19341 (2018)
43. V.I.Martynov, A.A.Pakhomov, I.E.Deyev, A.G.Petrenko. *BBA — Gen. Subjects*, **1862**, 2924 (2018)
44. L.Bai, P.F.Sun, Y.Liu, H.Zhang, W.B.Hu, W.S.Zhang, Z.P.Liu, Q.L.Fan, L.Li, W.Huang. *Chem. Commun.*, **55**, 10920 (2019)
45. G.L.Li, Y.Otsuka, T.Matsumiya, T.Suzuki, J.Y.Li, M.Takahashi, K.Yamada. Materials, 11, 1297 (2018)
46. E.Vosdewael, J.A.Pardoen, J.A.Vankoeveringe, J.Lugtenburg. *Recl. Trav. Chim. Pays-Bas*, **96**, 306 (1977)
47. G.B.Guseva, E.V.Antina, M.B.Berezin, R.S.Pavelyev, A.R.Kayumov, I.S.Sharafutdinov, O.A.Lodochnikova, D.R.Islamov, K.S.Usachev, S.V.Boichuk, L.E.Nikitina, S.A.Lisovskaya. *J. Photochem. Photobiol. A*, **401**, 112783 (2020)
48. R.Lincoln, L.E.Greene, C.Bain, J.O.Flores-Rizo, D.S.Bohle, G.Cosa. *J. Phys. Chem. B*, **119**, 4758 (2015)
49. A.A.Pakhomov, Y.N.Kononevich, A.A.Korlyukov, V.I.Martynov, A.M.Muzafarov. *Mendeleev Commun.*, **26**, 196 (2016)
50. J.Banuelos, V.Martin, C.F.A.Gomez-Duran, I.J.A.Cordoba, E.Pena-Cabrera, I.Garcia-Moreno, A.Costela, M.E.Perez-Ojeda, T.Arbeloa, I.L.Arbeloa. *Chem. – Eur. J.*, **17**, 7261 (2011)
51. T.Yogo, Y.Urano, Y.Ishitsuka, F.Maniwa, T.Nagano. *J. Am. Chem. Soc.*, **127**, 12162 (2005)
52. G.Duran-Sampedro, N.Epelde-Elezcano, V.Martinez-Martinez, I.Esnal, J.Banuelos, I.Garcia-Moreno, A.R.Agarrabeitia, S.de la Moya, A.Tabero, A.Lazaro-Carrillo, A.Villanueva, M.J.Ortiz, I.Lopez-Arbeloa. *Dyes Pigm.*, **142**, 77 (2017)
53. A.Kamkaew, S.H.Lim, H.B.Lee, L.V.Kiew, L.Y.Chung, K.Burgess. *Chem. Soc. Rev.*, **42**, 77 (2013)
54. C.S.Kue, S.Y.Ng, S.H.Voon, A.Kamkaew, L.Y.Chung, L.V.Kiew, H.B.Lee. *Photochem. Photobiol. Sci.*, **17**, 1691 (2018)
55. M.L.Agazzi, M.B.Ballatore, A.M.Durantini, E.N.Durantini, A.C.Tome. *J. Photochem. Photobiol. C*, **40**, 21 (2019)
56. E.Deniz, G.C.Isbasar, O.A.Bozdemir, L.T.Yildirim, A.Siemiarczuk, E.U.Akkaya. *Org. Lett.*, **10**, 3401 (2008)
57. K.Rurack, M.Kollmannsberger, J.Daub. *New J. Chem.*, **25**, 289 (2001)
58. A.Orte, E.Debroye, M.J.Ruedas-Rama, E.Garcia-Fernandez, D.Robinson, L.Crovetto, E.M.Talavera, J.M.Alvarez-Pez, V.Leen, B.Verbelen, L.C.D.de Rezende, W.Dehaen, J.Hofkens, M.Van der Auweraer, N.Boens. *RSC Adv.*, **6**, 102899 (2016)
59. J.Y.Tao, D.Sun, L.Sun, Z.Z.Li, B.Fu, J.Liu, L.Zhang, S.F.Wang, Y.Y.Fang, H.J.Xu. *Dyes Pigm.*, **168**, 166 (2019)
60. L.J.Patalag, P.G.Jones, D.B.Werz. *Angew. Chem., Int. Ed.*, **55**, 13340 (2016)
61. M.Nakamura, H.Tahara, K.Takahashi, T.Nagata, H.Uoyama, D.Kuzuhara, S.Mori, T.Okujima, H.Yamada, H.Uno. *Org. Biomol. Chem.*, **10**, 6840 (2012)
62. Y.S.Marfin, D.A.Merkushev, S.D.Usoltsev, M.V.Shipalova, E.V.Rumyantsev. *J. Fluoresc.*, **25**, 1517 (2015)
63. A.B.Descalzo, H.J.Xu, Z.L.Xue, K.Hoffmann, Z.Shen, M.G.Weller, X.Z.You, K.Rurack. *Org. Lett.*, **10**, 1581 (2008)
64. M.Nakamura, M.Kitatsuka, K.Takahashi, T.Nagata, S.Mori, D.Kuzuhara, T.Okujima, H.Yamada, T.Nakae, H.Uno. *Org. Biomol. Chem.*, **12**, 1309 (2014)
65. J.Wang, Q.H.Wu, C.J.Yu, Y.Wei, X.L.Mu, E.H.Hao, L.J.Jiao. *J. Org. Chem.*, **81**, 11316 (2016)
66. N.Zhao, S.T.Xuan, Z.H.Zhou, F.R.Fronczek, K.M.Smith, M.G.H.Vicente. *J. Org. Chem.*, **82**, 9744 (2017)
67. A.Loudet, R.Bandichhor, K.Burgess, A.Palma, S.O.McDonnell, M.J.Hall, D.F.O'Shea. *Org. Lett.*, **10**, 4771 (2008)
68. L.J.Jiao, Y.Y.Wu, Y.Ding, S.F.Wang, P.Zhang, C.J.Yu, Y.Wei, X.L.Mu, E.H.Hao. *Chem. – Asian J.*, **9**, 805 (2014)
69. J.L.Donnelly, D.Offenbartl-Stiegert, J.M.Marin-Beloqui, L.Rizello, G.Battaglia, T.M.Clarke, S.Howorka, J.D.Wilden. *Chem. – Eur. J.*, **26**, 863 (2020)
70. L.N.Sobenina, A.M.Vasil'tsov, O.V.Petrova, K.B.Petrushenko, I.A.Ushakov, G.Clavier, R.Meallet-Renault, A.I.Mikhaleva, B.A.Trofimov. *Org. Lett.*, **13**, 2524 (2011)
71. K.B.Petrushenko, I.K.Petrushenko, O.V.Petrova, L.N.Sobenina, I.A.Ushakov, B.A.Trofimov. *Asian J. Org. Chem.*, **6**, 852 (2017)
72. K.B.Petrushenko, I.K.Petrushenko, O.V.Petrova, L.N.Sobenina, B.A.Trofimov. *Dyes Pigm.*, **136**, 488 (2017)
73. I.K.Petrushenko, K.B.Petrushenko. *Spectrochim. Acta, Part A*, **138**, 623 (2015)
74. Y.Gabe, Y.Urano, K.Kikuchi, H.Kojima, T.Nagano. *J. Am. Chem. Soc.*, **126**, 3357 (2004)
75. W.Y.Lin, L.Yuan, Z.M.Cao, Y.M.Feng, J.Z.Song. *Angew. Chem., Int. Ed.*, **49**, 375 (2010)
76. G.Barin, M.D.Yilmaz, E.U.Akkaya. *Tetrahedron Lett.*, **50**, 1738 (2009)

77. J.Fan, M.Hu, P.Zhan, X.Peng. *Chem. Soc. Rev.*, **42**, 29 (2013)
78. J.Yang, H.Chen, I.R.Vlahov, J.X.Cheng, P.S.Low. *Proc. Natl. Acad. Sci. USA*, **103**, 13872 (2006)
79. R.Ziessel, G.Ulrich, J.H.Olivier, T.Bura, A.Sutter. *Chem. Commun.*, **46**, 7978 (2010)
80. Y.Zhao, Y.Zhang, X.Lv, Y.L.Liu, M.L.Chen, P.Wang, J.Liu, W.Guo. *J. Mater. Chem.*, **21**, 13168 (2011)
81. S.Xia, M.X.Fang, J.B.Wang, J.H.Bi, W.Mazi, Y.B.Zhang, R.L.Luck, H.Y.Liu. *Sens. Actuators B: Chem.*, **294**, 1 (2019)
82. Y.Hayashi, S.Yamaguchi, W.Y.Cha, D.Kim, H.Shinokubo. *Org. Lett.*, **13**, 2992 (2011)
83. O.Halter, I.Fernandez, H.Plenio. *Chem. – Eur. J.*, **23**, 711 (2017)
84. X.Y.Zhu, H.W.Yao, Y.J.Fu, X.F.Guo, H.Wang. *Anal. Chim. Acta*, **1048**, 194 (2019)
85. X.-Y.Zhu, H.Wu, X.-F.Guo, H.Wang. *Dyes Pigm.*, **165**, 400 (2019)
86. T.Uppal, X.Hu, F.R.Fronczek, S.Maschek, P.Bobadova-Parvanova, M.G.Vicente. *Chem. – Eur. J.*, **18**, 3893 (2012)
87. A.A.Pakhomov, I.E.Deyev, N.M.Ratnikova, S.P.Chumakov, V.B.Mironiuk, Y.N.Kononevich, A.M.Muzafarov, V.I.Martynov. *BioTechniques*, **63**, 77 (2017)
88. M.Collot, E.Boutant, M.Lehmann, A.S.Klymchenko. *Bioconjug. Chem.*, **30**, 192 (2019)
89. A.B.Descalzo, P.Ashokkumar, Z.Shen, K.Rurack. *ChemPhotoChem*, **4**, 120 (2019)
90. G.Fan, L.Yang, Z.J.Chen. *Front. Chem. Sci. Eng.*, **8**, 405 (2014)
91. H.J.Wories, J.H.Koek, G.Lodder, J.Lugtenburg, R.Fokkens, O.Driessen, G.R.Mohn. *Recl. Trav. Chim. Pays-Bas*, **104**, 288 (1985)
92. L.L.Li, J.Y.Han, B.Nguyen, K.Burgess. *J. Org. Chem.*, **73**, 1963 (2008)
93. F.Heisig, S.Gollos, S.J.Freudenthal, A.El-Tayeb, J.Iqbal, C.E.Muller. *J. Fluoresc.*, **24**, 213 (2014)
94. K.M.Bardon, S.Selfridge, D.S.Adams, R.A.Minns, R.Pawle, T.C.Adams, L.Takiff. *ACS Omega*, **3**, 13195 (2018)
95. A.Sutter, M.Elhabiri, G.Ulrich. *Chem. – Eur. J.*, **24**, 11119 (2018)
96. S.L.Niu, G.Ulrich, P.Retailleau, J.Harrowfield, R.Ziessel. *Tetrahedron Lett.*, **50**, 3840 (2009)
97. S.L.Niu, G.Ulrich, R.Ziessel, A.Kiss, P.Y.Renard, A.Romieu. *Org. Lett.*, **11**, 2049 (2009)
98. K.V.Ksenofontova, A.A.Ksenofontov, I.A.Khodov, E.V.Rumyantsev. *Izv. Vyssh. Ucheb. Zaved. Khim. Khim. Tekhnol.*, **63**, 4 (2020)
99. S.L.Zhu, J.T.Zhang, G.Vegesna, F.T.Luo, S.A.Green, H.Y.Liu. *Org. Lett.*, **13**, 438 (2011)
100. I.W.Badon, J.Lee, T.P.Vales, B.K.Cho, H.J.Kim. *J. Photochem. Photobiol. A*, **377**, 214 (2019)
101. A.L.Nguyen, K.E.Griffin, Z.H.Zhou, F.R.Fronczek, K.M.Smith, M.G.H.Vicente. *New J. Chem.*, **42**, 8241 (2018)
102. A.M.Courtis, S.A.Santos, Y.H.Guan, J.A.Hendricks, B.Ghosh, D.M.Szantai-Kis, S.A.Reis, J.V.Shah, R.Mazitschek. *Bioconjug. Chem.*, **25**, 1043 (2014)
103. A.Blazquez-Moraleja, D.Alvarez-Fernandez, R.P.Montero, I.Garcia-Moreno, V.Martinez-Martinez, J.Banuelos, I.Saenz-de-Santa-Maria, M.D.Chiara, J.L.Chiara. *Dyes Pigm.*, **170**, 107545 (2019)
104. T.Papalia, G.Siracusano, I.Colao, A.Barattucci, M.C.Aversa, S.Serroni, G.Zappala, S.Campagna, M.T.Sciortino, F.Puntoriero, P.Bonaccorsi. *Dyes Pigm.*, **110**, 67 (2014)
105. D.K.Mai, B.Kang, T.P.Vales, I.W.Badon, S.Cho, J.Lee, E.Kim, H.J.Kim. *Molecules*, **25**, 3340 (2020)
106. T.Uppal, N.V.S.D.K.Bhupathiraju, M.G.H.Vicente. *Tetrahedron*, **69**, 4687 (2013)
107. A.R.Sekhar, S.K.Sariki, R.V.R.Reddy, A.Bisai, P.K.Sahu, R.S.Tomar, J.Sankar. *Chem. Commun.*, **53**, 1096 (2017)
108. T.Zhang, C.Ma, T.T.Sun, Z.G.Xie. *Coord. Chem. Rev.*, **390**, 76 (2019)
109. C.Grazon, Y.Si, J.P.Placial, J.Rieger, R.Meallet-Renault, G.Clavier. *Photochem. Photobiol. Sci.*, **18**, 1156 (2019)
110. N.Song, L.Fu, Y.Liu, Y.Y.Li, L.Chen, X.Y.Wang, S.Liu, Z.G.Xie. *Dyes Pigm.*, **162**, 295 (2019)
111. D.Y.Gao, B.Y.Zhang, Y.B.Liu, D.H.Hu, Z.H.Sheng, X.J.Zhang, Z.Yuan. *Theranostics*, **9**, 5315 (2019)
112. A.Koltermann, U.Kettling, J.Bieschke, T.Winkler, M.Eigen. *Proc. Natl. Acad. Sci. USA*, **95**, 1421 (1998)
113. A.P.Demchenko. *Methods Appl. Fluoresc.*, **8**, 022001 (2020)
114. B.Hinkeldey, A.Schmitt, G.Jung. *ChemPhysChem*, **9**, 2019 (2008)
115. L.C.Dias de Rezende, M.Menezes Vaidergorn, J.C.Biazzotto Moraes, F.da Silva Emery. *J. Fluoresc.*, **24**, 257 (2014)
116. A.A.Pakhomov, Y.N.Kononevich, M.V.Stukalova, E.A.Svidchenko, N.M.Surin, G.V.Cherkaev, O.I.Shchegolikhina, V.I.Martynov, A.M.Muzafarov. *Tetrahedron Lett.*, **57**, 979 (2016)
117. I.V.Aksenova, R.T.Kuznetsova, I.P.Pozdnyakov, V.F.Plyusnin, M.B.Berezin, N.A.Bumagina, E.S.Jarnikova, M.V.Parkhats, B.M.Dzhagarov. *J. Photochem. Photobiol. A*, **344**, 206 (2017)
118. C.N.Allen, E.S.Harpur, T.J.B.Gray, B.H.Hirst. *Toxicol. in Vitro*, **5**, 183 (1991)
119. X.Liang, H.Luo, Y.Q.Lan, W.H.Zhu, J.Mack, Z.Hlatshwayo, T.Nyokong, Q.Y.Chen. *Macroheterocycles*, **11**, 421 (2018)
120. F.F.Han, Y.M.Xu, D.C.Jiang, Y.Qin, H.Y.Chen. *Anal. Biochem.*, **435**, 106 (2013)
121. C.S.Mahanta, S.Aparna, S.K.Das, B.B.Jena, B.R.Swain, M.Patri, B.P.Dash, R.Satapathy. *ChemistrySelect*, **5**, 8429 (2020)
122. *Molecular Probes.® Handbook — A Guide to Fluorescent Probes and Labeling Technologies (Online Version)*. Ch. 12; https://www.thermofisher.com/ru/ru/home/global/forms/mp-handbook-download-request-form-2014.html (Last access 12.09.2021)
123. D.Kand, L.Pizarro, I.Angel, A.Avni, D.Friedmann-Morvinski, R.Weinstain. *Angew. Chem., Int. Ed.*, **58**, 4659 (2019)
124. S.Rello, J.C.Stockert, V.Moreno, A.Gamez, M.Pacheco, A.Juarranz, M.Canete, A.Villanueva. *Apoptosis*, **10**, 201 (2005)
125. M.K.Kuimova, G.Yahioglu, J.A.Levitt, K.Suhling. *J. Am. Chem. Soc.*, **130**, 6672 (2008)
126. I.Lopez-Duarte, T.T.Vu, M.A.Izquierdo, J.A.Bull, M.K.Kuimova. *Chem. Commun.*, **50**, 5282 (2014)
127. I.G.Macara. *Microbiol. Mol. Biol. Rev.*, **65**, 570 (2001)
128. S.H.Son, A.Seko, S.Daikoku, K.Fujikawa, K.Suzuki, Y.Ito, O.Kanie. *ChemBioChem*, **17**, 630 (2016)

129. S.H.Son, S.Daikoku, A.Ohtake, K.Suzuki, K.Kabayama, Y.Ito, O.Kanie. *Chem. Commun.*, **50**, 3010 (2014)
130. F.Ali, S.Aute, S.Sreedharan, H.A.Anila, H.K.Saeed, C.G.Smythe, J.A.Thomas, A.Das. *Chem. Commun.*, **54**, 1849 (2018)
131. H.Lee, Z.Yang, Y.Wi, T.W.Kim, P.Verwilst, Y.H.Lee, G.I.Han, C.Kang, J.S.Kim. *Bioconjug. Chem.*, **26**, 2474 (2015)
132. C.Handschin, U.A.Meyer. *Pharmacol. Rev.*, **55**, 649 (2003)
133. S.D.Zucker, W.Goessling, M.L.Zeidel, J.L.Gollan. *J. Biol. Chem.*, **269**, 19262 (1994)
134. S.Xu, H.W.Liu, X.X.Hu, S.Y.Huan, J.Zhang, Y.C.Liu, L.Yuan, F.L.Qu, X.B.Zhang, W.Tan. *Anal. Chem.*, **89**, 7641 (2017)
135. B.K.McMahon, R.Pal, D.Parker. *Chem. Commun.*, **49**, 5363 (2013)
136. H.Xiao, P.Li, X.Hu, X.Shi, W.Zhang, B.Tang. *Chem. Sci.*, **7**, 6153 (2016)
137. T.Slanina, P.Shrestha, E.Palao, D.Kand, J.A.Peterson, A.S.Dutton, N.Rubinstein, R.Weinstain, A.H.Winter, P.Klan. *J. Am. Chem. Soc.*, **139**, 15168 (2017)
138. P.P.Goswami, A.Syed, C.L.Beck, T.R.Albright, K.M.Mahoney, R.Unash, E.A.Smith, A.H.Winter. *J. Am. Chem. Soc.*, **137**, 3783 (2015)
139. N.Rubinstein, P.Liu, E.W.Miller, R.Weinstain. *Chem. Commun.*, **51**, 6369 (2015)
140. A.T.Hoye, J.E.Davoren, P.Wipf, M.P.Fink, V.E.Kagan. *Acc. Chem. Res.*, **41**, 87 (2008)
141. L.V.Johnson, M.L.Walsh, L.B.Chen. *Proc. Natl. Acad. Sci. USA*, **77**, 990 (1980)
142. B.L.Sui, S.Tang, A.W.Woodward, B.Kim, K.D.Belfield. *Eur. J. Org. Chem.*, 2851 (2016)
143. T.Gao, H.He, R.Huang, M.Zheng, F.F.Wang, Y.J.Hu, F.L.Jiang, Y.Liu. *Dyes Pigm.*, **141**, 530 (2017)
144. H.K.Hall. *J. Am. Chem. Soc.*, **79**, 5441 (1957)
145. Z.Ye, C.Xiong, J.Pan, D.D.Su, L.T.Zeng. *Dyes Pigm.*, **155**, 30 (2018)
146. X.D.Kong, L.T.Di, Y.S.Fan, Z.K.Zhou, X.J.Feng, L.Z.Gai, J.W.Tian, H.Lu. *Chem. Commun.*, **55**, 11567 (2019)
147. A.H.Coons, H.J.Creech, R.N.Jones, E.Berliner. *J. Immunol.*, **45**, 159 (1942)
148. F.Thiebaut, S.J.Currier, J.Whitaker, R.P.Haugland, M.M.Gottesman, I.Pastan, M.C.Willingham. *J. Histochem. Cytochem.*, **38**, 685 (1990)
149. F.A.Green. *Inflammation*, **12**, 133 (1988)
150. N.Krall, F.P.da Cruz, O.Boutureira, G.J.L.Bernardes. *Nat. Chem.*, **8**, 102 (2016)
151. R.K.V.Lim, Q.Lin. *Chem. Commun.*, **46**, 1589 (2010)
152. J.A.Prescher, C.R.Bertozzi. *Nat. Chem. Biol.*, **1**, 13 (2005)
153. M.D.Best. *Biochemistry*, **48**, 6571 (2009)
154. Y.Kho, S.C.Kim, C.Jiang, D.Barma, S.W.Kwon, J.Cheng, J.Jaunbergs, C.Weinbaum, F.Tamanoi, J.Falck, Y.Zhao. *Proc. Natl. Acad. Sci. USA*, **101**, 12479 (2004)
155. K.L.Kiick, E.Saxon, D.A.Tirrell, C.R.Bertozzi. *Proc. Natl. Acad. Sci. USA*, **99**, 19 (2002)
156. E.Saxon, C.R.Bertozzi. *Science*, **287**, 2007 (2000)
157. A.E.Speers, G.C.Adam, B.F.Cravatt. *J. Am. Chem. Soc.*, **125**, 4686 (2003)
158. A.E.Speers, B.F.Cravatt. *Chem. Biol.*, **11**, 535 (2004)
159. V.V.Rostovtsev, L.G.Green, V.V.Fokin, K.B.Sharpless. *Angew. Chem., Int. Ed.*, **41**, 2596 (2002)
160. T.Kubota, T.Durek, B.B.Dang, R.K.Finol-Urdaneta, D.J.Craik, S.B.H.Kent, R.J.French, F.Bezanilla, A.M.Correa. *Proc. Natl. Acad. Sci. USA*, **114**, E1857 (2017)
161. R.Wombacher, V.W.Cornish. *J. Biophotonics*, **4**, 391 (2011)
162. A.Keppler, S.Gendreizig, T.Gronemeyer, H.Pick, H.Vogel, K.Johnsson. *Nat. Biotechnol.*, **21**, 86 (2003)
163. A.Keppler, H.Pick, C.Arrivoli, H.Vogel, K.Johnsson. *Proc. Natl. Acad. Sci. USA*, **101**, 9955 (2004)
164. N.B.Cole. *Curr. Protoc. Protein Sci.*, **73**, 30 (2013)
165. A.Gautier, A.Juillerat, C.Heinis, I.R.Correa Jr., M.Kindermann, F.Beaufils, K.Johnsson. *Chem. Biol.*, **15**, 128 (2008)
166. G.V.Los, L.P.Encell, M.G.McDougall, D.D.Hartzell, N.Karassina, C.Zimprich, M.G.Wood, R.Learish, R.F.Ohana, M.Urh, D.Simpson, J.Mendez, K.Zimmerman, P.Otto, G.Vidugiris, J.Zhu, A.Darzins, D.H.Klaubert, R.F.Bulleit, K.V.Wood. *ACS Chem. Biol.*, **3**, 373 (2008)
167. H.A.Benink, M.Urh. *Methods Mol. Biol.*, **1266**, 119 (2015)
168. C.G.England, H.Luo, W.Cai. *Bioconjug. Chem.*, **26**, 975 (2015)
169. L.W.Miller, Y.Cai, M.P.Sheetz, V.W.Cornish. *Nat. Methods*, **2**, 255 (2005)
170. S.S.Gallagher, J.E.Sable, M.P.Sheetz, V.W.Cornish. *ACS Chem. Biol.*, **4**, 547 (2009)
171. T.Y.Wang, L.J.Friedman, J.Gelles, W.Min, A.A.Hoskins, V.W.Cornish. *Biophys. J.*, **106**, 272 (2014)
172. T.Kobayashi, T.Komatsu, M.Kamiya, C.Campos, M.Gonzalez-Gaitan, T.Terai, K.Hanaoka, T.Nagano, Y.Urano. *J. Am. Chem. Soc.*, **134**, 11153 (2012)
173. S.R.Adams, R.E.Campbell, L.A.Gross, B.R.Martin, G.K.Walkup, Y.Yao, J.Llopis, R.Y.Tsien. *J. Am. Chem. Soc.*, **124**, 6063 (2002)
174. J.J.Lee, S.C.Lee, D.T.Zhai, Y.H.Ahn, H.Y.Yeo, Y.L.Tan, Y.T.Chang. *Chem. Commun.*, **47**, 4508 (2011)
175. Y.C.Chen, K.Tsao, S.L.Acton, J.W.Keillor. *Angew. Chem., Int. Ed.*, **57**, 12390 (2018)
176. I.Nikic, T.Plass, O.Schraidt, J.Szymanski, J.A.G.Briggs, C.Schultz, E.A.Lemke. *Angew. Chem., Int. Ed.*, **53**, 2245 (2014)
177. H.Sunahara, Y.Urano, H.Kojima, T.Nagano. *J. Am. Chem. Soc.*, **129**, 5597 (2007)
178. Y.S.Marfin, M.V.Shipalova, V.O.Kurzin, K.V.Ksenofontova, A.V.Solomonov, E.V.Rumyantsev. *J. Fluoresc.*, **26**, 2105 (2016)
179. Y.Huang, C.F.Li, W.J.Shi, H.Y.Tan, Z.Z.He, L.Y.Zheng, F.G.Liu, J.W.Yan. *Talanta*, **198**, 390 (2019)
180. S.Chowdhury, B.Rooj, A.Dutta, U.Mandal. *J. Fluoresc.*, **28**, 999 (2018)
181. W.W.Qin, W.Dou, V.Leen, W.Dehaen, M.Van der Auweraer, N.Boens. *RSC Adv.*, **6**, 7806 (2016)
182. D.D.Cheng, W.Q.Zhao, H.Z.Yang, Z.P.Huang, X.L.Liu, A.X.Han. *Tetrahedron Lett.*, **57**, 2655 (2016)
183. C.L.Zhang, Q.Sun, L.M.Zhao, S.W.Gong, Z.P.Liu. *Spectrochim. Acta, Part A*, **223**, 117295 (2019)
184. K.S.Choung, K.Marroquin, T.S.Teets. *Chem. Sci.*, **10**, 5124 (2019)
185. N.M.Cheruthu, T.Komatsu, T.Ueno, K.Hanaoka, Y.Urano. *Bioorg. Med. Chem. Lett.*, **29**, 126684 (2019)
186. T.T.Shu, Z.H.Yang, Z.T.Cen, X.K.Deng, Y.Deng, C.Z.Dong, Y.H.Yu. *Anal. Methods*, **10**, 5755 (2018)

187. S.S.Thakare, G.Chakraborty, A.B.More, S.Chattopadhyay, S.Mula, A.K.Ray, N.Sekar. *J. Lumin.*, **194**, 622 (2018)
188. Y.Zhang, X.Zheng, L.Zhang, Z.Yang, L.Chen, L.Wang, S.Liu, Z.Xie. *Org. Biomol. Chem.*, **18**, 707 (2020)
189. J.D.Luo, Z.L.Xie, J.W.Y.Lam, L.Cheng, H.Y.Chen, C.F.Qiu, H.S.Kwok, X.W.Zhan, Y.Q.Liu, D.B.Zhu, B.Z.Tang. *Chem. Commun.*, 1740 (2001)
190. R.R.Hu, C.F.A.Gomez-Duran, J.W.Y.Lam, J.L.Belmonte-Vazquez, C.M.Deng, S.J.Chen, R.Q.Ye, E.Pena-Cabrera, Y.C.Zhong, K.S.Wong, B.Z.Tang. *Chem. Commun.*, **48**, 10099 (2012)
191. P.Porcu, M.Vonlanthen, I.Gonzalez-Mendez, A.Ruiu, E.Rivera. *Molecules*, **23**, 2289 (2018)
192. J.B.Qiu, S.J.Jiang, H.Y.Guo, F.F.Yang. *Dyes Pigm.*, **157**, 351 (2018)
193. Z.G.Yang, Y.Wi, Y.M.Yoon, P.Verwilst, J.H.Jang, T.W.Kim, C.Kang, J.S.Kim. *Chem. – Asian J.*, **11**, 527 (2016)
194. D.H.Ma, D.Kim, T.Akisawa, K.H.Lee, K.T.Kim, K.H.Ahn. *Chem. – Asian J.*, **10**, 894 (2015)
195. D.D.Su, C.L.Teoh, S.Sahu, R.K.Das, Y.T.Chang. *Biomaterials*, **35**, 6078 (2014)
196. Y.T.Chen, L.Wan, X.Yu, W.J.Li, Y.Z.Bian, J.Z.Jiang. *Org. Lett.*, **13**, 5774 (2011)
197. F.Miao, S.Uchinomiya, Y.Ni, Y.T.Chang, J.S.Wu. *ChemPlusChem*, **81**, 1209 (2016)
198. M.L.Zhu, P.P.Xing, Y.B.Zhou, L.Gong, J.H.Zhang, D.D.Qi, Y.Z.Bian, H.W.Du, J.Z.Jiang. *J. Mater. Chem. B*, **6**, 4422 (2018)
199. M.Grossi, M.Morgunova, S.Cheung, D.Scholz, E.Conroy, M.Terrile, A.Panarella, J.C.Simpson, W.M.Gallagher, D.F.O'Shea. *Nat. Commun.*, **7**, 10855 (2016)
200. J.R.Casey, S.Grinstein, J.Orlowski. *Nat. Rev., Mol. Cell Biol.*, **11**, 50 (2010)
201. D.E.Clapham. *Cell*, **131**, 1047 (2007)
202. A.Miyawaki, J.Llopis, R.Heim, J.M.McCaffery, J.A.Adams, M.Ikura, R.Y.Tsien. *Nature (London)*, **388**, 882 (1997)
203. Y.N.Tallini, M.Ohkura, B.R.Choi, G.J.Ji, K.Imoto, R.Doran, J.Lee, P.Plan, J.Wilson, H.B.Xin, A.Sanbe, J.Gulick, J.Mathai, J.Robbins, G.Salama, J.Nakai, M.I.Kotlikoff. *Proc. Natl. Acad. Sci. USA*, **103**, 4753 (2006)
204. M.Kamiya, K.Johnsson. *Anal. Chem.*, **82**, 6472 (2010)
205. W.F.Duan, H.M.Wei, T.B.Cuia, B.X.Gao. *J. Mater. Chem. B*, **3**, 894 (2015)
206. K.Meuwis, N.Boens, F.C.De Schryver, J.Gallay, M.Vincent. *Biophys. J.*, **68**, 2469 (1995)
207. B.L.Sui, X.L.Yue, M.G.Tichy, T.H.Liu, K.D.Belfield. *Eur. J. Org. Chem.*, 1189 (2015)
208. B.J.Muller, S.M.Borisov, I.Klimant. *Adv. Funct. Mater.*, **26**, 7697 (2016)
209. Z.X.Yan, X.R.Lin, H.Y.Guo, F.F.Yang. *Tetrahedron Lett.*, **58**, 3064 (2017)
210. B.Chaigne-Delalande, F.Y.Li, G.M.O'Connor, M.J.Lukacs, P.Jiang, L.X.Zheng, A.Shatzer, M.Biancalana, S.Pittaluga, H.F.Matthews, T.J.Jancel, J.J.Bleesing, R.A.Marsh, T.W.Kuijpers, K.E.Nichols, C.L.Lucas, S.Nagpal, H.Mehmet, H.C.Su, J.I.Cohen, G.Uzel, M.J.Lenardo. *Science*, **341**, 186 (2013)
211. Q.T.Lin, J.J.Gruskos, D.Buccella. *Org. Biomol. Chem.*, **14**, 11381 (2016)
212. R.Treadwell, F.de Moliner, R.Subiros-Funosas, T.Hurd, K.Knox, M.Vendrell. *Org. Biomol. Chem.*, **16**, 239 (2018)
213. Q.T.Lin, D.Buccella. *J. Mater. Chem. B*, **6**, 7247 (2018)
214. P.A.Otten, R.E.London, L.A.Levy. *Bioconjug. Chem.*, **12**, 203 (2001)
215. M.P.Cuajungco, G.J.Lees. *Neurobiol. Dis.*, **4**, 137 (1997)
216. D.W.Choi, J.Y.Koh. *Annu. Rev. Neurosci.*, **21**, 347 (1998)
217. J.H.Weiss, S.L.Sensi, J.Y.Koh. *Trends Pharmacol. Sci.*, **21**, 395 (2000)
218. A.Harriman, L.J.Mallon, B.Stewart, G.Ulrich, R.Ziessel. *Eur. J. Org. Chem.*, 3191 (2007)
219. Y.Zhang, X.F.Guo, W.X.Si, L.H.Jia, X.H.Qian. *Org. Lett.*, **10**, 473 (2008)
220. P.J.Jiang, L.Z.Chen, J.Lin, Q.Liu, J.Ding, X.Gao, Z.J.Guo. *Chem. Commun.*, 1424 (2002)
221. M.S.Park, K.M.K.Swamy, Y.J.Lee, H.N.Lee, Y.J.Jang, Y.H.Moon, J.Yoon. *Tetrahedron Lett.*, **47**, 8129 (2006)
222. K.Kiyose, H.Kojima, Y.Urano, T.Nagano. *J. Am. Chem. Soc.*, **128**, 6548 (2006)
223. S.L.Zhu, J.T.Zhang, J.Janjanam, G.Vegesna, F.T.Luo, A.Tiwari, H.Y.Liu. *J. Mater. Chem. B*, **1**, 1722 (2013)
224. S.Atilgan, T.Ozdemir, E.U.Akkaya. *Org. Lett.*, **10**, 4065 (2008)
225. S.A.Gorbatov, M.A.Kozlov, I.E.Zlobin, A.V.Kartashov, I.V.Zavarzin, Y.A.Volkova. *Mendeleev Commun.*, **28**, 615 (2018)
226. S.Xia, J.J.Shen, J.B.Wang, H.L.Wang, M.X.Fang, H.W.Zhou, M.Tanasova. *Sens. Actuators B: Chem.*, **258**, 1279 (2018)
227. T.J.Jentsch, V.Stein, F.Weinreich, A.A.Zdebik. *Physiol. Rev.*, **82**, 503 (2002)
228. M.E.Moragues, R.Martinez-Manez, F.Sancenon. *Chem. Soc. Rev.*, **40**, 2593 (2011)
229. D.C.Gadsby, P.Vergani, L.Csanady. *Nature (London)*, **440**, 477 (2006)
230. S.Madhu, R.Kalaiyarasi, S.K.Basu, S.Jadhav, M.Ravikanth. *J. Mater. Chem. C*, **2**, 2534 (2014)
231. Y.Liu, C.B.Fan, S.Z.Pu. *Microchem. J.*, **158**, 105166 (2020)
232. A.Singh, M.Mohan, D.R.Trivedi. *ChemistrySelect*, **4**, 14120 (2019)
233. Z.Y.Zhan, Y.J.Jia, D.H.Li, X.L.Zhang, M.Hu. *Dalton Trans.*, **48**, 15231 (2019)
234. J.H.Jia, H.X.Zhao. *Org. Electron.*, **73**, 55 (2019)
235. Z.Xu, X.Chen, H.N.Kim, J.Yoon. *Chem. Soc. Rev.*, **39**, 127 (2010)
236. F.Wang, L.Wang, X.Q.Chen, J.Y.Yoon. *Chem. Soc. Rev.*, **43**, 4312 (2014)
237. P.Piyanuch, J.Sirirak, A.Kamkaew, O.Weeranantanapan, V.Promarak, K.Burgess, N.Wanichacheva. *ChemPlusChem*, **84**, 252 (2019)
238. J.Kaluzna-Czaplinska, E.Zurawicz, M.Michalska, J.Rynkowski. *Acta Biochim. Pol.*, **60**, 137 (2013)
239. D.M.Townsend, K.D.Tew, H.Tapiero. *Biomed. Pharmacother.*, **57**, 145 (2003)
240. F.J.T.Staal, S.W.Ela, M.Roederer, M.T.Anderson, L.A.Herzenberg, L.A.Herzenberg. *Lancet*, **339**, 909 (1992)
241. S.Zhang, C.N.Ong, H.M.Shen. *Cancer Lett.*, **208**, 143 (2004)
242. J.N.Dai, C.G.Ma, P.Zhang, Y.Q.Fu, B.X.Shen. *Dyes Pigm.*, **177**, 108321 (2020)
243. L.Y.Niu, Y.Z.Chen, H.R.Zheng, L.Z.Wu, C.H.Tung, Q.Z.Yang. *Chem. Soc. Rev.*, **44**, 6143 (2015)

244. J.Kang, F.J.Huo, J.B.Chao, C.Yin. *Spectrochim. Acta, Part A*, **195**, 16 (2018)
245. C.J.Wang, X.Xia, J.R.Luo, Y.Qian. *Dyes Pigm.*, **152**, 85 (2018)
246. F.F.Wang, Y.J.Liu, B.B.Wang, L.X.Gao, F.L.Jiang, Y.Liu. *Dyes Pigm.*, **152**, 29 (2018)
247. J.H.Gao, Y.F.Tao, J.Zhang, N.N.Wang, X.Ji, J.L.He, Y.B.Si, W.L.Zhao. *Chem. – Eur. J.*, **25**, 11246 (2019)
248. J.Nordberg, E.S.J.Arner. *Free Radical Biol. Med.*, **31**, 1287 (2001)
249. B.D'Autreaux, M.B.Toledano. *Nat. Rev., Mol. Cell Biol.*, **8**, 813 (2007)
250. C.Kunsch, R.M.Medford. *Circ. Res.*, **85**, 753 (1999)
251. H.E.Marshall, K.Merchant, J.S.Stamler. *FASEB J.*, **14**, 1889 (2000)
252. F.C.Fang. *Nat. Rev., Microbiology*, **2**, 820 (2004)
253. B.C.Dickinson, C.J.Chang. *Nat. Chem. Biol.*, **7**, 504 (2011)
254. S.G.Rhee. *Science*, **312**, 1882 (2006)
255. T.Finkel, M.Serrano, M.A.Blasco. *Nature (London)*, **448**, 767 (2007)
256. P.An, T.M.Lewandowski, Q.Lin. *ChemBioChem*, **19**, 1326 (2018)
257. M.S.Purdey, H.J.McLennan, M.L.Sutton-McDowall, D.W.Drumm, X.Z.Zhang, P.K.Capon, S.Heng, J.G.Thompson, A.D.Abell. *Sens. Actuators B: Chem.*, **262**, 750 (2018)
258. J.Xu, J.Zhai, Y.Xu, J.Zhu, Y.Qin, D.Jiang. *Analyst*, **141**, 2380 (2016)
259. H.Wiseman, B.Halliwell. *Biochem. J.*, **313** (Pt. 1), 17 (1996)
260. A.Ayala, M.F.Munoz, S.Arguelles. *Oxid. Med. Cell. Longev.*, 360438 (2014)
261. T.Az-ma, N.Saeki, O.Yuge. *Br. J. Pharmacol.*, **126**, 1462 (1999)
262. K.Lei, M.Sun, L.Du, X.Zhang, H.Yu, S.Wang, T.Hayat, A.Alsaedi. *Talanta*, **170**, 314(2017)
263. X.Qu, W.Song, Z.Shen. *Front. Chem.*, **7**, 598 (2019)
264. X.Y.Qu, Y.J.Bian, Y.Q.Chen, X.Q.Wei. *RSC Adv.*, **10**, 28705 (2020)
265. K.Selvakumar, P.Shah, H.B.Singh, R.J.Butcher. *Chem. – Eur. J.*, **17**, 12741 (2011)
266. G.Mugesh, A.Panda, H.B.Singh, N.S.Punekar, R.J.Butcher. *J. Am. Chem. Soc.*, **123**, 839 (2001)
267. S.T.Manjare, S.Kim, W.D.Heo, D.G.Churchill. *Org. Lett.*, **16**, 410 (2014)
268. P.P.Deshmukh, A.Navalkar, S.K.Maji, S.T.Manjare. *Sens. Actuators B: Chem.*, **281**, 8 (2019)
269. K.S.Madibone, P.P.Deshmukh, A.Navalkar, S.K.Maji, P.M.Badani, S.T.Manjare. *ACS Omega*, **5**, 14186 (2020)
270. A.D.De Grey. *DNA Cell Biol.*, **21**, 251 (2002)
271. M.M.Gaschler, B.R.Stockwell. *Biochem. Biophys. Res. Commun.*, **482**, 419 (2017)
272. P.Oleynik, Y.Ishihara, G.Cosa. *J. Am. Chem. Soc.*, **129**, 1842 (2007)
273. K.Krumova, L.E.Greene, G.Cosa. *J. Am. Chem. Soc.*, **135**, 17135 (2013)
274. L.E.Greene, R.Lincoln, G.Cosa. *J. Am. Chem. Soc.*, **139**, 15801 (2017)
275. J.Kusio, K.Sitkowska, A.Konopko, G.Litwinienko. *Antioxidants*, **9**, 88 (2020)
276. J.P.Gaut, G.C.Yeh, H.D.Tran, J.Byun, J.P.Henderson, G.M.Richter, M.L.Brennan, A.J.Lusis, A.Belaaouaj, R.S.Hotchkiss, J.W.Heinecke. *Proc. Natl. Acad. Sci. USA*, **98**, 11961 (2001)
277. C.C.Winterbourn, M.B.Hampton, J.H.Livesey, A.J.Kettle. *J. Biol. Chem.*, **281**, 39860 (2006)
278. R.K.Gupta, A.K.Patel, N.Shah, A.K.Choudhary, U.K.Jha, U.C.Yadav, P.K.Gupta, U.Pakuwal. *Asian Pac. J. Cancer Prev.*, **15**, 4405 (2014)
279. X.Q.Chen, F.Wang, J.Y.Hyun, T.W.Wei, J.Qiang, X.T.Ren, I.Shin, J.Yoon. *Chem. Soc. Rev.*, **45**, 2976 (2016)
280. Y.Jin, M.H.Lv, Y.F.Tao, S.Xu, J.L.He, J.Zhang, W.L.Zhao. *Spectrochim. Acta, Part A*, **219**, 569 (2019)
281. W.J.Shi, Y.Huang, W.C.Liu, D.Xu, S.T.Chen, F.G.Liu, J.Q.Hu, L.Y.Zheng, K.Chen. *Dyes Pigm.*, **170**, 107566 (2019)
282. L.J.Ignarro. *Hypertension*, **16**, 477 (1990)
283. R.Kamijo, H.Harada, T.Matsuyama, M.Bosland, J.Gerecitano, D.Shapiro, J.Le, S.I.Koh, T.Kimura, S.J.Green, T.W.Mak, T.Taniguchi, J.Vilcek. *Science*, **263**, 1612 (1994)
284. S.Moncada, R.M.J.Palmer, E.A.Higgs. *Pharmacol. Rev.*, **43**, 109 (1991)
285. H.X.Zhang, J.B.Chen, X.F.Guo, H.Wang, H.S.Zhang. *Anal. Chem.*, **86**, 3115 (2014)
286. L.A.Juarez, A.Barba-Bon, A.M.Costero, R.Martinez-Manez, F.Sancenon, M.Parra, P.Gavina, M.C.Terencio, M.J.Alcaraz. *Chem. – Eur. J.*, **21**, 15486 (2015)
287. J.Zhang, F.C.Pan, Y.Jin, N.N.Wang, J.L.He, W.J.Zhang, W.L.Zhao. *Dyes Pigm.*, **155**, 276 (2018)
288. A.Ballabio, V.Gieselmann. *Biochim. Biophys. Acta*, **1793**, 684 (2009)
289. M.A.Marletta. *Cell*, **78**, 927 (1994)
290. U.Forstermann, I.Gath, P.Schwarz, E.I.Closs, H.Kleinert. *Biochem. Pharmacol.*, **50**, 1321 (1995)
291. Z.Yu, J.Zhou, X.Dong, W.Zhao, Z.Chen. *Anal. Chim. Acta*, **1067**, 88 (2019)
292. S.Donzelli, M.G.Espey, D.D.Thomas, D.Mancardi, C.G.Tocchetti, L.A.Ridnour, N.Paolocci, S.B.King, K.M.Miranda, G.Lazzarino, J.M.Fukuto, D.A.Wink. *Free Radical Biol. Med.*, **40**, 1056 (2006)
293. K.M.Rusche, M.M.Spiering, M.A.Marletta. *Biochemistry*, **37**, 15503 (1998)
294. Z.Miao, S.B.King. *Nitric Oxide: Biol., Chem.*, **57**, 1 (2016)
295. H.J.Sun, Z.Y.Wu, L.Cao, M.Y.Zhu, X.W.Nie, D.J.Huang, M.T.Sun, J.S.Bian. *Pharmacol. Res.*, **159**, 104961 (2020)
296. A.T.Wrobel, T.C.Johnstone, A.Deliz Liang, S.J.Lippard, P.Rivera-Fuentes. *J. Am. Chem. Soc.*, **136**, 4697 (2014)
297. M.Royzen, J.J.Wilson, S.J.Lippard. *J. Inorg. Biochem.*, **118**, 162 (2013)
298. P.Liu, X.Jing, F.Yu, C.Lv, L.Chen. *Analyst*, **140**, 4576 (2015)
299. Z.Liu, Q.Sun. *Spectrochim Acta, Part A*, **241**, 118680 (2020)
300. G.L.Squadrito, W.A.Pryor. *Free Radical Biol. Med.*, **25**, 392 (1998)
301. R.Radi, A.Cassina, R.Hodara, C.Quijano, L.Castro. *Free Radical Biol. Med.*, **33**, 1451 (2002)
302. P.Pacher, J.S.Beckman, L.Liaudet. *Physiol. Rev.*, **87**, 315 (2007)
303. Z.N.Sun, H.L.Wang, F.Q.Liu, Y.Chen, P.K.Tam, D.Yang. *Org. Lett.*, **11**, 1887 (2009)
304. B.S.Wang, F.B.Yu, P.Li, X.F.Sun, K.L.Han. *Dyes Pigm.*, **96**, 383 (2013)
305. C.Zhao, J.An, L.Zhou, Q.Fei, F.Wang, J.Tan, B.Shi, R.Wang, Z.Guo, W.H.Zhu. *Chem. Commun.*, **52**, 2075 (2016)

306. E.W.Miller, J.Y.Lin, E.P.Frady, P.A.Steinbach, W.B.Kristan, R.Y.Tsien. *Proc. Natl. Acad. Sci. USA*, **109**, 2114 (2012)
307. J.M.Franke, B.K.Raliski, S.C.Boggess, D.V.Natesan, E.T.Koretsky, P.Zhang, R.U.Kulkarni, P.E.Deal, E.W.Miller. *J. Am. Chem. Soc.*, **141**, 12824 (2019)
308. K.Luby-Phelps. *Int. Rev. Cytol.*, **192**, 189 (2000)
309. H.L.Kee, C.Kirmaier, L.H.Yu, P.Thamyongkit, W.J.Youngblood, M.E.Calder, L.Ramos, B.C.Noll, D.F.Bocian, W.R.Scheidt, R.R.Birge, J.S.Lindsey, D.Holten. *J. Phys. Chem. B*, **109**, 20433 (2005)
310. M.A.Haidekker, E.A.Theodorakis. *Org. Biomol. Chem.*, **5**, 1669 (2007)
311. S.Requena, O.Ponomarchuk, M.Castillo, J.Rebik, E.Brochiero, J.Borejdo, I.Gryczynski, S.V.Dzyuba, Z.Gryczynski, R.Grygorczyk, R.Fudala. *Sci. Rep.*, **7**, 16761 (2017)
312. W.Miao, C.J.Yu, E.H.Hao, L.J.Jiao. *Front. Chem.*, **7**, 6 (2019)
313. S.Granick. *Science*, **253**, 1374 (1991)
314. Z.Yang, Y.He, J.H.Lee, N.Park, M.Suh, W.S.Chae, J.F.Cao, X.J.Peng, H.Jung, C.Kang, J.S.Kim. *J. Am. Chem. Soc.*, **135**, 9181 (2013)
315. Y.L.Wu, M.Stefl, A.Olzynska, M.Hof, G.Yahioglu, P.Yip, D.R.Casey, O.Ces, J.Humpolickova, M.K.Kuimova. *Phys. Chem. Chem. Phys.*, **15**, 14986 (2013)
316. J.A.Levitt, M.K.Kuimova, G.Yahioglu, P.H.Chung, K.Suhling, D.Phillips. *J. Phys. Chem. C*, **113**, 11634 (2009)
317. C.Wang, X.B.Song, L.C.Chen, Y.Xiao. *Biosens. Bioelectron.*, **91**, 313 (2017)
318. M.Kubankova, J.E.Chambers, R.G.Huber, P.J.Bond, S.J.Marciniak, M.K.Kuimova. *Methods Appl. Fluoresc.*, **7**, 044004 (2019)
319. M.M.Ogle, A.D.S.McWilliams, M.J.Ware, S.A.Curley, S.J.Corr, A.A.Marti. *J. Phys. Chem. B*, **123**, 7282 (2019)
320. B.X.Shen, L.F.Wang, X.Zhi, Y.Qian. *Sens. Actuators B: Chem.*, **304**, 127271 (2020)
321. L.L.Li, K.Li, M.Y.Li, L.Shi, Y.H.Liu, H.Zhang, S.L.Pan, N.Wang, Q.Zhou, X.Q.Yu. *Anal. Chem.*, **90**, 5873 (2018)
322. Y.He, J.Shin, W.J.Gong, P.Das, J.H.Qu, Z.G.Yang, W.F.Liu, C.Kang, J.L.Qu, J.S.Kim. *Chem. Commun.*, **55**, 2453 (2019)
323. X.B.Song, N.Li, C.Wang, Y.Xiao. *J. Mater. Chem. B*, **5**, 360 (2017)
324. G.H.Patterson. *J. Microsc.*, **243**, 1 (2011)
325. K.A.Lukyanov, D.M.Chudakov, S.Lukyanov, V.V.Verkhusha. *Nat. Rev., Mol. Cell Biol.*, **6**, 885 (2005)
326. S.Bettati, E.Pasqualetto, G.Lolli, B.Campanini, R.Battistutta. *Biochim. Biophys. Acta*, **1814**, 824 (2011)
327. M.Fernandez-Suarez, A.Y.Ting. *Nat. Rev., Mol. Cell Biol.*, **9**, 929 (2008)
328. J.Lippincott-Schwartz, G.H.Patterson. *Trends Cell. Biol.*, **19**, 555 (2009)
329. L.Wang, M.S.Frei, A.Salim, K.Johnsson. *J. Am. Chem. Soc.*, **141**, 2770 (2019)
330. Y.Zhang, S.Tang, L.Ravelo, J.Cusido, F.M.Raymo. *Methods Enzymol.*, **640**, 131 (2020)
331. S.S.Ragab, S.Swaminathan, E.Deniz, B.Captain, F.M.Raymo. *Org. Lett.*, **15**, 3154 (2013)
332. S.S.Ragab, S.Swaminathan, J.D.Baker, F.M.Raymo. *Phys. Chem. Chem. Phys.*, **15**, 14851 (2013)
333. T.A.Golovkova, D.V.Kozlov, D.C.Neckers. *J. Org. Chem.*, **70**, 5545 (2005)
334. L.Huang, Z.X.Gao, G.Han. *Part. Part. Syst. Charact.*, **34**, 1700223 (2017)
335. E.Deniz, S.Ray, M.Tomasulo, S.Impellizzeri, S.Sortino, F.M.Raymo. *J. Phys. Chem. A*, **114**, 11567 (2010)
336. Y.Zhang, S.Swaminathan, S.C.Tang, J.Garcia-Amoros, M.Boulina, B.Captain, J.D.Baker, F.M.Raymo. *J. Am. Chem. Soc.*, **137**, 4709 (2015)
337. L.Sansalone, S.C.Tang, J.Garcia-Amoros, Y.Zhang, S.Nonell, J.D.Baker, B.Captain, F.M.Raymo. *ACS Sensors*, **3**, 1347 (2018)
338. Y.Zhang, S.C.Tang, L.Sansalone, J.D.Baker, F.M.Raymo. *Chem. – Eur. J.*, **22**, 15027(2016)
339. X.M.Liu, Y.Zhang, J.D.Baker, F.M.Raymo. *J. Mater. Chem. C*, **5**, 12714 (2017)